UNIVERSITÄT TÜBINGEN

MASTER THESIS

Timing and spectral properties of the Be X-ray binary EXO 2030+375

Author:
Eva LAPLACE

Supervisors:
Prof. Andrea SANTANGELO
Dr. Tatehiro MIHARA

A thesis submitted in fulfillment of the requirements for the degree of Master of Science

in the

High Energy Astrophysics Group
Institut für Astronomie und Astrophysik

Eidesstattliche Erklärung

Hiermit erkläre ich, Eva LAPLACE, dass ich nach §17(4) des allgemeinen Teils der Studien- und Prüfungsordnung der Universität Tübingen für den Studiengang Physik mit akademischer Abschlussprüfung Master of Science (M. Sc.) die vorliegende Masterarbeit mit dem Titel „Timing and spectral properties of the Be X-ray binary EXO 2030+375“ selbständig verfasst habe. Darüber hinaus bestätige ich folgende Aussagen:

- Keine anderen als die angegebenen Hilfsmittel und Quellen wurden benutzt.
- Alle wörtlich oder sinngemäß aus anderen Werken übernommenen Aussagen wurden als solche gekennzeichnet.
- Die Arbeit ist weder vollständig noch in wesentlichen Teilen Gegenstand eines anderen Prüfungsverfahrens gewesen.
- Die Arbeit wurde weder vollständig noch in wesentlichen Teilen bereits veröffentlicht.

Ort, Datum:

Unterschrift:

UNIVERSITÄT TÜBINGEN

Zusammenfassung

Mathematisch-Naturwissenschaftliche Fakultät
Institut für Astronomie und Astrophysik

Master of Science

Timing and spectral properties of the Be X-ray binary EXO 2030+375

von Eva LAPLACE

In dem Be-Röntgendoppelsternsystem EXO 2030+375 wurden in den letzten 10 Jahren während jeder Umlaufbahn seit dem letzten Riesen-Röntgenausbruch (Typ II) in 2006 regelmäßige Ausbrüche mit niedriger Leuchtkraft (Typ I) beobachtet. Überraschenderweise wurden in den letzten zwei Jahren eine Änderung im Gesamtverhalten der Quelle beobachtet. Einige Röntgen-Ausbrüche fanden nicht statt, der durchschnittliche Röntgen-Fluss wurde schwächer, und es fand ein Übergang von einer globalen Beschleunigung der Drehung des Neutronensterns in den letzten Jahren zu einer konstante Drehung statt.
In der vorliegenden Masterarbeit untersuche ich den Ursprung dieser Änderungen, indem ich eine Zeit-und Spektralanalyse der Röntgendaten von EXO 2030+375 durchführe.
Die spektralen Eigenschaften der Quelle werden durch die erstmalige Analyse der Daten des japanischen Monitor of All-sky X-ray Image (MAXI) Teleskops, die in den letzten 6.5 Jahren kontinuierlich aufgenommen wurden, untersucht. Ich berechne das Orbit-gemittelte Spektrum der Quelle und analysiere systematisch das Spektrum von jedem Typ-I Ausbruch. Um die spektralen Änderungen innerhalb eines Orbits zu erforschen, wird das Orbit-aufgelöste Spektrum von EXO 2030+375 analysiert. Eine unabhängige Untersuchung wird durchgeführt, indem die Lichtkurve mit der Orbital-Periode gefaltet wird und indem das Härteverhältnis basierend auf drei Energiebänder berechnet wird. Zudem werden die spektralen Änderungen während eines Orbits über Fluss-aufgelöste Spektren untersucht.
Die Ergebnisse zeigen, dass das gemittelte Spektrum gut mit bisherigen Studien übereinstimmt. Allerdings sind die einzelnen Spektren der Typ-I Ausbrüche von niedriger Statistik und Hintergrundkontamination beeinträchtigt. Aus diesem Grund kann die Entwicklung der spektralen Parameter nicht eingeschränkt werden.
Ich finde außer einer Hauptspitze in der Nähe vom Periastron eine zweite, kleinere Spitze am Apastron. Eine ähnliche Beobachtung wurde schon früher basierend auf RXTE/ASM Daten gemeldet. Obwohl keine signifikanten spektralen Änderungen während der Hauptspitze beobachtet werden, gibt es Anzeichen für solche Änderungen währen des Apastrons. Dies wird durch die Studie der Fluss-ausgelösten und Orbit-aufgelösten Spektren bestätigt, in denen eine schwache Abhängigkeit der Leuchtkraft vom spektralen Index gefunden wird. Dies bestätigt frühere Ergebnisse, die auf die Analyse von RXTE Daten, die während eines Orbits von EXO 2030+375 aufgenommen wurden, beruhen.

Um die jüngsten Verhaltensänderungen von EXO 2030+375 besser zu verstehen, wird eine Untersuchung der zeitlichen Eigenschaften der Quelle durchgeführt. Das globale Verhalten der Quelle wird in den letzten 30 Jahren seit ihrer Entdeckung analysiert, indem alle verfügbaren Röntgendaten (basierend auf EXOSAT, BATSE, RXTE, Swift und MAXI), die Puls-Frequenz-Daten (basierend auf früheren Studien und neuesten Fermi/GBM Daten) und die Messungen der Hα Spektral-Linien gesammelt werden. Zudem wird die zeitliche Änderungen der Orbitalphase der Spitzen der Typ-I Ausbrüche untersucht. Außerdem werden die zeitlichen Eigenschaften der sogenannten "precursors", schwache Spitzen am Anfang eines Typ-I Ausbruchs, analysiert.
Ich finde bemerkenswerte Ähnlichkeiten zwischen den jüngsten Änderungen in EXO 2030+375 und Ereignissen, die zwischen 1993 und 1995 stattfanden. In dieser Zeit wurde der mittlere Röntgen-Ausbruchsfluss schwächer, Typ-I Röntgenausbrüche fanden nicht statt und die Drehung des Neutronensterns, die zuvor stetig beschleunigt wurde, wurde konstant. Kurz nach diesen Ereignissen wurde eine plötzliche Verschiebung der Spitze der Typ-I Ausbrüche beobachtet. Interessanterweise geschah dies fast genau zwischen den zwei Riesenausbrüchen der Quelle in den Jahren 1985 und 2006. Diese Ähnlichkeiten weisen auf die Existenz eines 10.5 oder 21 Jahre langen Zyklus der Quelle hin. Darauf basierend habe ich eine weitere Verschiebung der Orbitalphase der Typ-I Ausbruchsspitze um Dezember 2016 vorausberechnet. Die Beobachtung einer solchen Verschiebung im Juli 2016 bestätigt diese Voraussage und bekräftigt die Existenz einer Langzeitperiodizität in EXO 2030+375. Mehrere mögliche Interpretationen werden vorgestellt. Ich zeige, dass Kozai-Lidov Oszillationen in der Scheibe, die den Be-Stern umgibt, eine plausible Erklärung des Gesamtverhaltens ermöglichen.

UNIVERSITÄT TÜBINGEN

Abstract

Mathematisch-Naturwissenschaftliche Fakultät
Institut für Astronomie und Astrophysik

Master of Science

Timing and spectral properties of the Be X-ray binary EXO 2030+375

by Eva LAPLACE

The Be X-ray binary system EXO 2030+375 has shown recurring low-luminosity X-ray outbursts (type I) for the last 10 years. Surprisingly, changes in its regular behavior were observed during the last two years. Some X-ray outbursts were missed, the average X-ray flux level decreased, and a transition of the global spin up of the neutron star to a constant spin occurred.
In this Master thesis, I investigate the origin of these changes by performing a spectral and timing analysis of the X-ray data of EXO 2030+375.
The spectral properties of the source are studied by analyzing for the first time the last 6.5 years data from the Japanese Monitor of All-sky X-ray Image (MAXI) telescope. I compute the orbital phase-averaged spectrum of the source and conduct a systematic analysis of the spectra of each type I outburst. To understand the spectral variations along the orbit of the source, the orbital phase resolved spectrum of EXO 2030+375 is analyzed. An independent study is performed by folding the MAXI light-curve and computing the hardness ratio based on three energy bands. Moreover, I examine the orbital spectral changes with a flux resolved analysis of the MAXI spectra.
The results show that the MAXI phase average spectrum, modeled with a typical absorbed power-law with high-energy cutoff is in good agreement with previous studies. However, the studied spectra are strongly affected by low statistics and background contamination issues, and the evolution of the spectral parameters can thus not be constrained.
I find that the light-curve folded with the orbital period contains an interesting second peak at an orbital phase corresponding to the apastron passage of the neutron star in addition to the main peak shortly after the periastron passage. Such a feature was previously reported using RXTE/ASM data. While there are no significant spectral variations during the main peak of the orbital phase resolved light-curve, there are indications for spectral variations during the apastron passage. These findings are confirmed by the study of the flux and orbital phase resolved spectra of the source, which reveal a weak luminosity-dependence of the photon index. This supports previous studies based on the analysis of RXTE data.

To better understand the recent changes observed in EXO 2030+375, a study of the timing properties of EXO 2030+375 is conducted. The global source behavior in the last 30 years is analyzed by gathering all available X-ray data (based on EXOSAT, BATSE, RXTE, Swift and MAXI), pulse frequency data (based on previous studies of X-ray data and on recent Fermi/GBM data), the measurements of the equivalent width of the Hα line, and by studying the timing of the type I outburst peaks. In addition, I investigate the timing properties of the precursors of the type I outbursts using RXTE/ASM, Swift/BAT and MAXI/GSC data.
I find striking similarities between the recent changes and phenomena observed between 1993 and 1995. During this period, the average outburst flux decreases, type I X-ray outbursts are missed, and the spin frequency of the neutron star, which had been steadily increasing, starts to decrease. Shortly after these events, a sudden shift of the orbital phase shift of the type I outburst peak can be observed. Interestingly, this event occurs almost exactly in-between the two observed giant (type II) outbursts of the source which were observed in 1985 and 2006. These peculiar similarities indicate the existence of a 10.5 yr or 21 yr cycle in the source. Based on these observations, I predicted the occurrence of an orbital phase shift around 2016 December by estimating the long-term period with a folding method. The observation of an orbital phase shift in 2016 July confirms this prediction and strongly supports the existence of a long-term recurrence in EXO 2030+375. Several possible interpretations of the long-term behavior of the source are presented. I show that the existence of Kozai-Lidov oscillations in the circumstellar disk of the Be star constitutes a plausible explanation.

Contents

List of Figures

List of Tables

List of Abbreviations

ASM	**A**ll **S**ky **M**onitor
BAT	**B**urst **A**lert **T**elescope
BATSE	**B**urst **A**nd **T**ransient **S**ource **E**xperiment
Be disk	Circumstellar disk around the Be star in a Be X-ray binary system
BeXRB	**Be**/**X**-**r**ay **b**inary
CCD	**C**harge-**C**oupled **D**evice
CGRO	**C**ompton **G**amma-**R**ay **O**bservatory
CM	**C**enter of **M**omemtum
CRSF	**C**yclotron **R**esonant **S**cattering **F**eature
ESA	**E**uropean **S**pace **A**gency
EXOSAT	**E**uropean **X**-ray **O**bservatory **Sat**ellite
FOV	**F**ield **O**f **V**iew
GBM	**G**amma-ray **B**urst **M**onitor
GRB	**G**amma-**R**ay **B**urst
GSC	**G**as **S**lit **C**amera
GTI	**G**ood **T**ime **I**nterval
Hα	**H**ydrogen α
INTEGRAL	**Int**ernational **G**amma-**R**ay **A**strophysics **L**aboratory
IR	**I**nfra-**r**ed
ISS	**I**nternational **S**pace **S**tation
MAXI	**M**onitor of **A**ll-sky **X**-ray **I**mage
ME	**M**edium **E**nergy proportional counter
MJD	**M**odified **J**ulian **D**ate
OPS	**O**rbital **P**hase **S**hift
QPO	**Q**uasi-**p**eriodic **o**scillations
RMS	**R**oot **M**ean **Square**
RXTE	**R**ossi **X**-ray **T**iming **E**xplorer
SSC	**S**olid-state **S**lit **C**amera
XRT	**X**-**r**ay **T**elescope

Chapter 1

Introduction

In 1962, the first rocket with an X-ray experiment on-board was launched. As the atmosphere of the Earth absorbs high-energy photons, the exploration of the X-ray sky was only possible with the emergence of rockets and satellites, even though X-rays had been discovered long before by Röntgen in 1895. X-ray emission from the Sun had been observed in the 1950s and found to be significantly lower than its radiation in other wavelengths. The X-ray radiation from other stars was therefore expected to be insignificant. The main observational target of the rocket experiment, led by Riccardo Giacconi, was the Moon. X-rays were expected because of two reasons: the interactions between the lunar surface and the solar wind and the reflection of the solar X-ray radiation. Instead of observing the Moon, whose X-ray radiation was at a much lower energy than expected, the experiment led to the discovery of an extraordinarily bright X-ray source in the Scorpius region, named Sco X-1, which seemed to originate from outside the Solar System, and of a diffuse X-ray background (Giacconi et al., 1962).
When other missions started to explore the X-ray sky soon after, and the first X-ray satellites (Uhuru, Ariel-V, HEAO) were launched, it quickly became evident that the Universe was populated with point-like objects emitting strong X-ray radiation. The X-ray sky was found to be an ever-changing, violent place of extreme phenomena. Some point-like objects would suddenly appear and brighten before fading away (the transient sources), while others would always be visible (the persistent sources). This discovery enabled the observation of a new and unexpected aspect of the Universe, and marked the birth of a new field, X-ray astronomy (see, e.g., Santangelo and Madonia, 2014).
Some of the discovered sources showed a very regular pulsed emission. The first radio pulsars had just been discovered and it was soon apparent that the same objects were involved in these X-ray pulsars: neutron stars, extremely dense remnants of stellar explosions. Cen X-3, which was discovered by the Uhuru satellite (Giacconi et al., 1971), was the first X-ray source to exhibit pulsed emission. Unlike radio pulsars, it had a much longer period of 5s. A sinusoidal variation of the pulsed emission with a period of 2.1 days was found which revealed that this was a binary system with a very short orbital period. This finding was confirmed by the discovery of its optical counterpart shortly afterwards. Figure 1.1 shows the discovery light-curve of the pulsations from Cen X-3.

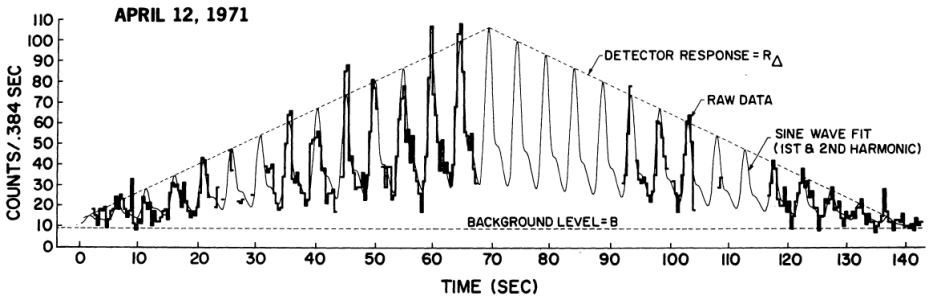

FIGURE 1.1: Discovery light-curve of the pulsed emission from Cen X-3, fitted with a sinusoidal function (from Giacconi et al., 1971).

Soon, many more binary X-ray sources were discovered. Their binary nature enabled the measurement of their masses, which corresponded to theoretical predictions for neutron stars and in some cases, for black holes. To explain the intense X-ray emission from these systems, a leading theory emerged, the accretion theory, which successfully explained how matter flow from the companion star to the compact object could produce such an intense X-ray radiation.

Be X-ray binaries (BeXRBs) are the most populated class of binary X-ray pulsars and belong to the high mass X-ray binaries (see, e.g. Reig, 2011). Today, 60 years after the discovery of these sources, surprisingly many of their properties are still poorly understood. What characterizes these systems are observational evidences for a circumstellar disk around the young and bright companion star of spectral type Be and their distinctive X-ray light-curves. Although there is little doubt that the very fast rotations of Be stars are linked to the formation of Be disks, the exact mechanisms involved are still unknown today. Furthermore, the formation history of BeXRBs and in particular the origin of their fast rotation is still debated to this day, with competing theories being an evolutionary spin up during the main sequence evolution (see, e.g., Granada et al., 2013) and a spin up due to accretion in a binary system (see, e.g., de Mink et al., 2013).

X-ray light-curves of transient BeXRBs are characterized by phases during which a fast increase of the X-ray flux, followed by a slower decrease of the flux can be observed on a time-scale of days to months, the so-called outbursts. Two classes of outbursts are typically distinguished: type I and type II. While the former ones are shorter, less bright, and can well be explained by matter capture at periastron, the latter are much brighter, last longer and their origin is still unclear, though most theories link them to the accretion of an enormous amount of matter directly from the circumstellar disk (Okazaki, Hayasaki, and Moritani, 2013; Martin et al., 2014a).

In this thesis, the spectral and timing properties of a particular BeXRB system, EXO 2030+375, are examined. The next chapter, Chapter 2, presents the theory of X-ray binaries and focuses on the particularities of BeXRBs. In Chapter 3, I introduce the main topic of this thesis, the BeXRB EXO 2030+375 and present its characteristics and the peculiar behavior change it exhibited in recent years. To understand the origin of this change, I investigate the spectral properties of the source in Chapter 4 and conduct a timing analysis in Chapter 5. The results are discussed and summarized in Chapter 6.

Chapter 2

Astrophysical background

2.1 Neutron stars

2.1.1 Discovery history

The existence of a neutron stars was first postulated in 1934 soon after the discovery of the neutron by James Chadwick in 1932 (Chadwick, 1932), when Walter Baade and Fritz Zwicky predicted its existence as the remnant of a core-collapse supernova (Baade and Zwicky, 1934). In 1939, the same object was postulated by Julius R. Oppenheimer and George Volkoff resulting from a solution of the relativistic equation for a pure neutron gas (Oppenheimer and Volkoff, 1939). Further predictions were made after these pioneering theoretical works, with a notable contribution from Franco Pacini, who argued that rotating neutron stars could produce radiation, explaining the origin of the energy required to power supernova remnants, which was a mystery at the time (Pacini, 1967). The first observational evidence for the existence of neutron stars was found during the same year.
At that time, radio astronomy was mainly focused on the study of quasars. Antony Hewish discovered that fluctuations in the radio signals of these objects at low frequencies were due to irregularities in the solar wind, providing a new way to discover objects of this class. Hewish ordered the construction of a radio array of high precision to allow for these kind of studies. His PhD student, Jocelyn Bell, studied the data of the first observational campaign. With careful monitoring, she discovered an unusual source in July 1967 which seemed to consist entirely of radio signals. In November 1967, the source was observed again and was seen to consist of periodical radio pulses with a period about 1.33 s : the first pulsar (short for "pulsating radio source") had been discovered (Hewish et al., 1968). Soon after, three additional such source were identified, marking the birth of pulsar astronomy (Pilkington et al., 1968).

2.1.2 Origin

Stars die in spectacular ways. Depending on their masses and on their environment, the way they die varies. However, it will usually involve a gigantic and extremely rapid explosion, known as a supernova. After such an event, the remnant of the star's inner core is often left over, and become an exotic extremely compact object, known as a white dwarf, a neutron star or a black hole.
In the typical stellar evolution of a single star of mass between 8 and 25 solar masses, the stellar remnant will be a neutron star. During its life, the star is sustained by nuclear fusion at its core, which produces a radiation

pressure in equilibrium with its gravitational compression (see, e.g. Longair, 2011).
When the conditions for nuclear fusion are not met anymore and hydrogen burning begins, the temperature of the core increases drastically and the time-scale for nuclear burning is greatly reduced, leading to a chain-reaction. As the temperature increases to 10^9 K, thermal electrons and positrons are created. Helium burning and then carbon, neon, oxygen and silicon burning induce tremendous losses of energy via the production of neutrino-antineutrino pairs, which are created by the annihilation of electrons and positrons and which escape the star because of their very small cross-sections. These energy losses will be countered by more nuclear reactions, until an iron core of about 1.5 $M_\odot$ is left.
The iron core will reach temperature high enough for inverse β-decay to take place, transforming protons and electrons into neutrons and electron neutrinos and inducing even more energy losses in a process known as neutronization. At the same time, iron nuclei will be disintegrated by high energy photons, loosing even more energy. The enormous neutrino losses will lead to a disappearance of the supporting pressure and to a free-fall collapse of the core which will last for less than a second.
The contraction of the core will result in high enough densities for electrons to be degenerate and as such to be governed by Fermi's exclusion principle: the high momenta of the particles will force them to occupy distinct quantum states and create a degeneracy pressure. In the case of neutron stars, the densities will be high enough for the electrons to become relativistic, and to induce β-decay which will convert protons into neutrons.
At a pressure exceeding 2×10^{14}g cm^{-3}, the density increases so much that the neutrons become degenerate. When this occurs, the pressure of the degenerate neutron gas is high enough to halt the gravitational collapse. What happens next is not entirely understood and is still being investigated. Simulations suggest the formation of an enormous shock wave which somehow generates the event we know as a supernova, during which most of the energy is carried away by neutrinos which were trapped inside the core, blowing away the outer layers of the star and creating the objects we know as neutron stars (Frank, King, and Raine, 2002).

2.1.3 Properties

The question of the composition of the inner-most part of a neutron star is one of the biggest unsolved problems of science, for the composition of neutron stars is governed by the physics of degenerate nuclear matter and in particular by its equation of state, which are still uncertain today. However there is a consensus on the likely composition of the outer layers of neutron stars as is pictured in Figure 2.1 and as is listed here:

1. surface layer: composed by a solid layer of atomic polymers of iron with a high conductivity parallel to the magnetic field

2. outer crust: This region has a density $\rho > 4.3 \times 10^{11}$g cm^{-3}, and its composition is similar to that of a white dwarf with a degenerate electron gas and a lattice of heavy nuclei, in which beta decay can occur, creating more and more neutrons.

3. inner crust: At densities $4.3 \times 10^{11}\mathrm{g\,cm^{-3}} < \rho < 2 \times 10^{11}\mathrm{g\,cm^{-3}}$, the lattice of nuclei is still present. However, when these nuclei become too neutron rich, a process called the neutron drip is induced, in which the nuclei change into a degenerate neutron gas and a degenerate relativistic electron gas in an equilibrium state.

4. neutron liquid region: At densities $\rho > 2 \times 10^{11}\mathrm{g\,cm^{-3}}$, it becomes energetically favorable to have free neutrons forming a liquid. The conditions are also met for protons to be superconducting.

5. inner core: the composition of the inner core remains unclear. One exciting possibility is the presence of exotic matter for example composed by strange quarks.

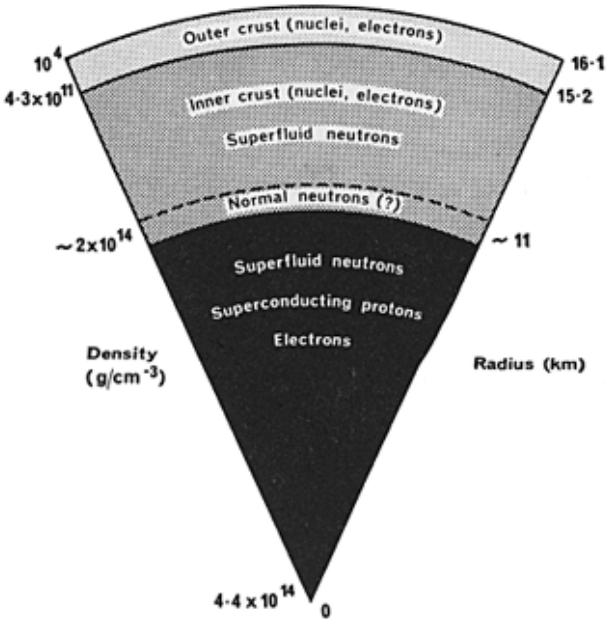

FIGURE 2.1: Model of the neutron star accretion structure. Credits:NASA/HEASARC

Neutron stars are expected to harbor extremely strong magnetic fields, which are the result of the conservation of the magnetic flux during the core-collapse of the progenitor star. The strength of the magnetic field is further sustained by a process called magnetic flux freezing, which couples the magnetic field to the ionized plasma.
Since the discovery of neutron stars, there has been strong evidence supporting the existence of exceptionally high magnetic fields in neutron stars, including the polarization of radiation from radio pulsars, together with the rotation of the polarization plane and the discovery of cyclotron resonant scattering features in the X-ray spectra of X-ray binaries (Trümper et al., 1978).
Another characteristic of neutron stars is their extremely high rotational velocity, in some cases up to their breaking velocity, as in the case of millisecond pulsars, for example.

2.2 Accretion

The classical stellar energy production mechanisms cannot explain the energies observed in the X-ray or the gamma-range for X-ray binaries. In fact, the classical energy production of stars, fusion, is not efficient enough to account for these energies.
Another mechanism had to be found, accretion, which is based on the conversion of gravitational energy to radiation energy (Frank, King, and Raine, 2002). It can be pictured as follows: matter or gas with total mass m accumulates in free-fall from infinity onto an object with mass M and radius R_*. The gravitational potential energy is converted to the free-fall kinetic energy and radiated away as heat once the matter reaches the surface of the object.
Assuming that all the gravitational energy $\mathrm{E_g}$ is released in form of radiation energy $\mathrm{E_{rad}}$, we obtain:

$$\Delta E_{\mathrm{acc}} = \frac{GmM}{R_*} \tag{2.1}$$

for the total accretion energy. The corresponding radiation luminosity is

$$L = \frac{dE}{dt} = \frac{GMdm}{R_* dt} = \frac{GM\dot{m}}{R_*} \tag{2.2}$$

with $\dot{m}$ the mass accretion rate. The luminosity is often expressed using the Schwarzschild radius, $r_{\mathrm{g}} = \frac{2GM}{c^2}$. We obtain $GM = \frac{r_{\mathrm{g}}c^2}{2}$ and therefore

$$L = \frac{r_{\mathrm{g}}\dot{m}c^2}{2R_*} = \xi\dot{m}c^2, \tag{2.3}$$

with $\xi = \frac{r_{\mathrm{g}}}{2R_*}$ the so-called accretion efficiency. This quantity is strongly dependent on the compactness of the object considered. Thus, it is natural to expect efficient energy production from accretion in compact objects such as neutron stars, black holes and white dwarfs.
For white dwarfs, this process is less efficient than fusion, but still has to be accounted for, since nuclear fusion only occurs during run-away reactions on the surface during which the available fuel is rapidly burnt (Frank, King, and Raine, 2002).
Since black hole have a larger compactness than neutron stars, one would expect that accretion would be more efficient for these objects. However, one has to consider that black holes do not have a surface and that the accretion process thus varies.
In fact, matter falling onto the black hole conserves its angular momentum and, due to some fluctuations in the gravitational potential, will have some angular momentum and acquire rotational energy. Due to centrifugal forces, the matter will be prevented from falling onto the black hole and collapse along the rotational axis to form an accretion disk.
The disk is governed by viscous forces, which allow matter in the disk to spread outwards, taking angular momentum with it and enabling matter inside the disk to fall onto the compact object. In addition, viscous forces act as a friction force and radiate away heat, an effect which is mostly observed in black holes.

The formation of such a disk is not limited to black holes, rather, it is a universal process which is involved in explaining planet formation, the properties of AGNs, and Quasi Periodic Oscillations (QPOs) in binary systems. Accretion in binary systems can be divided into two main categories:

1. Roche-Lobe overflow: During the evolution of a binary system, the orbital separation may shrink or/and one of the stars may increase in size. Matter from the outer envelop of this star may then cross the edge of its gravitational potential and be transferred to the companion star.

2. Wind accretion: Matter transfer which occurs when a compact object passes through the strong wind created by a young and massive star.

2.2.1 Roche-Lobe overflow

As of today, the best understood accretion mechanism is the Roche-Lobe overflow. It is associated to the mathematician Edouard Roche who studied the survival of planetary satellites in the 19th century. The mathematical description of this mechanism makes two assumptions which are typically met in real systems: both stars can be regarded as point masses and orbit each other on Keplerian orbits which can be approximated as circular. Considering the orbit of a test particle with negligible mass in this system, the gravitational potential created by the interaction of both stars can be characterized. In the frame of reference rotating with the binary system, centered around the center of momentum of the system, CM, a centrifugal potential is added to the gravitational potential. The equipotential surfaces can be described as

$$\phi = \frac{GM_1}{r_1} + \frac{GM_2}{r_2} - \frac{\omega^2 r^2}{2} = \text{const}, \tag{2.4}$$

with M_i the masses of the stars, r_i the distance to each star, ω the angular velocity of the binary system and r the distance to the rotation axis (e.g., Longair, 2011).

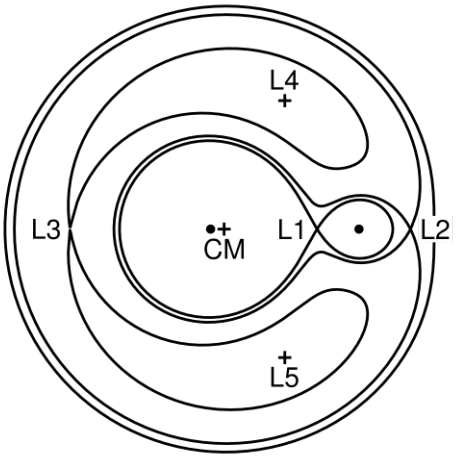

FIGURE 2.2: Contours of the equipotential surfaces of a binary system with a mass ratio of q=10. The Lagrangian points L1 to L5 and the Center of Momentum are indicated. [By Philip D. Hall - Own work, CC BY-SA 4.0]

An example of equipotential surfaces for a mass ratio of 10:1 is shown in Figure 2.2. The lines show the 2D cut of the equipotential surfaces and the equilibrium Lagrangian point 1 – 5. The most interesting equipotential line is the one shaped as a figure-of-eight which surrounds both stars. The surfaces around each star are known as the Roche-Lobes, which meet at the Lagrangian L1 point, the saddle point. This can be understood as a high mountain pass between two valley. From this analogy, the accretion mechanism can be easily understood: The star with the larger mass expands until it fills its Roche lobe. At the L1 point, matter can flow to the Roche lobe of the second star.
Close to the star, the equipotentials can be understood as the edge of the gravitational potential of each star, which is a circle in 2 dimensions. The same happens far away from the systems, where particles feel the gravitational potential of the binary system as a circle around the CM.

2.2.2 Wind accretion

In systems containing a young and massive star (O, B) in a close orbit with the compact object, the effect of the strong stellar wind becomes relevant. A typical wind of a donor star with a mass M_* and a radius R_* is ejected in every direction and its velocity v_w can be estimated as the velocity needed to escape the gravitational potential of the star

$$v_\mathrm{w} \sim v_\mathrm{esc} = \sqrt{\frac{2GM_*}{R_*}}. \tag{2.5}$$

For typical values, the wind velocity is largely supersonic, which means that the gas pressure can be neglected and that the wind can be described as a collection of particles. As the compact object orbits the star, it can only capture a tiny fraction of the stellar wind: the particles for which the gravitational potential energy due to the compact object is greater than their kinetic energy. For a compact object with mass M_CO with an orbital velocity v_CO, accretion is therefore only possible at a certain radius r_acc in a

cylindrical region around the relative wind direction $v_{\rm rel} = v_{\rm w} + v_{\rm CO}$.

$$r_{\rm acc} \sim \frac{2GM_{\rm CO}}{v_{\rm rel}^2} \tag{2.6}$$

2.2.3 Accreting pulsars

When accretion occurs in a system containing a neutron star, the process is influenced by the extremely strong magnetic field of the neutron star. Matter reaching the neutron star (which is typically ionized), is stopped from falling directly on the surface as it reaches the region of influence of the magnetic field at a radius known as the Alfvén radius. From there, it is funneled along the magnetic field lines onto the magnetic poles of the neutron star, where it finally reaches the surface (e.g., Longair, 2011).
The energy of the in-falling matter is released in form of thermal radiation in the X-ray band in a radiation beam from a hot spot on the pole of the neutron star. Because of the misalignment of the magnetic axes of the neutron star and its spinning axis, a pulsating signal is detected when the radiation beam passes through the line-of-sight of the observer. Such an object is an X-ray pulsar. An artist's impression of a neutron star summarizing its properties is shown in Fig. 2.3.

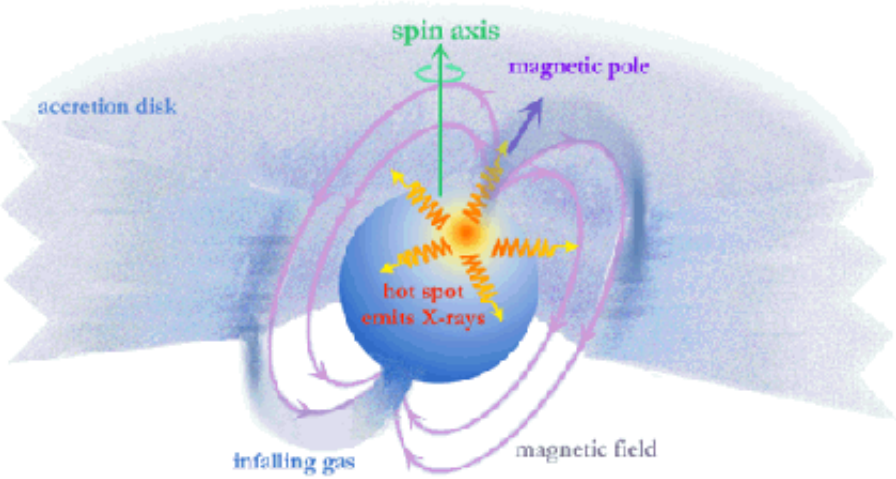

FIGURE 2.3: Artist's impression of an accreting neutron star.
Credits:NASA/Chandra

While X-ray pulsars involve the same objects as radio pulsars, namely neutron stars, their energy source is completely different: the radio beam of radio pulsars is fueled by the rotational energy of the pulsar, effectively slowing it down. In the case of X-ray pulsars, the energy source is accretion (Frank, King, and Raine, 2002).
When examining the evolution of the pulse period of X-ray pulsars, two main types of variations are observed. The first is a period modulation which can be accounted for by the orbital motion of the pulsar. In fact, a pulsar acts similarly to a clock rotating around an object: the frequency is periodically Doppler shifted. This provides an independent way of calculating the orbital period and the mass function of such a system which is

often also more reliable, as it is relatively free of external effects changing the parameters of the model.
The second type of variation is a steady decrease of the pulse period or "long-term spin-up" on a typical time-scale of 10^4 yr, which is occasionally interrupted by short periods of spin-down.
This can be explained by the accretion process. In fact, not only energy, but also angular momentum is transferred to the pulsar. In this case, its rotation velocity increases and its pulse period decreases ("spin up"). The periods of "spin-down" are mainly explained by changes in the accretion torque and by internal changes of the neutron star structure.

2.3 Be X-ray binaries

2.3.1 Overview

X-ray binaries are divided in several sub-classes which exhibit different properties. Be X-ray binaries (BeXRBs) build the most populated of these sub-classes. They are composed by a Be star and by a neutron star (and more rarely by a black hole (e.g., Munar-Adrover et al., 2014)). Be stars are defined as (O9-B2)-type stars from which hydrogen α (Hα) emission lines have been observed at least once (e.g., Reig, 2011). These young stars with masses ranging roughly between $6 - 24\ M_\odot$ are known to rotate very rapidly close to their braking velocity. Their strong optical emission lines and an excessive infrared radiation indicate the presence of an excretion disk of ejected material surrounding them. The rapid rotation of the Be star is an insufficient explanation for the formation of the excretion disk, which remains unclear, with several candidates being stellar pulsations (Smith, 1994) and magnetic fields (Rivinius et al., 2001a).
BeXRBs are characterized by their strong and transient X-ray emission which originates in accretion of matter from the excretion disk of the companion star onto the neutron star. Quasi Periodic Oscillations (QPOs) are exhibited by many BeXRBs and indicate the presence of a transient accretion disk surrounding the neutron star (Longair, 2011).
These systems have an eccentric orbit (e > 0.1), a relatively long orbital period (from a week to several months) and there are some observational indications for a significant inclination of the orbital plane with respect to the spin of the Be star (Martin et al., 2014a).

2.3.2 Optical emission lines and infrared excess

BeXRBs sometimes exhibit emission lines in their optical spectra. Especially prominent lines are Hydrogen α and Helium α lines. Their origin is best explained by the presence of a large circumstellar disk of expelled material around the stellar companion, the excretion disk, which re-emits the radiation received from the star depending on its composition. The width and the shape of the lines, and their evolution can give crucial information about the size and the geometry of the disk.
Compared to isolated stars of the same spectral type (B), the optical companion in BeXRBs have an excessively strong infrared radiation. The presence of a circumstellar disk can also explain this observation by the re-emission of radiation at this wavelength.

In some systems, the presence or the absence of a disk can be clearly distinguished by studying optical and infrared observations, as for example in the case of X Per, as shown in Figure 2.4 (Reig, 2011). In the infrared band, the spectrum clearly shifts from a higher flux in the presence of a disk to a lower flux. In the optical band, Hα and He emission lines become absorption lines in the absence of a disk.

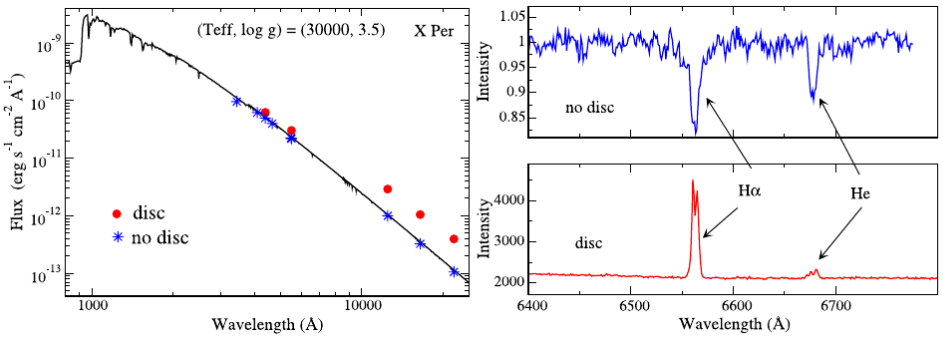

FIGURE 2.4: Infrared and optical spectra from X Per. the difference rising from the presence or absence of a circumstellar disk is clearly observed (from Fig. 4 in Reig, (2011))

Another property of BeXRBs is the so-called V/R variability. The shape of the optical spectral lines of BeXRBs is complex and most often double peaked. Monitoring the ratio of the blue/violet peak and of the red peak (V/R), a quasi-cyclic variability is observed in both isolated Be stars and BeXRBs. In general, the time-scale of the V/R variability is shorter for BeXRBs (1 – 5 yr) than for isolated Be stars (2 – 11 yr) (Okazaki, 1997). The V/R variability is typically interpreted with the presence of a global one-armed oscillation passing through the disk.

2.3.3 X-ray spectra

The X-ray spectra of most BeXRBs correspond to a typical accreting pulsar spectrum: an absorbed power-law with a photon index in the range $1 - 2$ with an exponential cut-off. A fluorescent iron Kα line is also often present in most sources at around 6.4 keV and cyclotron resonant scattering absorption features and their harmonics have been reported for a large number of BeXRBs. It is also worth noting that BeXRBs are distinct from X-ray binaries with OB supergiant stars, as they have low absorption column densities and weak Iron K lines (see, e.g, Makishima et al., 1990).
The power-law with an exponential cut-off is understood to be formed by the Compton scattering of photons by the accreted plasma (see, e.g., Longair, 2011). The absorption arises from the intra-galactic absorption between the observer and the source, while the iron line reveals the abundance of this element in the accreted matter and is thought to be produced by the interaction of hard X-rays from the neutron star with the optically thick matter at the inner edge of the accretion disk.
The discovery of cyclotron lines in several spectra of accreting pulsars has been fundamental for the understanding of these systems (Trümper et al.,

1978). The cyclotron line and its harmonics are formed by the resonant scattering of photons trapped in the dense part of the accretion column and of Landau electrons, whose kinetic energy is quantized because of the strong magnetic field. It provides an independent method for estimating the magnetic field of the neutron star and the variations of the line constrain existing accretion models.

2.3.4 Corbet diagram

X-ray pulsars can be classified using the Corbet diagram, the relation between their spin period and their orbital period. Interestingly, BeXRBs occupy a distinct portion of this diagram, as they appear to have a linear relation between both parameters, with very few exceptions (for example SAX J2103.5+4545), as shown in Figure 2.5.

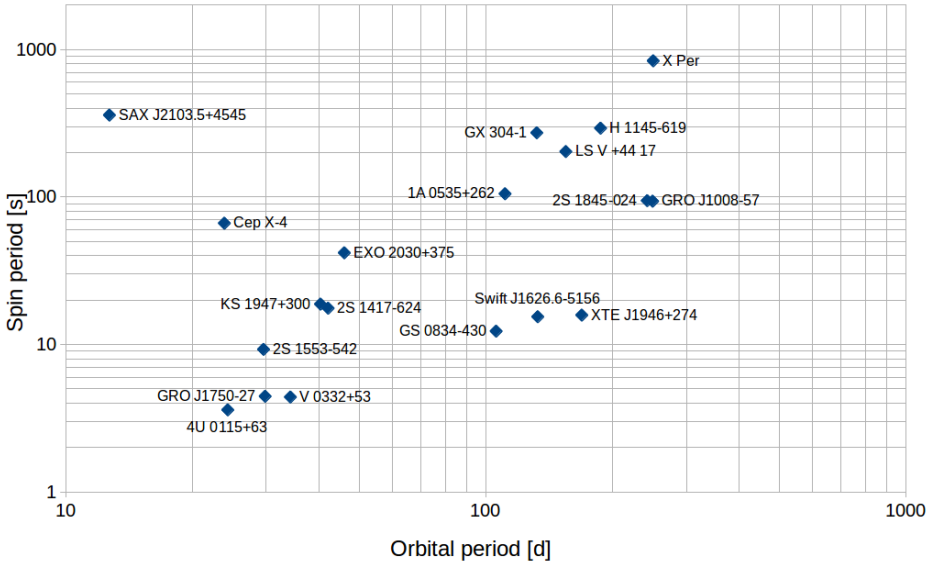

FIGURE 2.5: Corbet diagram of confirmed BeXRBs, from Laplace, (2015). The errors are smaller than the symbols.

This peculiar link between the rotation of the pulsar and its orbit is usually explained by the existence of an equilibrium state of the forces acting on the pulsar. Consequently, the Alfvén radius and the co-rotation radius are almost the same (see section 2.2.3). As the Alfvén radius depends on the density of the medium and thus on the orbital period, a linear relation arises with the spin period. Empirically, this relation can be approximated by a power-law with an additional correction for the eccentricity of the orbit (see Corbet, 1984).

2.3.5 Outbursts

The transient X-ray emission from BeXRBs is called an outburst. During such an event, the X-ray luminosity of the system increases until it reaches a maximum and then slowly decreases again. Two main types of outbursts are distinguished:

- **Type I outbursts**, also known as normal outbursts; with a luminosity of $L_X \sim 10^{36} - 10^{37}$ erg s^{-1}. They are thought to be the result of the accretion of material at periastron, when the neutron star is closest to the companion star, and typically occur periodically with a period equal to the orbital period (e.g., Reig, 2011).

- **Type II outbursts**, also known as giant outbursts, are characterized by being about an order of magnitude more luminous than type I outbursts with a luminosity of $L_X \geq 10^{37}$ erg s^{-1}. These outbursts can last for several orbital periods and are characterized by a harder X-ray spectrum and the frequent observation of a cyclotron resonant scattering feature.
  Giant outbursts are usually believed to occur randomly (Stella, White, and Rosner, 1986; Okazaki and Negueruela, 2001) and their origin remains unclear, more than 50 years after the discovery of BeXRBs. The very high luminosities and the long timescales can be explained by the accretion of an enormous amount of matter directly from the circumstellar disk, but the mechanism enabling this accretion are still difficult to explain. Recent theories and simulations suggest that a transfer of matter directly from the disk can be achieved in misaligned systems if the disk is warped (Okazaki, Hayasaki, and Moritani, 2013) and if it has an increased eccentricity (Martin et al., 2014a).

Typical examples of BeXRB light-curves are shown in Fig. 2.6.

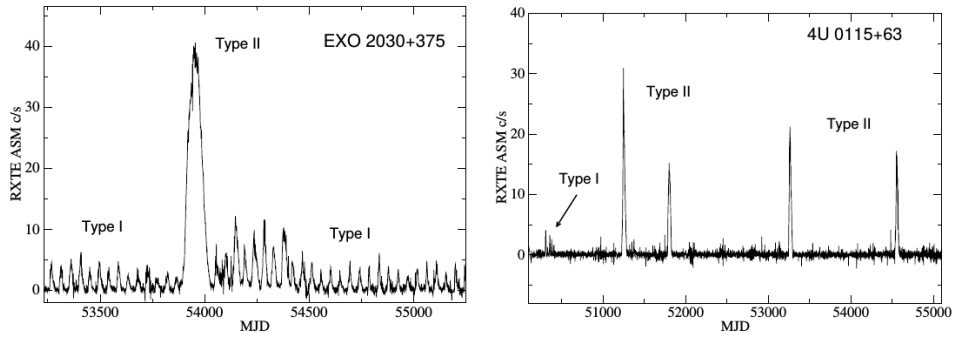

FIGURE 2.6: Typical light-curves of two transient BeXRBs, EXO 2030+375 on the left plot and 4U 0115+63 on the right, from "Be/X-ray binaries", Fig. 9. Both exhibit the two categories of outbursts.

2.3.6 Explanatory model

As described above, BeXRBs exhibit a number of interesting properties. Several attempts have been made to achieve a unifying explanation for their characteristics. To this day, many uncertainties remain, but the most widely accepted interpretation is the decretion or excretion disk model (Okazaki and Negueruela, 2001; Lee, Saio, and Osaki, 1991; Porter, 1999; Negueruela and Okazaki, 2001). Its key element is the presence of a circumstellar disk around the Be star which is formed episodically by matter outflows from the equatorial region around the star. Angular momentum is transferred from the star to the inner edge of the disk. When the velocity of the material becomes Keplerian, it is transported outwards by viscosity (similarly to

an accretion disk, but in the opposite direction).
Due to resonant and tidal interactions with the neutron star, the disk becomes truncated at a certain radius. For most Be X-ray binaries, the truncation occurs at a 4:1 resonant radius, where the orbital period of the matter in the disk is four times smaller than the binary orbital period. This resonant radius is smaller than that of the Lagrangian L1 point for observed parameters of BeXRBs (Okazaki and Negueruela, 2001). As a result, in only a few configurations matter can be transferred through the L1 point and cause regular outbursts, as is seen for most Be X-ray binaries.
Because of the truncation of disk, the circumstellar disk in a Be X-ray binary system should be smaller and denser than that of a single Be star. Regular outbursts can occur when the disk is large enough for enabling matter transfer, replenishing the accretion disk around the neutron star and causing a type I X-ray outburst every periastron passage.
Fig. 2.7 shows examples of orbital models derived for 6 known BeXRBs from the classification of their optical companions (and therefore from their masses) and from their orbital parameters (Okazaki and Negueruela, 2001). The models are centered on the Be star and clearly illustrate the difference in the Roche equipotential regions both at periastron and at apastron, as well as the trajectory of the Lagrangian L1 point. The Be disk can easily be pictured as extending up to the resonant radii. Only if the disk extends further, matter can be captured by the neutron star during the periastron passage and create a type I outburst.

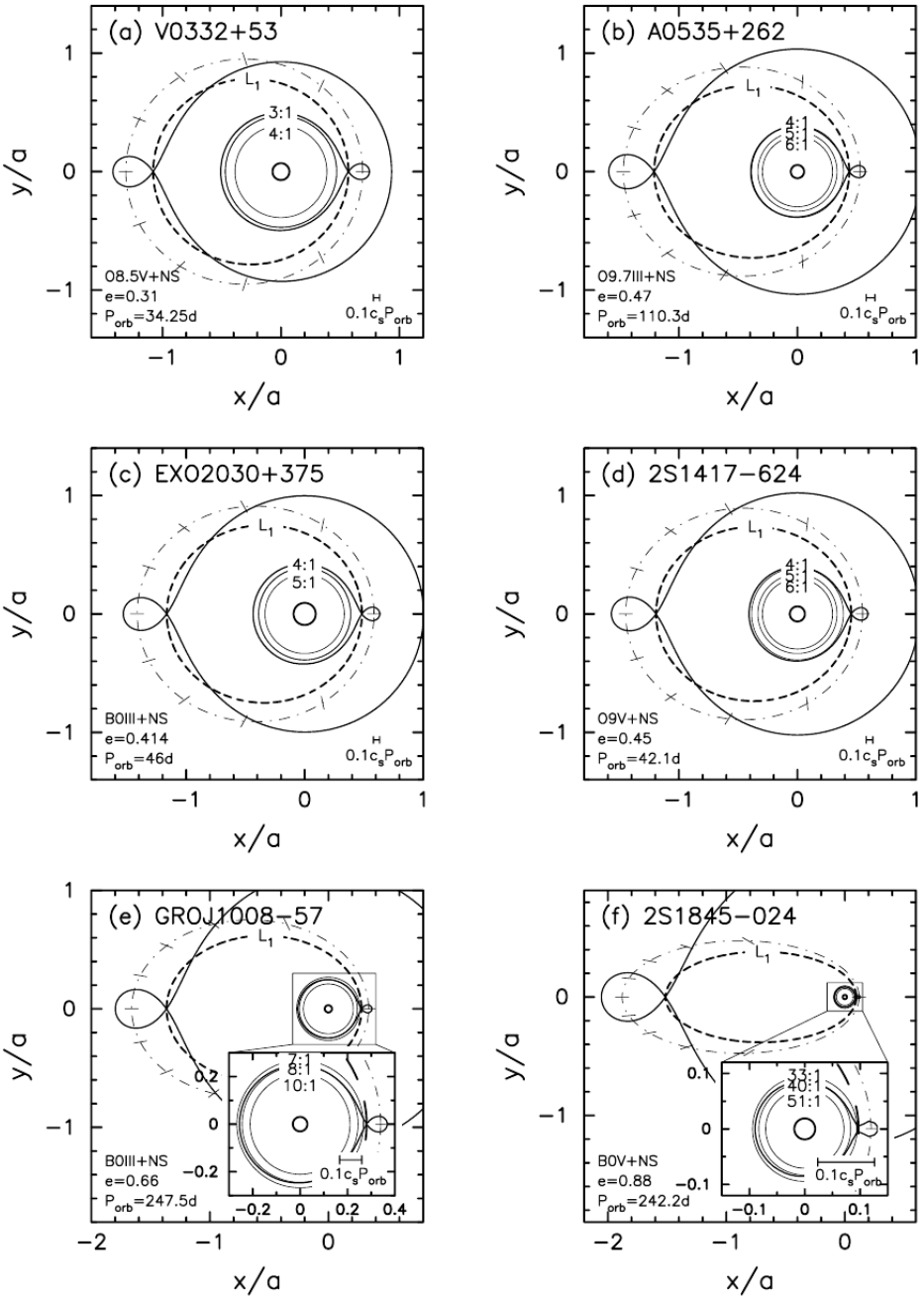

FIGURE 2.7: Orbital models derived for 6 well-known BeXRBs from Okazaki and Negueruela, (2001), Fig. 2. The models are centered on the Be star, which is represented by an open circle and surrounded by solid lines labeled with the resonance radii at which the truncation occurs for viscosities $\alpha = 0.3$, 0.1, and 0.03 (starting from the outside). The dash-dotted line represents the orbit of the neutron star and the solid lines indicate the critical Roche equipotentials lobes at both periastron and apastron, where the position of the neutron star is marked with a cross. The thick dashed line represents the position of the first Lagrangian point (L1) around the orbit. For each panel, at the lower-left corner, the parameters used for the model are shown and at the lower-right corner, the distance scale corresponding to 0.1cs $P_{\rm orb}$ is indicated.

The decretion disk model can explain the observed V/R variability by the presence of a one-armed density perturbation propagating through the disk, effectively warping its outer edges (Kato, 1983; Okazaki, 1996; Hummel and Hanuschik, 1997). The shape of the Hα line will be changed depending on the location of the high density part of the disk with respect to the observer and its moving direction. If the density perturbation is moving towards the observer, the blue part will be enhanced and similarly the red part will be enhanced when it moves away from the observer, resulting in the observed V/R variability.
However, many problems remain to be addressed by this model, such as the effect of the irradiation of the Be disk by the central star or an explanation of the mechanism leading to sufficiently high angular momentum transfer for the formation of such a disk.
Difficulties also arise when trying to explain the presence of type II outbursts, as they require a significantly higher matter transfer. This can be achieved in a configuration in which the disk is both highly inclined and warped in such a way that the outer edge of the Be disk reaches the orbit of the neutron star.
However, such a configuration would be highly unstable and result in a rapid disk loss or disruption after the giant outburst, a consequence which is not observed for all BeXRBs. Moreover, this explanation is contradicted by the duration of the type II outbursts, which can last several orbital periods and therefore require a steady matter flow.
Martin et al., (2014a) showed that the formation of giant outbursts can be best explained by the presence of a both highly eccentric and misaligned disk. A promising explanation for achieving such eccentricities is the presence of Kozai-Lidov oscillations in the circumstellar disk.

2.4 Kozai-Lidov Oscillations

2.4.1 Overview

Kozai-Lidov (KL) oscillations are an effect of orbital mechanics which is commonly observed in the Universe when three celestial bodies interact in a certain configuration. When a small body with negligible mass (for example a comet) orbits one of the celestial bodies of a binary system (for example the Sun and Jupiter) with an initially high inclination of the orbit with respect to the binary orbit, its orbit will be perturbed by the other binary member in such a way that periodical oscillations will appear.
This phenomenon was first described independently by Michael Lidov in 1961 and Yoshihide Kozai in 1962 (Kozai, 1962; Lidov, 1962). Yoshihide Kozai was studying the problem of the influence of Jupiter on asteroids around the Sun and found that Jupiter would induce a periodic exchange of the orbit inclination and eccentricity of the asteroid.
Michael Lidov, who was working on the orbit of artificial satellites around the Earth, realized that the same oscillations would be observed in the orbit of these satellites due to a perturbation produced by gravitational interactions with external bodies. Since then, KL oscillations have been observed in several configurations and shown to have a critical importance in the formation of planets and in explaining the origin of highly eccentric orbits of multiple star systems and extra-solar planets.

This phenomenon can be generalized as follows: Consider a test particle with a negligible mass and two celestial bodies (the primary with mass $M_{\rm a}$ and the perturber, with mass $M_{\rm b}$) orbiting each other. The configuration is such that the test particle orbit is significantly smaller than the perturber orbit.
If the test particle is initially in a circular orbit (eccentricity $e_{\rm p_0} = 0$) and the initial inclination of the orbit $i_{\rm p_0}$ with respect to the orbital plane of the binary is high, ($39^\circ \leq i_{\rm p_0} \leq 141^\circ$), periodic oscillations will appear. Following the conservation of the angular momentum component perpendicular to the the test particle orbit, the eccentricity $e_{\rm p}$ and the inclination $i_{\rm p}$ of the test particle orbit will be exchanged periodically. This can be expressed mathematically as

$$\cos i_{\rm p} \sqrt{1 - e_{\rm p}^2} \approx \text{const.} \tag{2.7}$$

The analytical period $\tau_{\rm KL}$ of the oscillations is

$$\tau_{\rm KL} \approx \frac{P_{\rm orb}^2}{P_{\rm p}} \frac{M_{\rm A} + M_{\rm B}}{M_{\rm B}} \left(1 - e_{\rm b}^2\right)^{\frac{3}{2}}, \tag{2.8}$$

with $P_{\rm orb}$ the orbital period of the binary, $P_{\rm p}$ the orbital period of the particle, and $e_{\rm b}$ the eccentricity of the binary orbit (e.g., Martin et al., 2014b).
Figure 2.8 shows a simulation of the evolution of the eccentricity and the inclination of a test particle orbit at an initial radius of $0.2a$, with a the orbital separation of the binary. The initial inclination is of $i_{\rm p_0} = 60^\circ$ and $M_{\rm A} = M_{\rm B}$. The exchange of the eccentricity and of the inclination can be clearly observed.

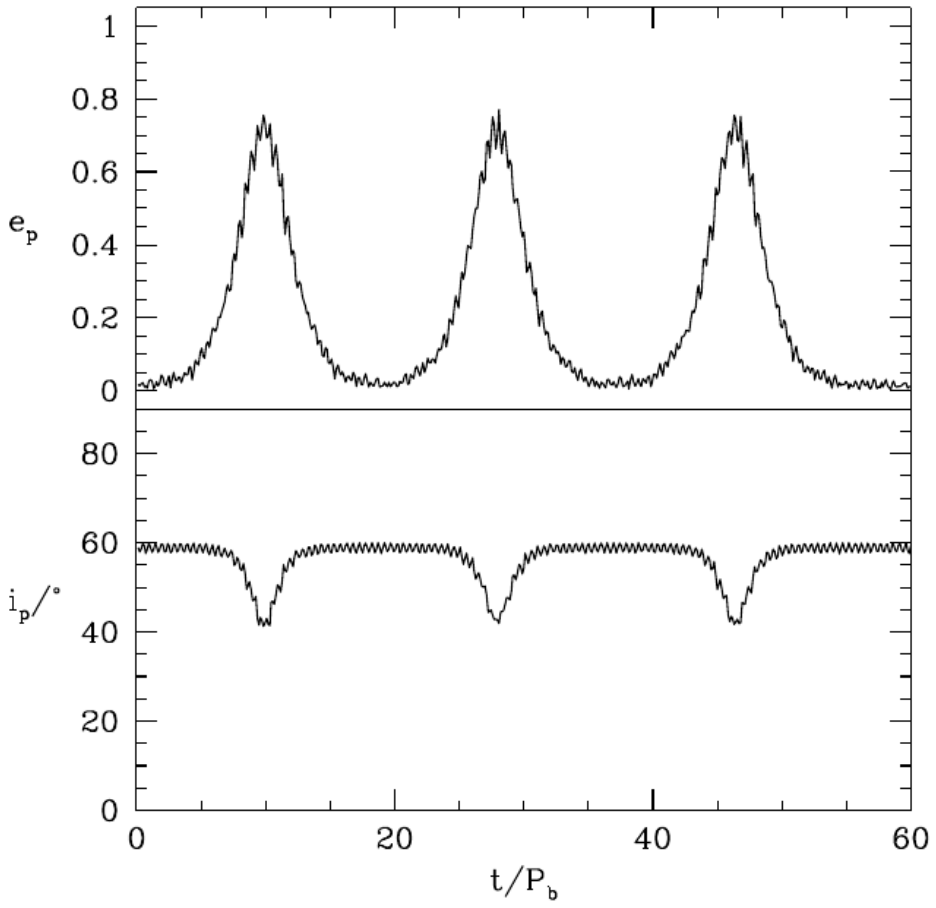

FIGURE 2.8: Simulation of the evolution of the eccentricity and of the inclination of a test particle (details see text) from Fig. 1 in Martin et al., (2014b)

2.4.2 KL oscillations in hydrodynamical disks

The effect of KL oscillations on accretion disks has been studied for the first time by Martin et al., (2014b) using 3D hydrodynamical simulations and further discussed in Fu, Lubow, and Martin, (2015a) and Fu, Lubow, and Martin, (2015b). The authors showed that in a binary system in which one of the stars is surrounded by a disk, KL oscillations can arise if the initial disk inclination is high enough. Contrary to the single particle scenario, the oscillations get damped with time, as pictured in Figure 2.9. The case of Be X-ray binaries was considered by the authors, who discussed the possibility that KL oscillations of the disk could give rise to type II outbursts. The increased eccentricity of the disk could enable the neutron star to pass through, or close enough to the disk to capture the enormous amount of matter expected for a type II outburst, even at a distance larger than the periastron (Martin et al., 2014a).

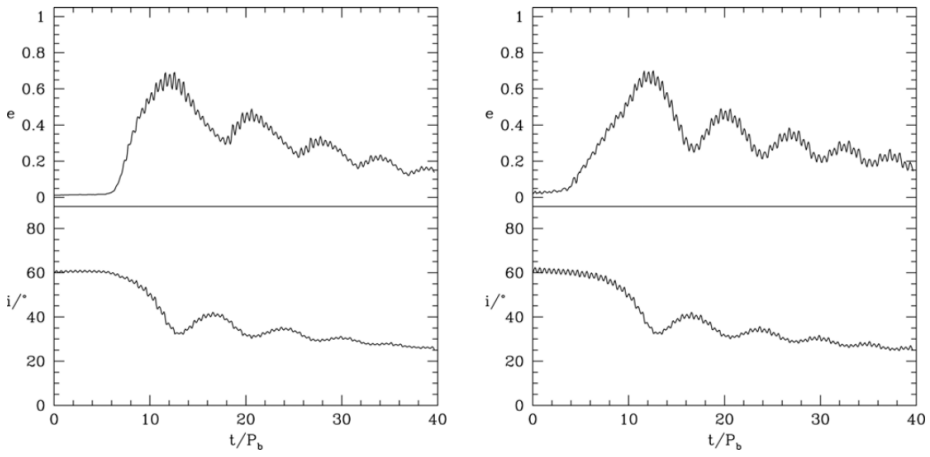

FIGURE 2.9: Simulation of the evolution of the eccentricity and of the inclination of a hydrodynamical disk (details see text) from Fig. 3 in Martin et al., (2014b)

The time-scale of a KL cycle for disks can be approximated by applying the rigid disks theory. In the case of a Be X-ray binary system with $M_{\rm Be}$ the mass of the Be star, $M_{\rm NS}$ the mass of the neutron star, with an orbital separation of a, and an orbital period $P_{\rm orb}$ the KL cycles time-scale can be estimated. The disk is described by a radius R, an inner disk radius $R_{\rm in}$, an outer disk radius of $R_{\rm out}$, and a surface density Σ. The global disk oscillation time-scale can be estimated as

$$< \tau_{\rm KL} > \approx \frac{\int_{R_{\rm in}}^{R_{\rm out}} \Sigma R^3 \sqrt{\frac{GM_{\rm Be}}{R^3}} dR}{\int_{R_{\rm in}}^{R_{\rm out}} \frac{\Sigma R^3}{\tau_{\rm KL}} \sqrt{\frac{GM_{\rm Be}}{R^3}} dR} \tag{2.9}$$

Assuming that the surface density follows a power law $\Sigma \propto R^{-p}$, the oscillation time-scale can be approximated by

$$\frac{\tau_{\rm KL}}{P_{\rm orb}} \approx \frac{(4-p)}{(\frac{5}{2}-p)} \left(\frac{a}{R_{\rm out}}\right)^{\frac{3}{2}} \sqrt{\frac{M_{\rm Be}}{M_{\rm NS}} \left(\frac{M_{\rm Be}}{M_{\rm NS}} + 1\right)}, \tag{2.10}$$

(Martin et al., 2014b). This equation does not take into account the inclination dependence of the oscillations. Fu, Lubow, and Martin, (2015a) studied the effect of changed inclination on the time-scale and found that it is valid up to a factor of 2. The timescale of Kozai-Lidov oscillations becomes longer, the start time slightly later, and the amplitude smaller with a decreasing inclination angle.

Chapter 3

EXO 2030+375

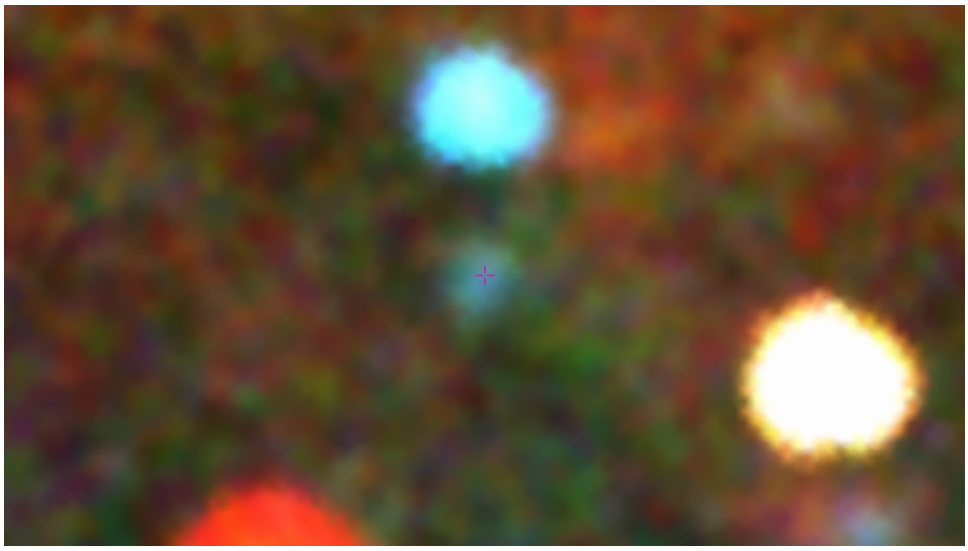

FIGURE 3.1: MAXI 4.5 yr integrated image of EXO 2030+375, indicated by a cross in the center of the image, which has a FOV of 22°. The proximity of two bright X-ray sources is seen, with Cyg X-3 at the top of the image and Cyg X-1 at the bottom right of the image. The upper part of an old supernova remnant, Cyg Loop, can be distinguished in the bottom left part of the image. The spectral difference between the sources' X-ray emission is clearly visible, since the color indicates the X-ray energy, with soft X-rays (2 – 4 keV) in red, medium X-rays (4 – 8 keV) in green and hard X-rays (8 – 16 keV) in blue. This image was generated using Aladin Lite[1](Boch and Fernique, 2014).

3.1 Overview

EXO 2030+375, discovered in 1987 May 17 during a giant outburst (Parmar et al., 1985), was one of the first accreting pulsars for which Quasi Periodic Oscillations (QPOs) were observed and the first source to show the correlation between the outburst luminosity and the spin period derivative predicted by the accretion theory (Parmar et al., 1989). The 42 s pulse period revealed that the source contains a magnetized neutron star. Soon after the discovery, optical and infrared observations discovered a counterpart with a B0 Ve spectral type and classified the system as a BeXRB (Coe et al., 1988). EXO 2030+375 is located within our galaxy and is visible in the galactic

[1] http://aladin.u-strasbg.fr/AladinLite/

plane in the Cygnus region. As showed in Figure 3.1, two much brighter X-ray sources are found close to it: Cyg X-1, one of the brightest sources in the X-ray sky and Cyg X-3, which are both classified as micro-quasars. The proximity of these sources may contaminate observations of EXO 2030+375 and care has to be taken when analyzing its X-ray data (see, e.g., Camero Arranz et al., 2005).
The orbital parameters of the source were found early on (Parmar et al., 1989; Stollberg et al., 1999) and determined more precisely later, with an orbital period of $P_{\rm orb} = 46.021$ d and an eccentricity of $e = 0.4190$ (Wilson, Finger, and Camero-Arranz, 2008).
The relatively short orbital period and the very regular activity of this source makes it one of the best studied systems of its kind. Continuous monitoring from several generations of X-ray instruments have enabled the observation of over 200 type I and of 2 type II outbursts. In addition, the source was part of an optical/infrared monitoring program of BeXRBs, the Southampton-Valencia campaign, which enabled regular observations with the Isaac Newton Telescope and the William Herschel Telescope, both located at the Roque de Los Muchachos observatory in La Palma (Spain) and from the 5 m Hale telescope at Palomar mountain in California (U.S.A.) (Reig et al., 1998).

3.2 X-ray light-curve

After the discovery of the giant outburst in 1987, EXO 2030+375 was observed only a few more times in the following years. The monitoring of the source started in 1991 April with the launch of the Compton Gamma Ray Observatory (CGRO) and its X-ray instrument, the Burst And Transient Source Experiment (BATSE), and continued with the Rossi X-ray Timing Explorer (RXTE) and its All Sky Monitor (ASM) instrument, launched end of December 1995. Both missions provided a continuous monitoring of the source until their operations ended in 2000 June and 2012 January, respectively.
A continuous monitoring of the source was achieved with the start of three more X-ray monitors still active today: the Burst Alert Telescope on-board the Swift satellite (launched end of 2004); the Monitor of All-sky X-ray Image (MAXI) on the International Space Station (ISS), launched in 2009 August; the Gamma-ray Burst Monitor (GBM) on-board the Fermi satellite, launched in 2008 June.
Moreover, other X-ray and Gamma-ray instruments have carried out pointed observations of the source, providing more detailed information on the spectral properties and the short-term timing behavior of EXO 2030+375.

3.2.1 Type I outbursts

Overview

Since the discovery of the source 30 years ago, EXO 2030+375 displayed very regular type I outburst with a typical peak luminosity of about $L_{1-20\,\rm keV} \sim 1.5 \times 10^{37}$ erg s^{-1} (assuming a distance of 7.1 kpc, Wilson, Fabregat, and Coburn, (2005)). This remarkable regularity enabled a precise

determination of the orbital parameters of the source (Wilson et al., 2002). When BATSE started monitoring the source in 1992, the X-ray flux was fading. In fact, it was even reported that the source had become quiescent (Reig et al., 1998). A more detailed follow-up analysis showed that while the outburst had indeed started to become fainter, only some of them were completely missing (Wilson et al., 2002).
The average flux started increasing again and a type I outburst could be observed for each periastron passage until the second giant outburst occurred in 2006 May. The type I outbursts after the giant outburst were unusually bright and it was suggested that they are part of a different category of outbursts (Wilson, Finger, and Camero-Arranz, 2008).

Precursors

Despite being very regular, the type I outbursts can have complex shapes (Kuehnel et al., 2015). As first discussed by Camero Arranz et al., (2005), who analyzed INTEGRAL, BATSE and RXTE/PCA data, an initial spike before the main peak was observed for several outbursts.
The authors reported similar observations with different instruments and a few cases in which a possible second spike after the main peak was observed. In addition, the time interval between the precursor and the main peak was found to have a constant value of 4 days, as shown in Fig. 3.2.

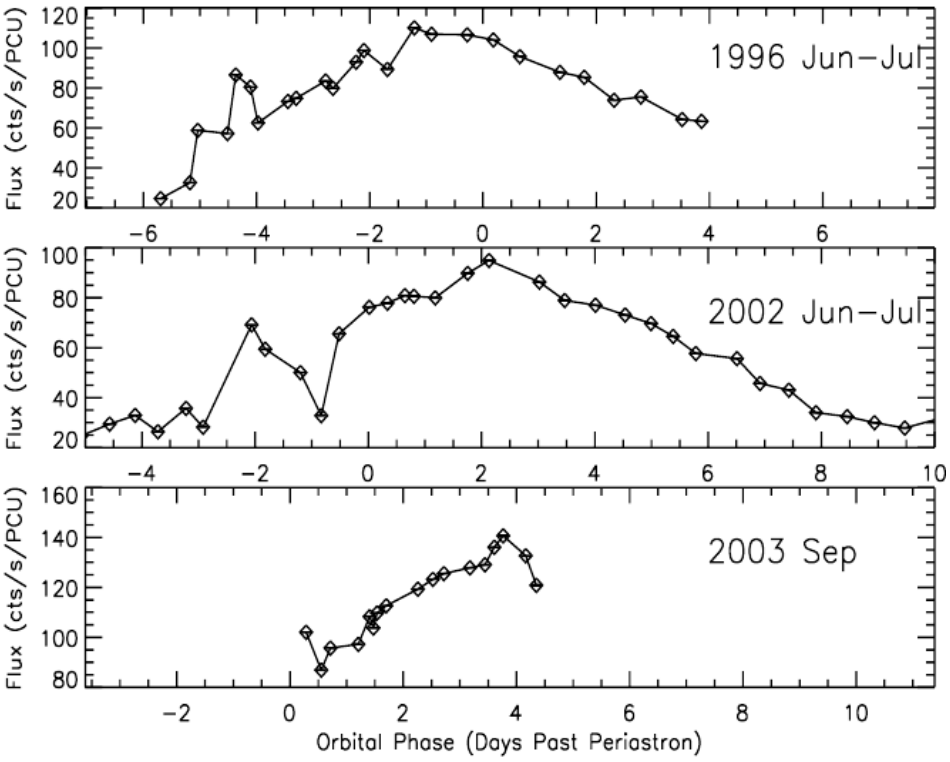

FIGURE 3.2: Orbital phase resolved light-curves of three outbursts observed with RXTE/PCA from Camero Arranz et al., (2005). A precursor is clearly seen in the two upper panels.

The shape of the outburst was interpreted as resulting from a passage of the neutron star through the outer envelop of the disk and accretion of material at periastron for the initial spike and the main outburst peak, respectively.
In this work, I investigate the shape of the outbursts and the presence of a precursor for all observed outbursts using RXTE/ASM, Swift/BAT and MAXI data.

Orbital phase shift

EXO 2030+375 was the second BeXRB system to display an orbital phase shift (OPS). Monitoring the orbital phase of the type I outbursts peak using a simple Gaussian model and precisely determined orbital parameters, Wilson et al., (2002) found that there was a major shift of the outburst peak in 1995, around MJD 50000. The outburst peak shifted from an almost constant value of 5 days *after* periastron to about 5 days *before* periastron. Interestingly, the same phenomenon was observed around the second giant outburst in 2006, with the same amplitude, but in the opposite direction (Wilson, Finger, and Camero-Arranz, 2008). The peaks of the normal outbursts just before the giant outburst shifted gradually, until they reached ∼13 days after periastron Baykal et al., (see 2008) and Wilson, Finger, and Camero-Arranz, (2008) as is shown in Fig. 3.3.

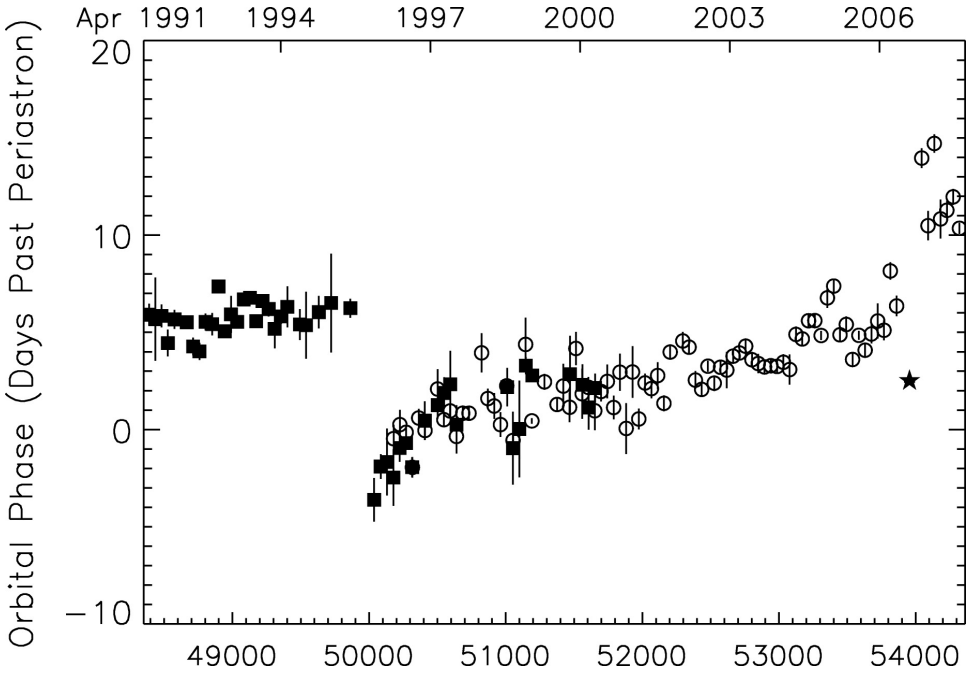

FIGURE 3.3: Evolution of the peak phase of the type I outbursts from Wilson, Finger, and Camero-Arranz, (2008), Fig. 10. The star indicates the peak time of the giant outburst 2006.

Based on phenomenological similarities, I predicted the observation of an OPS in December 2016 (Laplace et al., 2017). In 2016 July, as I reported in Laplace et al., (2016), an OPS was observed. In this thesis, I present the

indications which have led to make this prediction and discuss the implications of the observation of a new OPS for the understanding of the physical processes in place.

3.2.2 Giant outbursts

Overview

Two giant outbursts have been observed in EXO 2030+375. The first, during which the source was discovered (Parmar et al., 1985; Parmar et al., 1989), reached a luminosity of $L_{1-20\,\mathrm{keV}} \sim 2 \times 10^{38}$ erg s^{-1} (assuming a distance of 7.1 kpc, (Wilson, Fabregat, and Coburn, 2005)), as reported in Klochkov et al., (2007). Unfortunately, because it was only shortly after the outburst peak, it is not possible to determine how long this outburst lasted. The discovery light-curve is shown in Fig. 3.4.

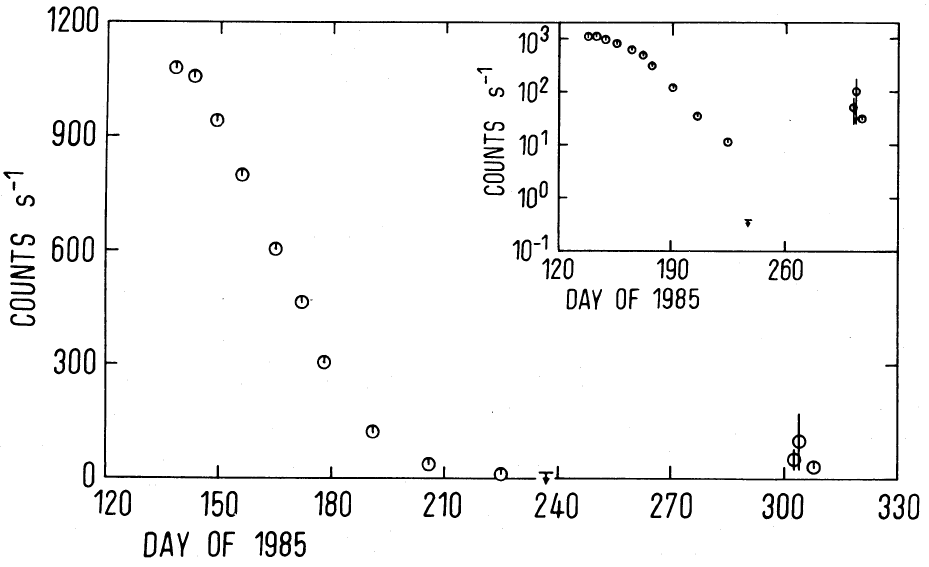

FIGURE 3.4: Light-curve of the discovery giant outburst of EXO 2030+375 as observed by EXOSAT/ME from Parmar et al., (1989), Fig. 1. The insert shows the same light-curve with a logarithmic scale.

The second giant outburst, which occurred in 2006 May-September (Corbet and Levine, 2006; Krimm et al., 2006; McCollough et al., 2006), was observed as a Target Of Opportunity by INTEGRAL and Swift and studied extensively. Klochkov et al., (2007) reported that the outburst reached a lower luminosity than the first with $L_{1-20\,\mathrm{keV}} \sim 1.2 \times 10^{38}$ erg s^{-1}. The outburst lasted for 3 orbital periods and its shape was asymmetric. Baykal et al., (2008) modeled it with a double Gaussian.

$\dot{P} \propto L$ relation

EXO 2030+375 is the first source to have shown the correlation between luminosity and spin period derivative expected from accretion theory (Parmar et al., 1989; Ghosh and Lamb, 1979). During the first giant outburst, a dramatic spin up of the source was observed with a characteristic time-scale

of $-P/\dot{P} \simeq 30$ yr. The spin-up rate was found to be strongly luminosity dependent with $-\dot{P} \propto L^{1.08-1.35}$.
The second giant outburst was also marked by a dramatic spin up, but with a slightly longer time-scale $-P/\dot{P} \simeq 40$ yr than that of the first giant outburst (Klochkov et al., 2007). Just as for the first giant outburst, a correlation between the luminosity and the spin up rate was reported. Using simple accretion theory and assuming typical values for the neutron star parameters, the magnetic field strength of the neutron star can be estimated as $B \simeq 1 - 4 \times 10^{12}$ G (Klochkov et al., 2007).

3.2.3 QPOs

EXO 2030+375 was one of the first accreting X-ray pulsars to exhibit Quasi Periodic Oscillations (QPOs) (Parmar et al., 1989). EXOSAT observations a few months after the first giant outburst in 1985 revealed a series of 6 X-ray flares recurring quasi-periodically every 3.96h.
Decades later, INTEGRAL observed QPOs during the rising phase of a normal outburst in 2010 November – December (Klochkov et al., 2011). The flares were very similar in global shape (fast rise followed by slow decay) and relative amplitude to the QPOs in 1985 but had a somewhat longer recurrence period of ∼7h.
These observations suggest that normal outbursts in EXO 2030+375 are indeed triggered by accretion of matter from an accretion disk around the neutron star, as the presence of instabilities at the inner edge of the accretion disk are the most likely cause of QPOs for this source (Klochkov et al., 2011).

3.3 Spin frequency

3.3.1 Spin frequency evolution

The spin frequency of EXO 2030+375 has changed dramatically since the first observations of the source. As explained above, during both giant outbursts, the strong spin up of the spin frequency was correlated with the luminosity. An overview of the spin frequency evolution of the source as reported in the literature is shown in Figure 3.5.

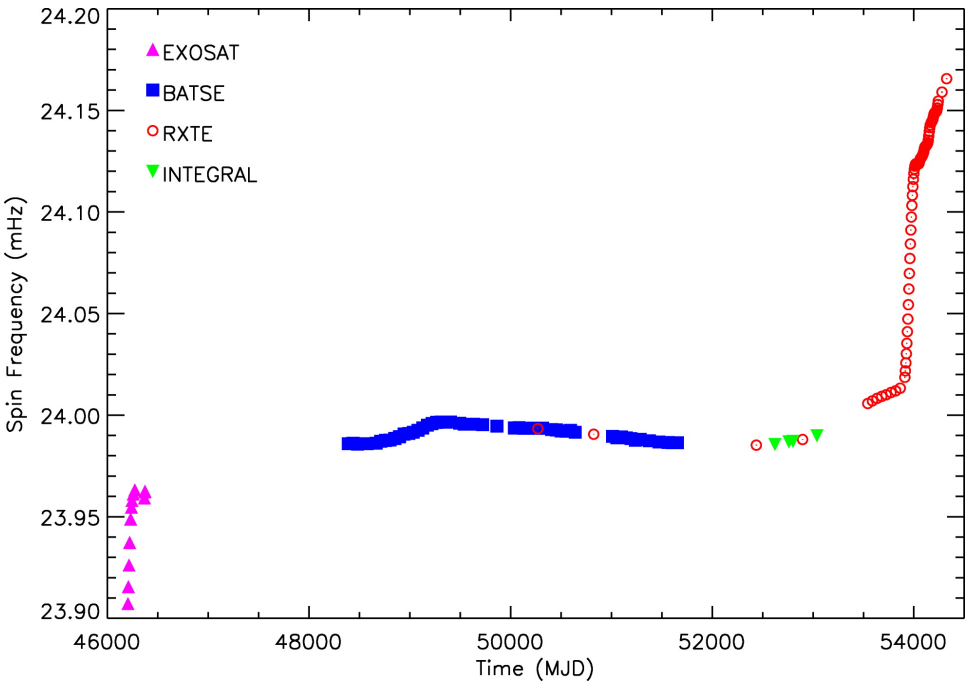

FIGURE 3.5: Spin frequency evolution of EXO 2030+375 from Wilson, Finger, and Camero-Arranz, (2008), Fig. 9.

After the first giant outburst, the spin frequency continued to increase more slowly until 1995, when it reached a plateau and then started to spin down slowly for about 6 yr, after which it started to slowly spin up again (Wilson, Finger, and Camero-Arranz, 2008). During the second giant outburst in 2006, the spin frequency increased dramatically again and then changed to a slower global spin up trend.

3.3.2 Pulse profile

The pulse profile of EXO 2030+375 has been very well studied with several instruments, starting with EXOSAT (Parmar, White, and Stella, 1989). The quality of the measurements and the many years of monitoring of the source have enabled a detailed study of the dependency on other parameters, such as the luminosity, along with precise measurements of the spin period.

The pulse profile of EXO 2030+375 is complex and was found to strongly depend on the luminosity (Parmar, White, and Stella, 1989). At low luminosities, the profile consists of a smooth asymmetric pulse and a smaller pulse separated by 180°. When the luminosity increases, the profile becomes increasingly complex with multiple peaks. At high luminosities, the pulse which was smaller for low luminosities becomes dominant and the main pulse becomes smaller.

While pulse profiles determined using BATSE data found double peaked profiles and no significant luminosity dependence (Stollberg et al., 1999), studies with RXTE/PCA (Reig and Coe, 1998) confirmed the findings from EXOSAT. During the giant outburst in 2006, the pulse profile was studied for energies above ∼20 keV (Klochkov et al., 2007), confirming the luminosity dependence. In addition, Klochkov et al., (2008) showed a strong link between the spectral parameters and the pulse profile. Based on this work,

Sasaki et al., (2010) reconstructed the neutron star emission and geometry and found that it could be best explained by a configuration in which one of the magnetic poles of the neutron star is closer to the line-of-sight and in which both poles become invisible to the observer for a short time during the neutron star orbit.
After the 2006 giant outburst, the pulse profile during a normal outburst in 2007 May was studied using Suzaku data (Naik et al., 2013). The authors reported a significant energy dependence and the presence of narrow dips in the complex shaped pulse profile at low energies (2 – 70 keV). The pulse profile at higher energies (40 – 600 keV) revealed the asymmetric profile reported in previous studies. Monitoring the pulse dependency of the spectral parameters using a partial covering model, the authors found that the only parameter significantly changing during the presence of the dips was the ionization parameter. This finding was interpreted as an indication for the presence of phase locked matter streams around the neutron star.
Another normal outburst in 2012 May with lower luminosity was analyzed using Suzaku data and the pulse profile was found to be very different from the previous outburst. While the pulse profile at low energies (0.5 – 10 keV) and at high energies (55 – 70 keV) displayed a single asymmetric peak, the profile at intermediate energies (12 – 55 keV) changed to a broad double-peaked profile. The strong dependence on spectral parameters confirmed the findings from Klochkov et al., (2008).
Using XMM Newton, the pulse profile during the rise of an outburst in 2014 May was analyzed (Ferrigno et al., 2016). The authors discovered a narrow dip-like feature with a width of about 100th of the spin period, as shown in Fig. 3.6.

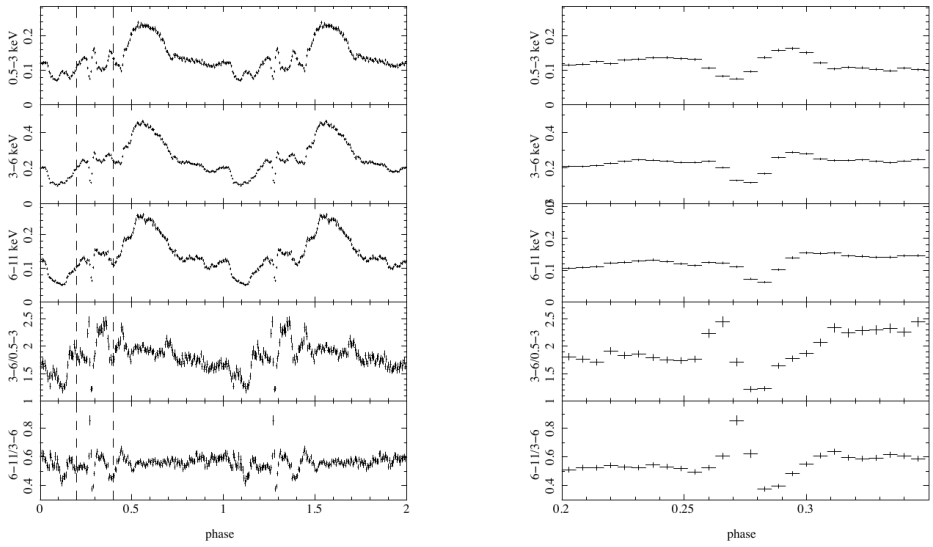

FIGURE 3.6: Pulse profiles and hardness ratio of EXO 2030+375 calculated from XMM Newton/EPIC-pn data, from Fig. 1 and 2. in Ferrigno et al., (2016). The right-hand side figure is a zoom of the narrow dip-like feature at a pulse phase of ∼0.27 in the left figure.

A pulse-dependent spectral analysis of this observation and of the two Suzaku observations in 2007 and 2012 described above was carried out. The

parameters were found to vary significantly and the authors interpreted this feature as due to the passage of the accretion stream through the line of sight of the observer. EXO 2030+375 is the only high-mass X-ray pulsar so far to show such a feature in its pulse profile.

3.4 X-ray spectrum

3.4.1 Overview

The X-ray spectrum of EXO 2030+375 was first determined during the discovery giant outburst with EXOSAT in the 2 – 25 keV enery range as being that of a typical accreting pulsar, mainly described by an absorbed power-law with a high-energy cutoff and an iron line at ∼6.5 keV (Parmar et al., 1989; Reynolds, Parmar, and White, 1993). A significant change of the spectrum was observed as the outburst decayed, with the luminosity decreasing by a factor 100, the cutoff energy decreasing from 20 to 10 keV and the spectrum becoming harder with a photon index changing from 1.8 to 1.3.
The first spectrum of a normal outburst was determined using RXTE observations in 1996 July (Reig and Coe, 1999). While the hard part of the spectrum was described by a cutoff powerlaw, the lower energy part of the spectrum up to ∼10 keV was modeled with a black-body component with a temperature of kT ∼ 1.2 keV and an emission radius of ∼1 km. Both the temperature of the black-body component and the width of the iron line showed weak correlations with the luminosity. The high energy part of the spectrum (17 – 65 keV) was studied for the first time and found to be consistent with previous findings. An absorption feature in the spectrum was modeled with a cyclotron line at 36 keV.
A broadband spectrum of the source (3 – 300 keV) was obtained for the first time using INTEGRAL observations of a type I outburst in 2002 December (Camero Arranz et al., 2005). The spectrum was described by a black-body component with kT ∼8 keV at low energies and by a power-law with a photon index of 2 at high energies.
During the giant outburst which started in 2006 May, a broadband spectrum (3 – 120 keV) was obtained with INTEGRAL (Klochkov et al., 2007). It was modeled by an absorbed power-law with a photon index of 1.93, a cutoff energy of 26 keV and an iron line a 6 – 7 keV. The authors reported the presence of features between 10 and 20 keV which could be modeled by either two absorption lines at ∼10 and ∼20 keV (tentatively interpreted as cyclotron lines) or by a broad emission line or "bump" around 14 keV.
A spectrum of the same outburst, but using combined RXTE/PCA and HXTE data, showed the same features as in the INTEGRAL spectrum (Wilson, Finger, and Camero-Arranz, 2008). The authors claimed the existence of a cyclotron resonant scattering feature at around 10 keV. The spectral parameters were somewhat different from the best fit to INTEGRAL data, with a photon index of 1.7 and a cutoff energy of 20 keV.
After the giant outburst, the broadband (1 – 200 keV) Suzaku spectrum of a normal outburst which occurred in 2007 May was analyzed (Naik et al., 2013). In addition to the iron line, its very high spectral resolution enabled the clear detection of five S and Si lines. The authors used a partial covering high energy cutoff model with either a neutral or partially ionized absorber and parameters consistent with previous models with a photon index of

∼1.3 and a cutoff energy of at 12 keV. The obtained spectrum is shown in Fig. 3.7.

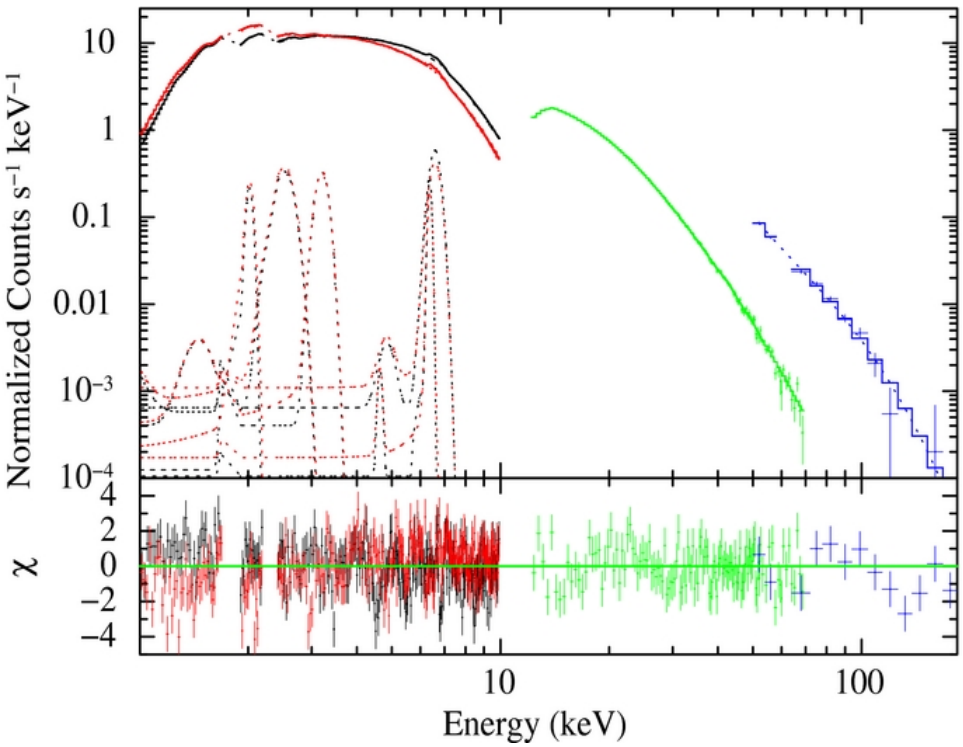

FIGURE 3.7: Suzaku spectrum of EXO 2030+375 combining data from the XIS, PIN and GSO detectors, from Naik et al., (2013), Fig.6. Spectral emission lines of S ans Si elements are clearly seen and the model is fitted with a partial covering high energy cutoff model with a partially ionized absorber.

The partially ionized absorber model resulted in a better fit and as explained above, its increase in the proximity of the dips in the pulse profile led to the interpretation of the presence of several accretion streams phase-locked with the neutron star. No evidence for the previously reported cyclotron lines was found.
Another Suzaku spectrum of a normal outburst was studied in 2012 May, which had a much lower luminosity than in the previous study (Naik and Jaisawal, 2015). Unlike for the previously studied outburst, no S or Si lines were detected and only a weak iron line was found at 6.4 keV. The 1 – 100 keV spectrum was modeled equally well with three continuum models: a partial covering high energy cut-off power-law model, (ii) a partially absorbed power-law with high-energy exponential rolloff and (iii) a partial covering Negative and Positive power law with EXponential model. No absorption feature was found in the spectrum, further contradicting the previous claims.
XMM-Newton data of the rise of an outburst in 2014 May was modeled using a phenomenological Comptonization continuum and a combination of homogeneous and inhomogeneous absorbers (Ferrigno et al., 2016). Comparisons were carried out with the two Suzaku observations described above.
In this work, I present the first systematic analysis of MAXI spectra (2 – 20 keV) of this source during the last 7 years and study the spectral variations.

3.5 Optical/IR observations

3.5.1 Hα line and IR history

In 1993 June/July, measurements of the infra-red flux and of the Hα line were taken during a single type I outburst observed by BATSE (Norton et al., 1994). No significant change of the infra-red flux or of the equivalent width of the Hα line were detected during the outburst. The authors concluded that the measurements were not precise enough to understand the accretion mechanism in place during type I outbursts and that less than 1% of the X-ray emission was reprocessed in the infra-red and optical wavelength.
As mentioned before (see section 3.1), EXO 2030+375 was part of a large monitoring campaign of BeXRBs and as such, has been observed several times in the infrared and optical wavelengths. The evolution of the Hα line and of the infra-red flux in the JHK bands could thus be determined (Reig et al., 1998). The authors found a significant decrease of the optical and infrared flux which was correlated with a drop in X-ray flux around 1995. They interpreted this trend as the begin of a disc-loss phase of the Be star. Subsequent observations revealed that the optical, infrared and X-ray flux was increasing again, indicating that the density of the Be disk was increasing (Wilson et al., 2002). The evolution of the infrared flux can be seen in Fig. 3.8.

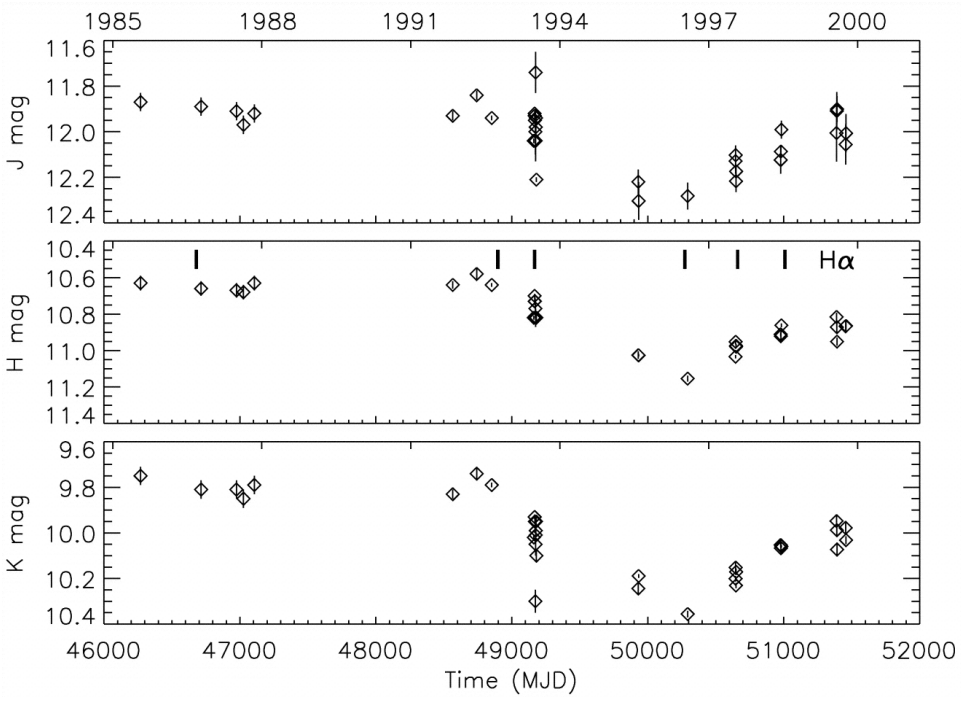

FIGURE 3.8: Evolution of the infrared flux in the JHK band around MJD 50000 from Wilson et al., (2002) Fig. 10. The measurements of the Hα line are indicated by bars in the second panel.

In addition, the Hα line profiles changed as well, as shown in Fig. 3.9, evolving from a single peak just before the OPS in 1995 to a complex multi-peaked shape afterwards, indicating that this event was linked to dramatic

changes in the Be disk.

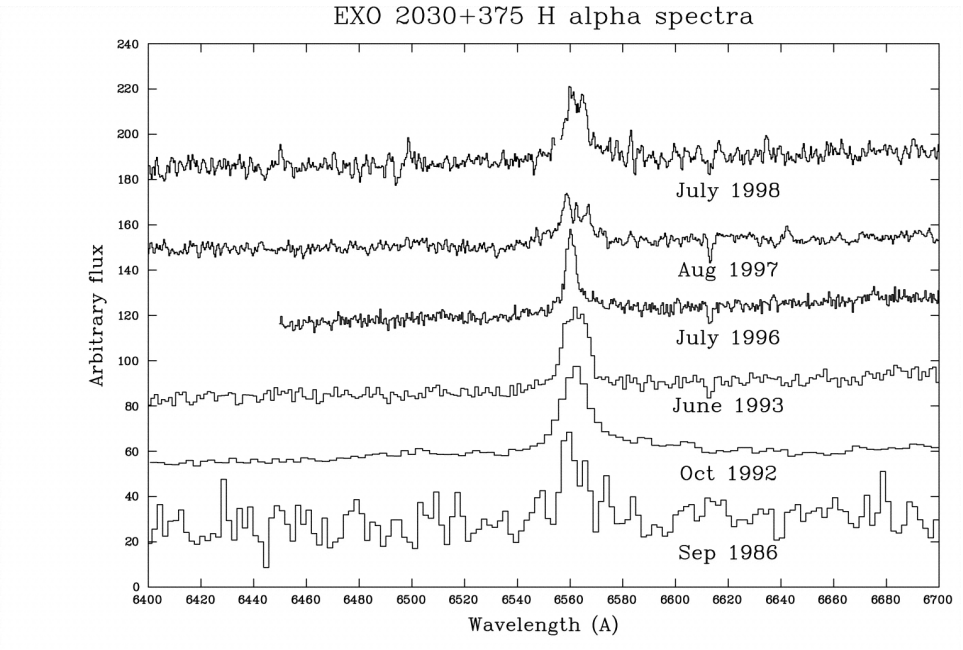

FIGURE 3.9: Evolution of the the Hα emission line around MJD 50000 from Wilson et al., (2002) Fig. 11.

During the giant outburst in 2006, optical data were obtained with ROTSEIIId, the Robotic Optical Transient Experiment located in Bakırlıtepe, Antalya (Turkey) (Baykal et al., 2008). The optical flux decreased slightly before the type II outburst but remained unchanged during and after the giant outburst. Three measurements of the Hα line were made after the giant outburst. All observations displayed a single-peaked shape and a constant equivalent width which was significantly larger than the measurements reported in 1995.
For this work, I made use of a privately communicated measurement of the Hα line reported by Iain Steele. The measurement took place on 2014 December 7 and shows a single-peaked profile with an equivalent width of 11 ± 2 Å. This value is similar to the measurements before the OPS in 1995.

3.5.2 IR polarization

A significant infra-red polarization was found during the observation of the type I outbursts of EXO 2030+375 in 1993 June/July (Norton et al., 1994). However, the study could not determine whether the polarization was intrinsic to the source or due to the polarization of the interstellar medium.

3.5.3 Optical polarization

In 2014, optical polarization studies of EXO 2030+375 measured the highest linear polarization (19%) ever detected for a classical Be or Be X-ray binary system (Reig et al., 2014). The authors argued that such a high polarization cannot be accounted for by the interstellar medium and that a significant fraction must be intrinsic to the source.
The high polarization was interpreted as originating from the alignment of

non-spherical ferromagnetic grains in the Be disk due to the high neutron star magnetic field. The relatively short orbital period of the system ensures that the alignment is not lost and effectively produces a high optical linear polarization. This model predicts an increased polarization during type I outbursts in BeXRBs.

3.6 Recent changes

In the 7 yr since the giant outburst, a type I outburst could be observed in EXO 2030+375 during each periastron passage. However, starting around 2012 July, the X-ray flux of the source started to decrease. Some outburst were even not detected by the observing X-ray monitors, while others could still be observed. Simultaneously, the long-term spin-up of the source slowed down and reached a plateau, as detected in Fermi/GBM observations (Fuerst et al., 2016).
All these changes for this otherwise very predictable source were intriguing. To understand the origin of these changes and their link to previous observations of the source, I investigated the long-term spectral and timing changes of EXO 2030+375. In this thesis, I report on the results of this research.

Chapter 4

Spectral studies of EXO 2030+375 with MAXI

4.1 Introduction

The X-ray spectral properties of EXO 2030+375 have been studied extensively in the past (see section 3.4). The spectrum of the source during type I outbursts is usually modeled by an absorbed cut-off power-law model with a photon index of $\gamma \sim 1.2 - 2$, typical for accreting pulsars, and a cutoff energy around 15 keV at higher energies. The first studies of type I outbursts in this source have included a black-body component describing the soft part of the spectrum (see, e.g., Reig and Coe, 1999; Camero Arranz et al., 2005), while the most recent studies based on Suzaku observations included a partial absorber component (Naik et al., 2013; Naik and Jaisawal, 2015).
In this thesis, I study the X-ray spectral properties of the source by studying for the first time MAXI spectra of EXO 2030+375 observed during the last seven years. As mentioned in section 3.6, the global behavior of EXO 2030+375 has changed dramatically in recent years, with a drop of the X-ray flux, missing X-ray outbursts and a transition from a global spin up to a constant spin frequency (Fuerst et al., 2016). Here, I investigate whether or not these changes in the global behavior are visible in the MAXI spectra and their evolution. This may help to determine the physical origin of these changes.
In addition, I present the first orbital phase resolved and the first phase-averaged spectral analysis of EXO 2030+375. Since MAXI is designed to nearly continuously monitor X-ray sources, it is particularly well suited for studies of their long-term evolution. For example, MAXI has been successfully used to study the orbital spectral changes of several X-ray binaries, such as Vela X-1 (Malacaria et al., 2016) or 4U 1538 - 52 (Rodes-Roca et al., 2015).

4.2 Observations and methods

4.2.1 MAXI

The Monitor of All-sky X-ray Image (MAXI) is a Japanese instrument onboard the International Space Station (ISS) that has been continuously monitoring X-ray sources since the beginning of its operations in 2009 August (Matsuoka et al., 2009). It is the first astronomical instrument on the ISS

and consists of two instruments: the Gas Slit Camera (GSC) and the Solid-state Slit Camera (SSC). The GSC consists of 12 cameras and a proportional counter filled with Xenon and has a time resolution of 0.1 ms. It has a large detection area of 5350 cm^2 and covers the energy range 2 – 30 keV (Mihara et al., 2011).

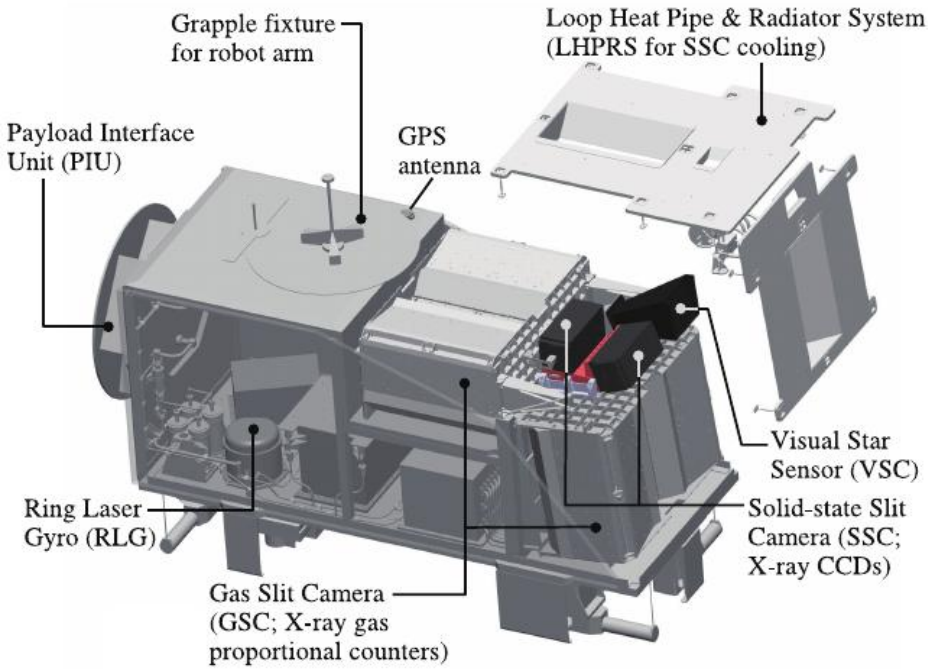

FIGURE 4.1: Schematics of the composition of MAXI, from Matsuoka et al., (2009), Fig. 1. The two science instruments GSC and SSC can be clearly distinguished.

The secondary instrument, SSC, operates in the 0.7 – 7 keV energy range (Tomida et al., 2011). It consists of 32 chips of X-ray Charge-Coupled Devices (CCDs), has a time resolution of 5.8 s, and a smaller field of view of 200 cm^2 with a sensitivity of 5 mCrab/week.
Every 92 minutes, the ISS completes an orbit around the Earth, which enables MAXI to observe the entire X-ray sky, except regions in the direction of the Sun. As a result, the MAXI data are useful to study the long-term variations of X-ray sources.

FIGURE 4.2: Exterior view of MAXI mounted on the Japanese module of the ISS with the Earth in the background, from Rainey, (2014), Credits:NASA.

4.2.2 Methods

I extracted spectra from a 1.6 circular degree region around the source, with an annular background region using the MAXI on-demand processing[1]. Only data with a minimum flux of 0.05 GSC ph/s/cm^2 were selected to maximize the spectral sensitivity.
For this analysis, I used the X-ray spectral analysis software XSPEC version 12.9.1 (Arnaud, 1996). To achieve an efficient analysis while studying the evolution of the spectra, I used PyXspec version 2.0, which is part of the XSPEC package with the open source programming language Python version 2.7.2.
To ensure the use of χ^2 statistics, all spectral channels were grouped to have at least 30 counts per bin using GRPPHA, which is part of the NASA FTOOLS (Blackburn, 1995).
The orbital solution from Wilson, Finger, and Camero-Arranz, (2008) for the orbital phase resolved analysis.

4.3 Spectral properties

4.3.1 Long-term spectral evolution of the type I outbursts

I investigated the spectral evolution of EXO 2030+375 by selecting all the outbursts observed with MAXI during the last 6.5 years. To avoid background contamination issues, I only selected outbursts with a flux above 0.05 MAXI/GSC ph/s/cm^2 and retrieved them using the Good Time Intervals (GTI) feature of the MAXI on-demand process. The MAXI light-curve with the selected outbursts marked in red can be found in Figure A.1 in the appendix A.

[1] http://maxi.riken.jp/mxondem

Average spectrum

The average MAXI spectrum was obtained by combining SSC (0.7 – 7 keV) and GSC (2 – 20 keV) data of the selected outbursts. To ensure consistency with previous studies, I fitted the spectrum with a phenomenological absorbed power-law model with high energy cutoff. The model is described by

$$M(E) = Ke^{N_{\rm H}\sigma(E)}E^{-\gamma}\begin{cases} e^{\frac{E_{\rm cut}-E}{E_{\rm fold}}} & \text{if } E \geq E_{\rm cut} \\ 1 & \text{if } E \leq E_{\rm cut} \end{cases}, \tag{4.1}$$

with K the normalization in units of photon keV^{-1} cm^{-2} s^{-1}, the $N_{\rm H}$ the equivalent hydrogen column density in units of 10^{22} cm^{-2}, $\sigma(E)$ the photo-electric absorption cross section, γ the photon index, $E_{\rm cut}$ the cutoff energy in keV and $E_{\rm fold}$ the folding energy in keV.
Because of known calibration issues with the 1 – 2 keV energy range of SSC (Tomida et al., 2011) and the low statistics at energies smaller than 1 keV, I only considered the 2 – 20 keV energy range. In the spectral model I included a first absorption component to take into account the contribution of the Galactic interstellar medium along the line of sight to the source. I obtained a value of $N_{\rm H1} = 9.5 \times 10^{21}$ cm^{-2} using the HEASARC tool nH column density[2] for EXO 2030+375. In this way a second absorption component $N_{\rm H2}$ takes into account the "intrinsic" absorption, i.e. the X-ray extinction caused by the material close to the X-ray emitting region. The best fit model is shown in Fig. 4.3 and the corresponding best fit parameters are summarized in table 4.1.

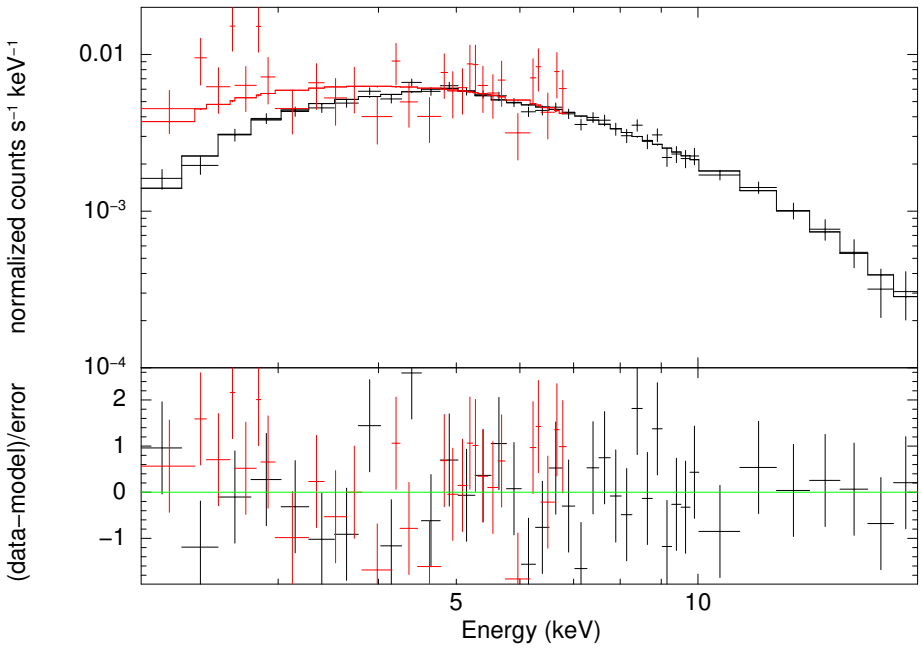

FIGURE 4.3: Average MAXI 2 – 20 keV spectrum during the type I outbursts of EXO 2030+375. The two instruments GSC and SSC are represented in black and red colors, respectively. The top panel shows the data modeled with an absorbed powerlaw with high-energy cut-off. The residuals are shown in the bottom panel.

[2] https://heasarc.gsfc.nasa.gov/cgi-bin/Tools/w3nh/w3nh.pl

TABLE 4.1: Fit parameters for the average MAXI outburst spectrum. The unabsorbed flux is indicated in units of 10^{-10}erg s^{-1} cm^{-2}.

Parameter	Fit
$N_{\rm H1}$ $(\times 10^{22}{\rm cm}^{-2})$	0.95
$N_{\rm H2}$ $(\times 10^{22}{\rm cm}^{-2})$	$0.87^{+1.2}_{-0.87}$
Photon index	$0.9^{+0.3}_{-0.5}$
Norm $(\times 10^{-2})$	2.67 ± 0.02
$E_{\rm cut}$ [keV]	$6.7^{+1.2}_{-1.7}$
$E_{\rm fold}$ [keV]	$7.5^{+2.0}_{-1.5}$
$F_{\rm SSC}$	1.03 ± 0.11
Flux (2 – 20 keV)	$5.9^{+0.3}_{-0.2}$
Flux (2 – 7 keV)	2.6 ± 0.3
χ^2/d.o.f.	65.9/61

This result is consistent with previous studies (see Reig and Coe, 1999).

Outburst evolution

The MAXI spectra of each outburst suffer from poor statistics, in particular at low energy. Data from MAXI/SSC was also too sparse to improve the fit for all outbursts. As a consequence, the absorption coefficient could not be constrained. In addition, the absorption parameters and the photon index are typically strongly coupled by the fitting process, especially if the spectrum is affected by low statistics. Therefore, to estimate the photon index, I fitted the spectra by using only events with energy $E \geq 5.3$ keV. At this energy the spectral modulation produced by the absorption column density is negligible and hence does not influence the photon index. To estimate the other parameters, I thus reduced the energy range at low energies until the absorption would not change the determination of the photon index. However, with this method, the coupling of the photon index and the cut-off and folding energy could not be neglected. Consequently, the long-term evolution of the parameters could not be determined.

4.3.2 Orbital phase resolved spectroscopy

Hardness ratio

To investigate whether or not a spectral variation is observed along the orbit of EXO 2030+375, I analyzed the background-subtracted light-curve of EXO 2030+375 in three different energy bands: 2 – 4 keV, 4 – 10 keV and 10 – 20 keV. I then studied the hardness ratio of the source, which is given by the ratio of light-curves with different energy bands. Using this method is a common solution for investigating the spectral variability of sources which are either faint or whose spectra have insufficient statistics.
In Fig. 4.4, I show the 6.5 yr MAXI light-curve folded with the orbital period (42 d) and binned with an orbital phase of 0.015. In the 4 – 10 keV band, the highest flux is detected, whereas the two other energy bands have a very similar lower flux. The main peak of the folded light-curve has the same asymmetric shape in all energy bands, with a small dip at the orbital

phase 0.1. The small excess seen in all energy bands around a phase of 0.9 is most likely due to the precursor already observed in several outbursts (see Chapter 5) at this phase. Interestingly, a smaller peak is observed at apastron, around 0.6 – 0.7 orbital phase, especially in the hard band (10 – 20 keV).

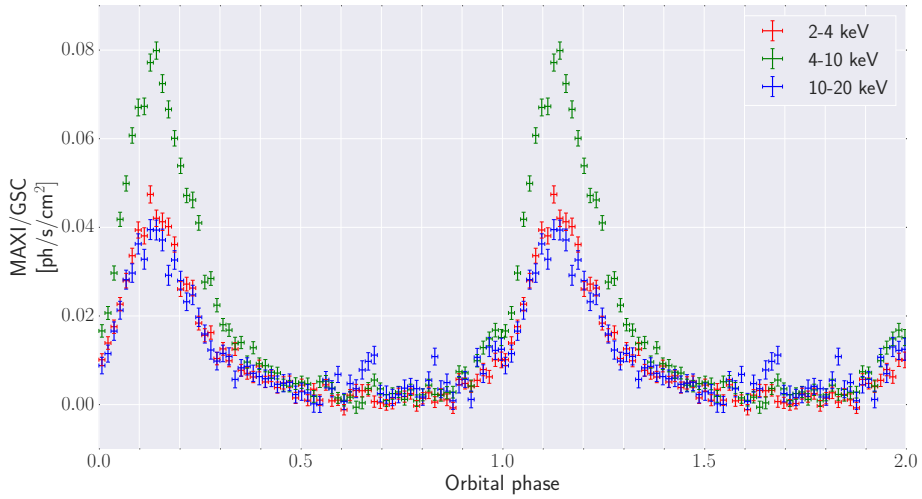

FIGURE 4.4: Orbital phase resolved MAXI/GSC light-curve of EXO 2030+375.

I construct the hardness ratio H between all energy bands, which is defined as

$$H = \frac{F_{\text{hard}}}{F_{\text{soft}}} \tag{4.2}$$

with F_{hard} and F_{hard} the flux in the harder and the softer energy band, respectively. Fig. 4.5 shows the light-curve and all the hardness ratios folded with the orbital period. I note that negative flux values, especially at an orbital phase of ~ 0.7, are due to a substantial overestimation of the background at lower fluxes. To take into account additional systematic errors, I adapted the bin size and estimated a systematic error of 3% by computing the histogram of the flux in each energy band.

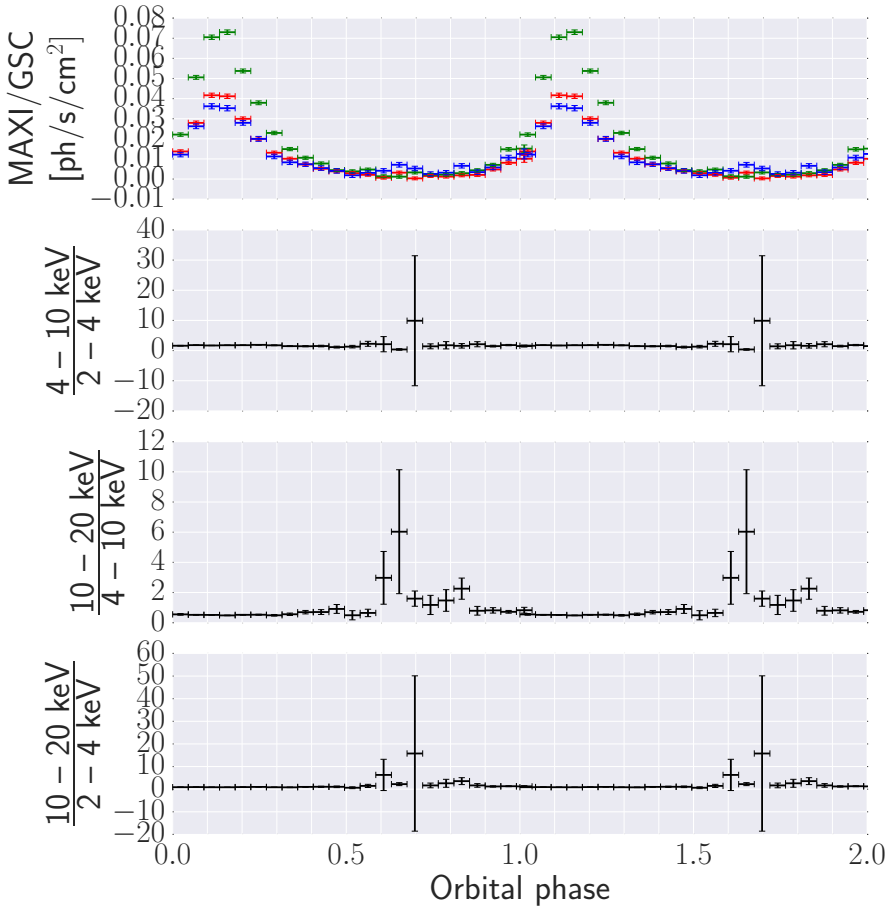

FIGURE 4.5: From top to bottom: orbital phase resolved light-curve binned with 0.045 orbital phase and hardness ratios of the energy bands 2 – 4, 4 – 10 and 10 – 20 keV, colored in red, green, and blue, respectively. A systematic error of 3% was included.

Around the periastron, where the flux is higher and the folded light-curve shows a peak, the hardness ratios are constant. This indicates that the source does not show a significant spectral variability during outbursts. In contrast, variations can be observed between orbital phases of 0.5 and 1, i.e. around apastron. While no significant spectral changes are observed between the soft (2 – 4 keV) and the medium (4 – 10 keV) energy bands, there are indications for spectral variability between the hard energy band (10 – 20 keV) and the softer energy bands, especially at an orbital phase of around 0.85.

Spectral analysis

A phase-averaged spectrum was generated using the MAXI on-demand process (see section 4.3.1). However, it was found to be highly background-contaminated due to its location, even at high energies, and could therefore not be used as a reference for the evolution of the spectral parameters during the outburst.
Instead, I compared the evolution of the spectral parameters with respect to

the peak spectrum, obtained by combining data in the orbital phase range 0.1 – 0.2. To compare the MAXI orbital resolved spectra, I defined the following five phase ranges with a high signal to noise ratio: 0 – 0.1, 0.2 – 0.3, 0.3 – 0.4, 0.4 – 0.8, 0.9 – 1 and extracted the spectra using the MAXI on-demand process.

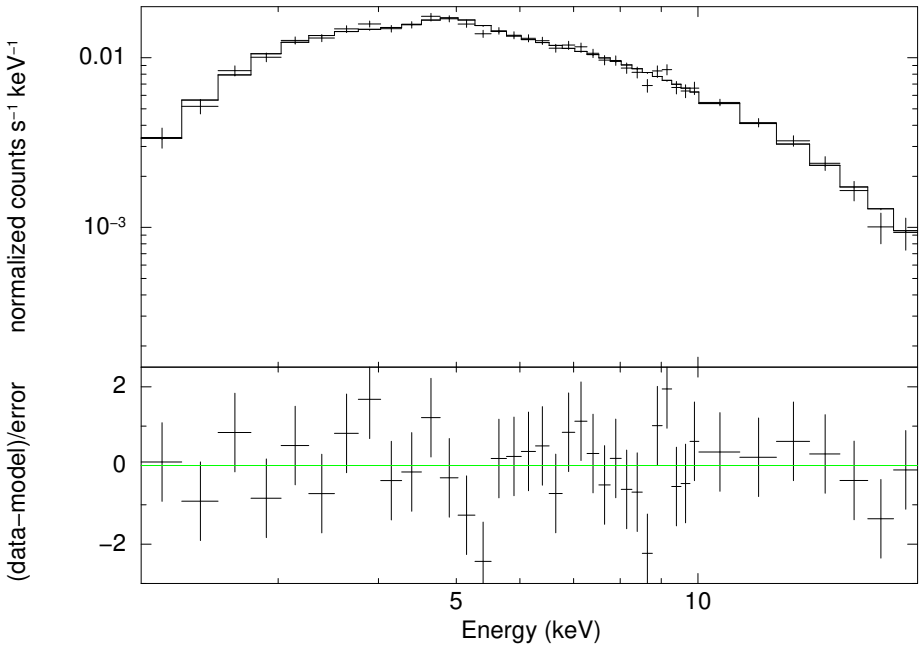

FIGURE 4.6: MAXI 2 – 20 keV orbital phase resolved spectrum at the peak phase (0.1 – 0.2) of the folded light-curve. The top panel shows the data with an absorbed power-law with high-energy cut-off. The residuals are shown in the bottom panel.

The peak spectrum was fit with the same model as the average outburst model, that is, an absorbed power-law with high energy cutoff. In this case, the equivalent hydrogen column density could be constrained. The best fit spectrum is shown in Fig. 4.6. The best-fit parameters are summarized in Table 4.2 and are consistent with the results obtained for the average spectrum (see Table 4.1).

TABLE 4.2: Fit parameters for the orbital phase resolved MAXI spectrum at the peak phase (0.1 – 0.2). The unabsorbed flux is indicated in units of 10^{-9}erg s^{-1} cm^{-2}.

Parameter	Fit
$N_{\rm H}$ $(\times 10^{22}{\rm cm}^{-2})$	$2.32^{+0.73}_{-0.69}$
Photon index	1.02 ± 0.16
Norm $(\times 10^{-2})$	$9.59^{+0.03}_{-0.02}$
$E_{\rm cut}$ [keV]	$7.6^{+1.2}_{-0.8}$
$E_{\rm fold}$ [keV]	$9.7^{+2.2}_{-1.6}$
Flux (2 – 20 keV)	1.87 ± 0.07
χ^2/d.o.f.	33.24/34

As a first step, I compared the spectra at different orbital phases by building the ratio of the best fit peak model and the data (see Fig. A.2 in the Appendix A).
From these comparisons, it is clear that the orbital variations of the spectral parameters cannot be well constrained, even though there are indications for spectral changes at the phases 0.3 – 0.4 and 0.9 – 1.

4.3.3 Flux resolved analysis along the orbit

To further study the spectral variability in EXO 2030+375 I performed flux resolved spectroscopy. I selected three flux intervals from the MAXI 2 – 20 keV light-curve with a similar observation time, and, in the case of the low flux, a similar signal to noise ratio, namely the low flux range (0.05 – 0.1 GSC ph s^{-1} cm^{-2}), the medium flux range (0.1 – 0.17 GSC ph s^{-1} cm^{-2}) and the high flux range (0.17 – 0.35 GSC ph s^{-1} cm^{-2}). These ranges, from lower to higher flux, correspond to the apastron passage of the neutron star, the beginning and end phases of the outburst, and to the outburst peak, respectively. To avoid background contamination, the lower flux range was set to start from an arbitrary value of 0.05 MAXI/GSC ph s^{-1} cm^{-2}.
For a consistent comparison, I determined the best fit model for the highest flux interval using the same phenomenological absorbed power-law with high-energy cutoff model. The obtained best fit model is shown in Fig. 4.7, the unfolded spectrum in Fig. 4.8, and the corresponding parameters in Tables 4.3. These parameters are consistent with the previously determined values for the average spectrum and for the orbital phase resolved spectrum at the peak of the outburst (see Table 4.1 and 4.2). Therefore, this result supports the approach of using flux resolved spectroscopy to probe the orbital changes of the source.
As a first probe of the existence of a spectral variability, I calculated the ratio between the best model obtained for the highest flux range and the other ranges. These results are shown in Fig. 4.9.

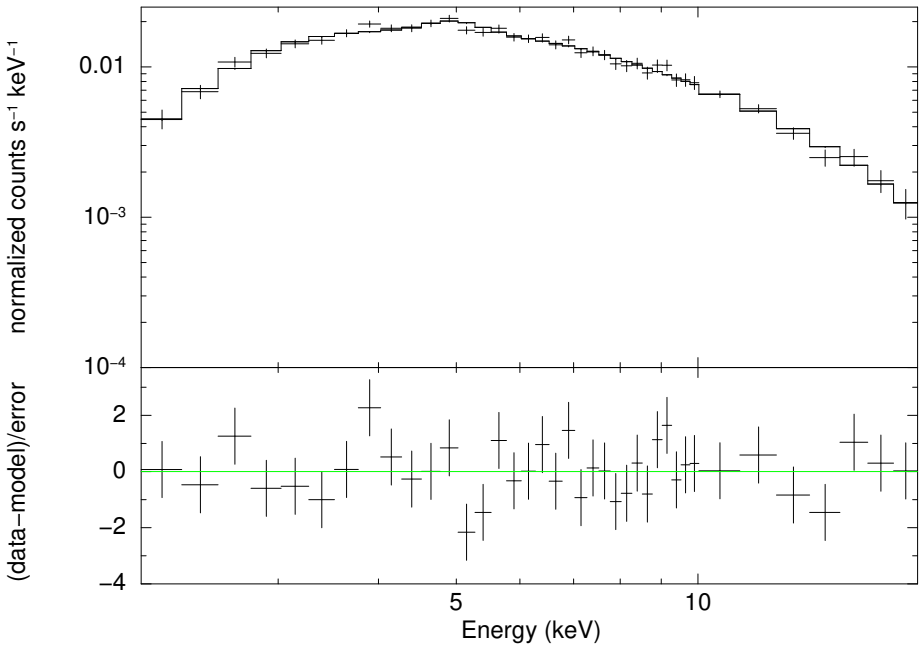

FIGURE 4.7: MAXI 2 – 20 keV flux resolved spectrum in the highest flux range (0.17 – 0.35 GSC ph s^{-1} cm^{-2}). The top panel shows the data fitted with an absorbed powerlaw model with high-energy cut-off. The residuals are shown in the bottom panel.

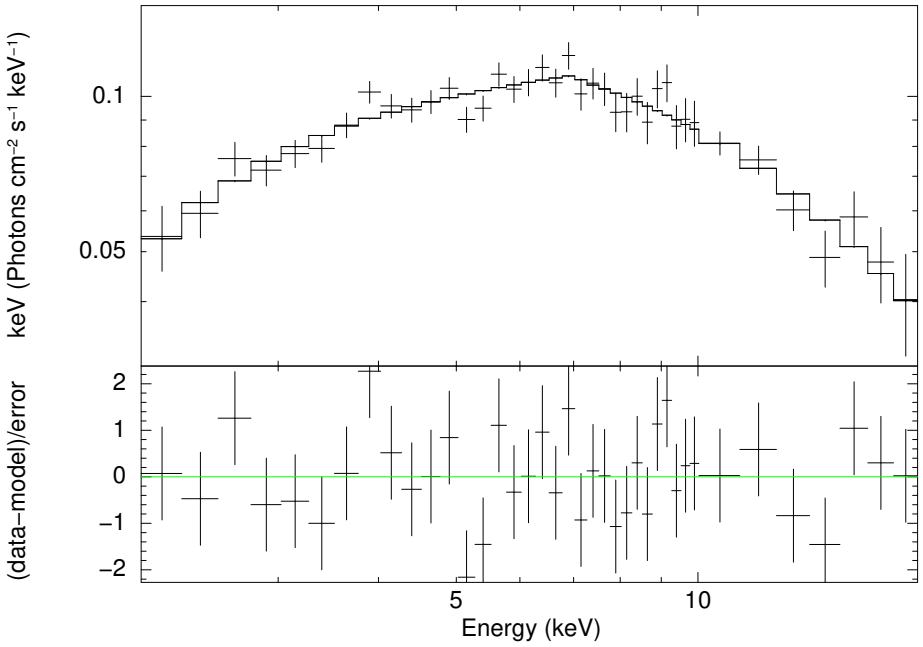

FIGURE 4.8: MAXI 2 – 20 keV unfolded flux resolved spectrum in the highest flux range (0.17 – 0.35 GSC ph s^{-1} cm^{-2}). The top panel shows the data fitted with an absorbed powerlaw model with high-energy cut-off. The bottom panel contains a plot of the residuals.

TABLE 4.3: Fit parameters for the orbital phase resolved MAXI spectrum at the peak phase (0.1 – 0.2). The unabsorbed flux is indicated in units of 10^{-9}erg s^{-1} cm^{-2}.

Parameter	Fit
$N_{\rm H}$ $(\times 10^{22}{\rm cm}^{-2})$	1.5 ± 0.9
Photon index	0.8 ± 0.2
Norm $(\times 10^{-2})$	$7.95^{+0.04}_{-0.03}$
$E_{\rm cut}$ [keV]	$7.1^{+1.3}_{-0.8}$
$E_{\rm fold}$ [keV]	$11.7^{+2.5}_{-1.6}$
Flux (2 – 20 keV)	2.2 ± 0.1
χ^2/d.o.f.	32.87/34

From these figures, it is clear that there is indeed a spectral variation between the low and the two higher flux ranges, while there is no clear difference between the two higher flux ranges.
As a quantitative approach, I fitted the spectra with the same model described above. Unfortunately, insufficient statistics prevent us to constrain the parameters of the model for the lower energy range. Indeed, as can be distinguished in Fig. 4.9 (a), the effect of the interstellar absorption is not observed in this flux range.

4.4 Conclusion

The last 6.5 years of MAXI spectra of EXO 2030+375 were analyzed for the first time. I constructed the average spectrum and fitted it with a phenomenological absorbed power-law with high-energy cutoff model. These results are consistent with previous results reported for type I outbursts of the source (Reig and Coe, 1999; Camero Arranz et al., 2005; Naik et al., 2013). Due to low statistics, my systematic study of X-ray outbursts during the last 6.5 years could not constrain the model parameters.
Studying the orbital phase resolved MAXI light-curve and computing the hardness ratios, I found no spectral variability during the main peak of the folded light-curve. However, I observe indications for spectral variations between the end and the rise of the main peak. I find an interesting second peak at apastron, during which spectral variability is observed. Such a peak was reported before in a study based on RXTE data (Reig et al., 1998).
A comparison of MAXI spectra of 5 orbital phase ranges and the peak phase points to a weak luminosity-dependence of the photon index, which appears to become harder during the main peak. This supports previous indications of such a dependence (Reig and Coe, 1999). In addition, the study of the flux resolved spectra confirms the indications of spectral variations between low and high fluxes.
Unfortunately, this study was highly limited by insufficient statistics and further investigations are needed to better understand the spectral variations of EXO 2030+375.

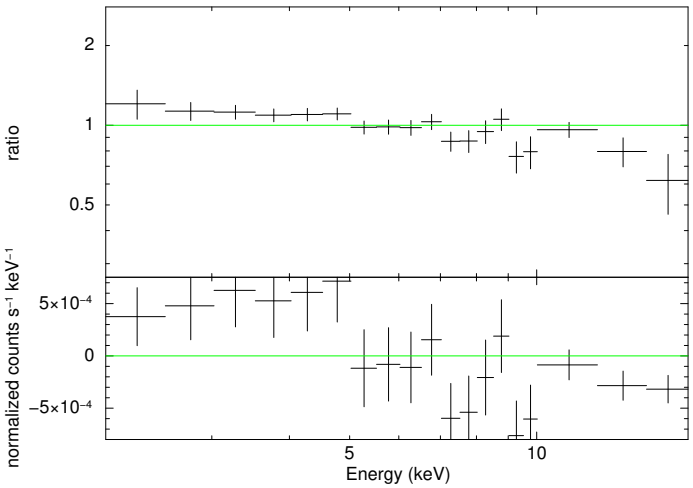

(a) Low flux range

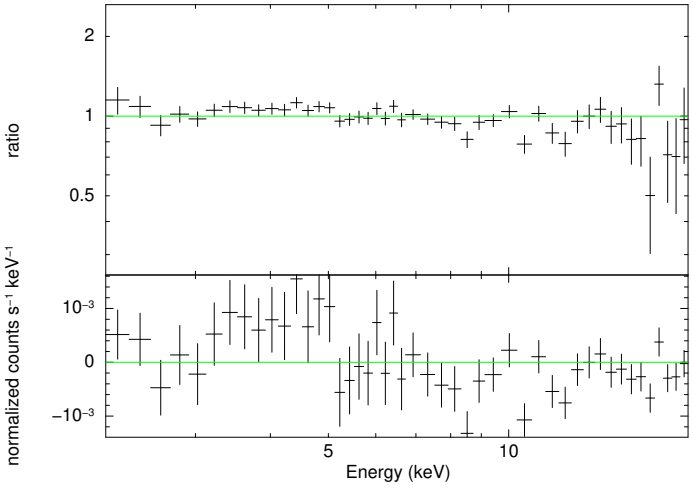

(b) Medium flux range

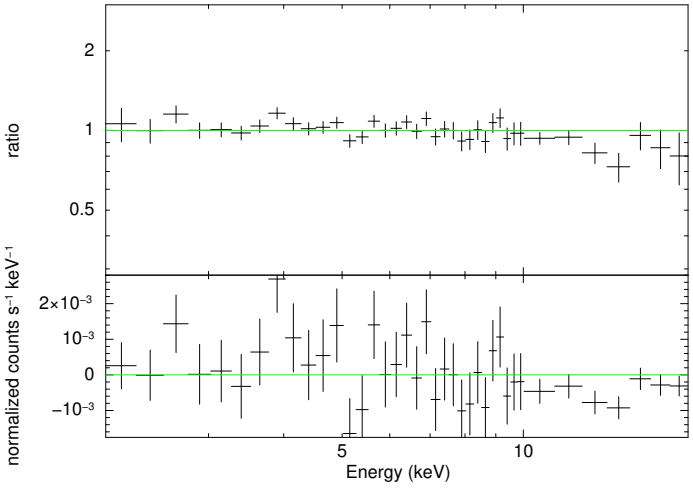

(c) High flux range

FIGURE 4.9: Ratio of the MAXI/GSC spectra obtained for different flux ranges and the best fit model of the highest flux range. Residuals are shown in the lower panels.

Chapter 5

Timing studies of EXO 2030+375

5.1 Overview

In this chapter, I present a study of the behavior of EXO 2030+375 in the last 30 years since its discovery, focusing especially on its X-ray light-curve. In particular, I examine the relationship between the recent changes displayed by the source, with a drop in flux, missing outbursts and a transition from a steadily increasing frequency to a constant spin frequency and similar changes ~ 21 yrs earlier. The analysis of the observed long-term phenomenology and arguments about the physical phenomena responsible for these observations led to the formulation of predictions concerning the next events displayed by the source. The observation of either an OPS (see section 3.2.1) or a giant outburst around December 2016 is predicted. This work has been published in a refereed journal (Laplace et al., 2017).
I present the observation of an orbital phase shift in July 2016 (Laplace et al., 2016).

5.2 Instruments

A number of monitoring instruments are used for this study, for which the data are publicly available online.

5.2.1 Archival data

EXOSAT/ME

The European X-ray Observatory Satellite (EXOSAT), after which EXO 2030+375 is named, was the first X-ray mission of the European Space Agency (ESA) (Korte et al., 1981). It was launched in 1983 May and was operative until 1986 May.
Among the most important achievements of EXOSAT, there is the discovery of QPOs in accreting X-ray pulsars, of which EXO 2030+375 was the first example (Parmar et al., 1985), and in LMXBs, as well as the measurement of iron lines in both galactic and extra-galactic sources (Santangelo and Madonia, 2014).

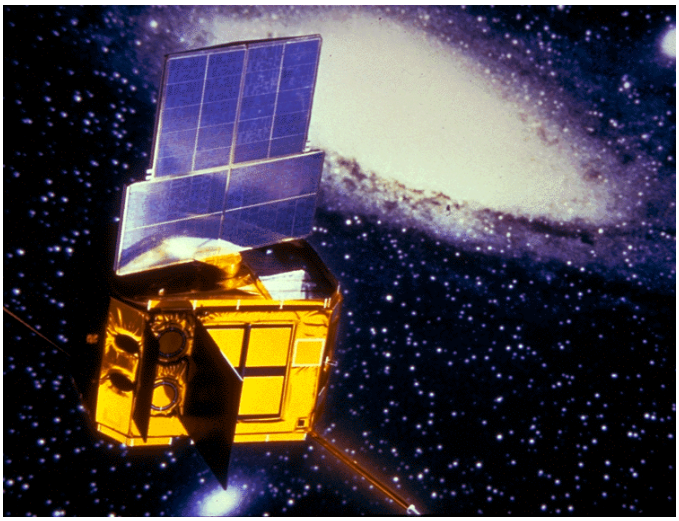

FIGURE 5.1: Artist's impression of EXOSAT from *EXOSAT > EXOSAT Home Page*

In this study, I make use of the data from the Medium Energy (ME) proportional counter, which was operating in the 1-50 keV range and had a field of view (FOV) of 45 arcmin and spanned an area of 1600cm^2 (Turner, Smith, and Zimmermann, 1981). I used data reported in the literature for this study (Parmar et al., 1989; Parmar, White, and Stella, 1989; Reynolds, Parmar, and White, 1993).

RXTE/ASM

The Rossi X-ray Timing Explorer was launched in December 1995 and was operative until January 2012. This long-lasting mission enabled a long-term view of the X-ray sky and led to many discoveries, such as establishing the existence of magnetars, observing the first millisecond accreting X-ray pulsar, the frame-dragging effect in the vicinity of black holes and determining the size of the smallest black hole known. The mission carried three major instruments: the Proportional Counter Array (PCA), operating in the low energy range (2 – 60 keV), the High-Energy X-ray Timing Experiment (HEXTE) for the high energy range (15 – 250 keV), and the All Sky Monitor (ASM). While both PCA and HEXTE were pointing instruments designed to observe specific targets, the ASM was continuously observing 80% if the sky per minute. It was operative in the 2 – 10 keV band, and was composed by three wide angle scanning shadow cameras with Xenon proportional counters achieving a total collecting area of $90\ \text{cm}^2$ (Levine et al., 1996).

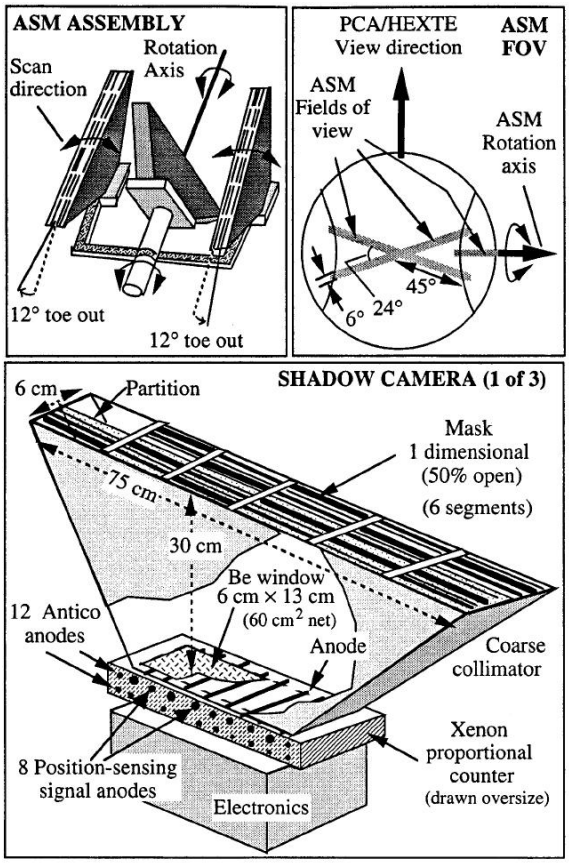

FIGURE 5.2: Overview of the configuration in which the scanning shadow cameras were placed on the ASM onboard RXTE, from (Levine et al., 1996), Fig. 1. The top-left schematics shows the ASM, the top-right the field of view of the cameras and the bottom image details the components of a scanning shadow camera.

For this study, I used archival data[1] of the ASM instrument.

5.2.2 Monitoring data

MAXI/GSC

As explained in section 4.2.1, MAXI is a monitoring X-ray instrument onboard the ISS. Its main instrument, the Gas Slit Camera (GSC), is sensitive to an energy range of 2 – 30 keV and has a time resolution of 0.1 ms (Mihara et al., 2011). I used the publicly available light-curves of the official MAXI website[2] for this study.

Swift/BAT

Swift is an X-ray satellite which was launched in 2004 and designed specifically for the search of Gamma-ray bursts (GRBs). Its monitoring instrument, the Burt Alert Telescope (BAT), is searching for transient events in the 15 – 50 keV band and covers 80% to 90% of the sky per day (Barthelmy

[1] http://heasarc.gsfc.nasa.gov/docs/xte/ASM/sources.html
[2] http://maxi.riken.jp/top/

et al., 2005). In addition, Swift carries two more instruments, the X-Ray telescope (XRT), which is a pointing instrument consisting of a Wolter type I telescope with 12 nested mirrors and is initially designed to precisely determine the origin of GRBs with a precision of 2 arcseconds in the 0.5 – 10 keV band, and the Ultraviolet/optical telescope (UVOT), which is mainly used to detect optical afterglows of GRBs.

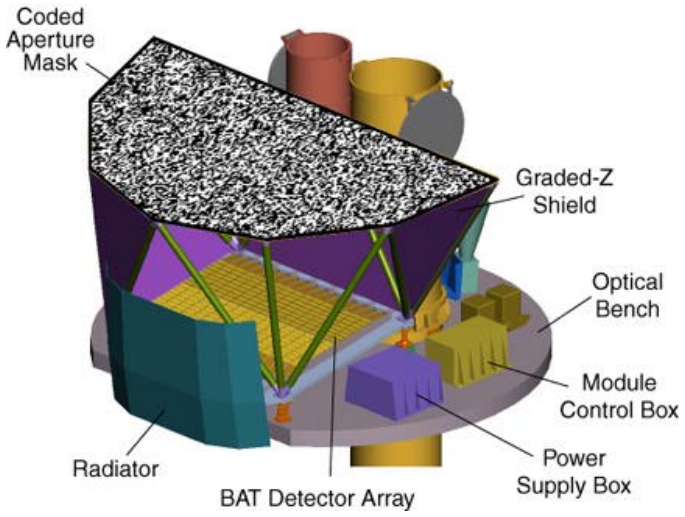

FIGURE 5.3: Schematics of the BAT instrument onboard Swift, from *Swift: About Swift - BAT Instrument Description*.

The BAT is a coded aperture imaging instrument with a large detection area ($5200\ \mathrm{cm}^2$), which is composed by 256 modules of 128 elements and has a sensitivity of 16 mCrab. Publicly available data were taken from the official website[3], the Hard X-rays Transient Monitor (Krimm et al., 2013).

Fermi/GBM

The Fermi Gamma-Ray Space Telescope, launched in 2008, is dedicated to the study of the gamma-ray sky. It carries two main instruments: the Large Area Telescope (LAT), an imaging telescope operating in the 20 MeV – 300 GeV energy range with a FOV of about 20% of the sky, and the Gamma-ray Burst Monitor (GBM) specifically designed to study GRBs, which is operative between 8 keV and 40 MeV (Meegan et al., 2009).

[3] http://swift.gsfc.nasa.gov/results/transients/

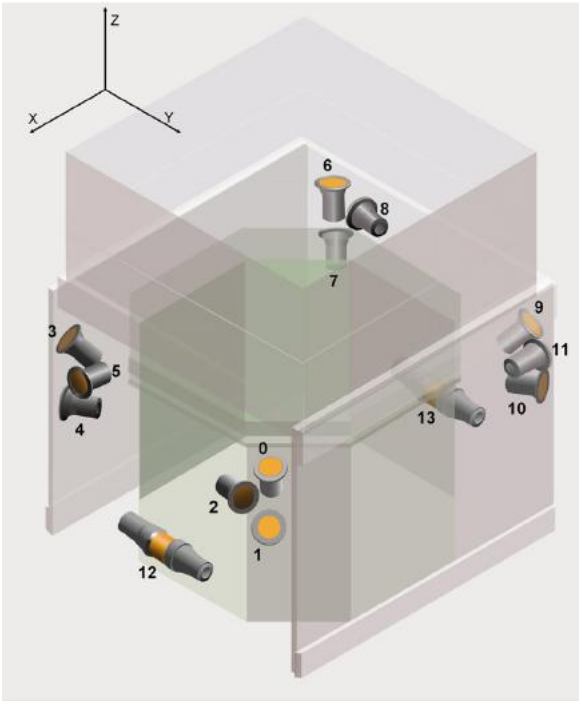

FIGURE 5.4: Location of the NaI and BGO detectors on the Fermi satellite from (Meegan et al., 2009), Fig. 4.

The GBM instrument consists of 2 Sodium Iodide (NaI) and 2 Bismuth Germanate (BGO) scintillation detectors with a time resolution of 2 μs. For this study, the public pulsar data[4] were used. These data are already processed light-curves extracted from the GBM instrument after integrating observations between 1 and 4 days. A pulse search is run which automatically folds the light-curves using frequencies of known pulsars in the observed region as a reference, using two of the 8 channels of the NaI detectors. The frequencies are corrected for the binary motion for sources where the binary orbit is known, such as for example for EXO 2030+375, using the orbital parameters derived in Wilson, Finger, and Camero-Arranz, (2008). The program returns frequencies and an R.M.S. pulsed flux.

5.3 The global evolution of EXO 2030+375

5.3.1 Overview

Recent monitoring data of several instruments are combined with previously published X-ray and optical data to understand the phenomena displayed by EXO 2030+375 in the context of its history.
Figure 5.5 presents an overview of the entire behavior of the source, where the light curve and the evolution of the spin frequency, the timing of the peak, and the equivalent width of the Hα line are shown.

[4] http://gammaray.nsstc.nasa.gov/gbm/science/pulsars.html

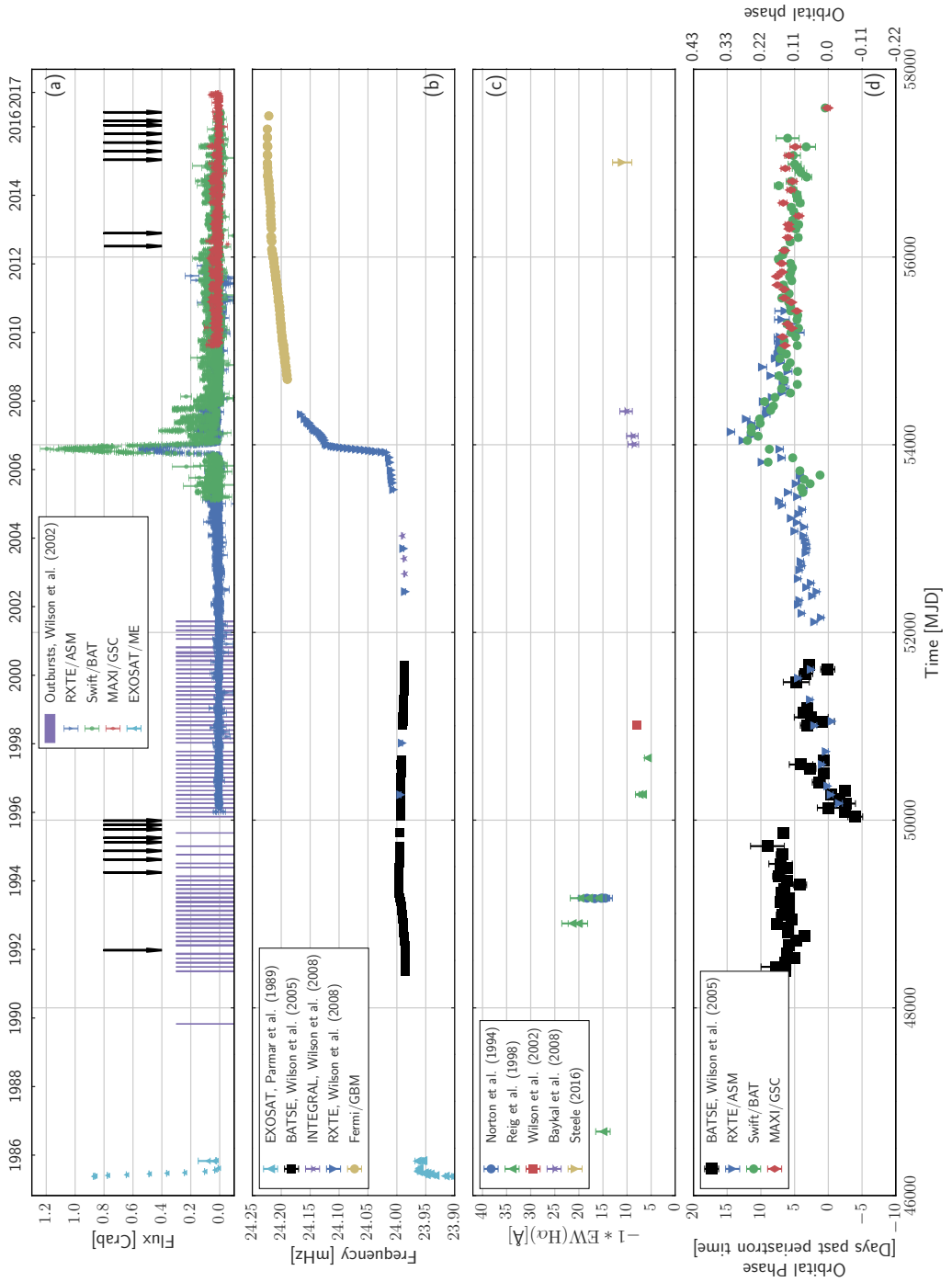

FIGURE 5.5: Global evolution of EXO 2030+375 over the last 30 yr. Panels (a),(b),(c),(d) show the evolution of the light-curve, spin frequency, and Hα line equivalent width of EXO 2030+375, and of the orbital phase of the peaks of the type I outbursts, respectively.

5.3.2 Light curve

I combined data from EXOSAT/ME data as reported in Parmar et al., (1989) and monitoring data from RXTE/ASM, Swift/BAT and MAXI/GSC in the

light-curve Fig. 5.5 panel (a). For better comparison, the flux of each instrument was rescaled to the Crab flux with a value of 1 Crab $= 3.6$ counts s^{-1} cm^{-2} (Matsuoka et al., 2009), 1 Crab $= 0.22$ counts s^{-1} cm^{-2} (Krimm et al., 2013), and 1 Crab $= 75.5$ counts s^{-1} cm^{-2} (Levine et al., 1996) for MAXI (2-20 keV), Swift/BAT (15-50 keV), and RXTE/ASM (1-12 keV), respectively. BATSE outbursts listed in Wilson et al., (2002) are indicated as violet rectangles and black arrows pinpoint the periastron passages during which no type I outbursts were detected using the orbital solution from Wilson, Finger, and Camero-Arranz, (2008).
It is interesting to note that during the both periods of missing outbursts (1994/1995 and 2014/2015), a similar number of outbursts were not observed and that this occurred with the same frequency.

5.3.3 Spin frequency

In Fig. 2, panel (b), the evolution of the spin frequency is shown, combining data from Wilson, Finger, and Camero-Arranz, (2008), as well as recent Fermi/GBM data. As detailed in section 3.3.1, during the two giant outbursts, a dramatic spin-up of the neutron star was observed (MJD 46200 and MJD 54000). The subsequent transition to a slower spin up followed by a constant spin is remarkably similar both around MJD 49300, before the pulsar started spinning down, and for the most recent measurements.
It can also be noted that the latest data points strongly indicate that the source is starting to spin down, as was reported in Laplace et al., (2016) and Laplace et al., (2017), and as was confirmed later from Swift/XRT and NuSTAR measurements (Kretschmar et al., 2016).

5.3.4 Hα line equivalent width

Infrared and optical observations can give crucial information about the Be disk size and geometry (see, e.g., Reig, 2011). In particular, the Hα line and the variations of its shape and equivalent width give strong indications of the changes occurring in the disk. In Fig. 5.5, panel (c), all published measurements of the Hα line equivalent width (Norton et al., 1994; Reig et al., 1998; Wilson et al., 2002; Baykal et al., 2008) are combined.
As it was recently reported in Steele, (2016a), since the Hα measurements communicated in Steele, (2016c) and (Steele, 2016b) were carried out with the wrong positioning, I did not include them in this work.
At present as before the OPS which occurred in 1995, an increase of the equivalent width can be observed, followed by a dramatic drop of the equivalent width (MJD 50500). Because of the very sparse observations of the source, it remains unclear how the Hα line evolved just before the OPS (see also Fig. 3.8 and Fig. 3.9). However, infrared photometry measurements indicate a drop in magnitude at least 100 days before the OPS in 1995 (Reig et al., 1998; Wilson et al., 2002) which has been interpreted as an indication for the beginning of a disk-loss phase.

5.3.5 Monitoring of the type I outbursts peaks

In Figure 5.5 panel (d), I investigate the evolution of the orbital phase of the type I outburst peak. In the past, this value has been shown to change

significantly, as reported in section 3.2.1. To perform this study, I fitted monitoring data from RXTE/ASM, Swift/BAT and MAXI separately and converted the resulting peak time into an orbital phase using the solution from Wilson, Finger, and Camero-Arranz, (2008). In previous studies, a Gaussian function was used for monitoring the outburst peak. However, since the resolution of the modern monitoring instruments is much higher today, I used more accurate models for the fits. Previous studies have shown that type I outbursts can have a range of different shapes (Kuehnel et al., 2015). Consequently, I used four different models to fit type I outbursts: the Gaussian model used in previous studies, (Eq. 5.1), a Lorentzian model (Eq. 5.2), an asymmetric Gaussian model similar to the one used in Kuehnel et al., (2015) (Eq. 5.3), and in the case of certain outbursts displaying an initial spike, the fit could be improved with an additional Gaussian component.

$$F_{\text{Gaussian}}(x) = K \cdot \exp\left(\frac{-(x-\mu)^2}{2\sigma^2}\right) \tag{5.1}$$

$$F_{\text{Lorentzian}}(x) = \frac{K\sigma}{\pi\left(\sigma^2 + (x-\mu)^2\right)} \tag{5.2}$$

The parameters K, μ, and σ represent the scaling factor, the location of the peak, and the standard deviation, respectively. For the asymmetric Gaussian function, the parameters F_{max}, t_{max}, σ_{rise}, and σ_{decline} specify the highest value at the peak, the peak time, and the standard deviation of the Gaussian function at the rising and declining phase, respectively.

$$F_{\text{assymetric Gaussian}}(x) = F_{\text{max}} \begin{cases} \exp\left(-\frac{(x-t_{\text{max}})^2}{2\sigma_{\text{rise}}^2}\right) & \text{for } x < t_{\text{max}} \\ \exp\left(-\frac{(x-t_{\text{max}})^2}{2\sigma_{\text{decline}}^2}\right) & \text{for } x \geq t_{\text{max}} \end{cases} \tag{5.3}$$

The peak time for each outburst was obtained from the model resulting in the best fit and then converted into an orbital phase with the orbital solution of Wilson, Finger, and Camero-Arranz, (2008). For each instrument, I fitted each orbit separately. To verify whether or not a systematic bias had been introduced in the determined peak time by the use of multiple models, I compared the determined peak time for each functions and for different data sets. The orbital phase of the peak as a function of time is shown in Fig. 5.6, with the results from different models used.

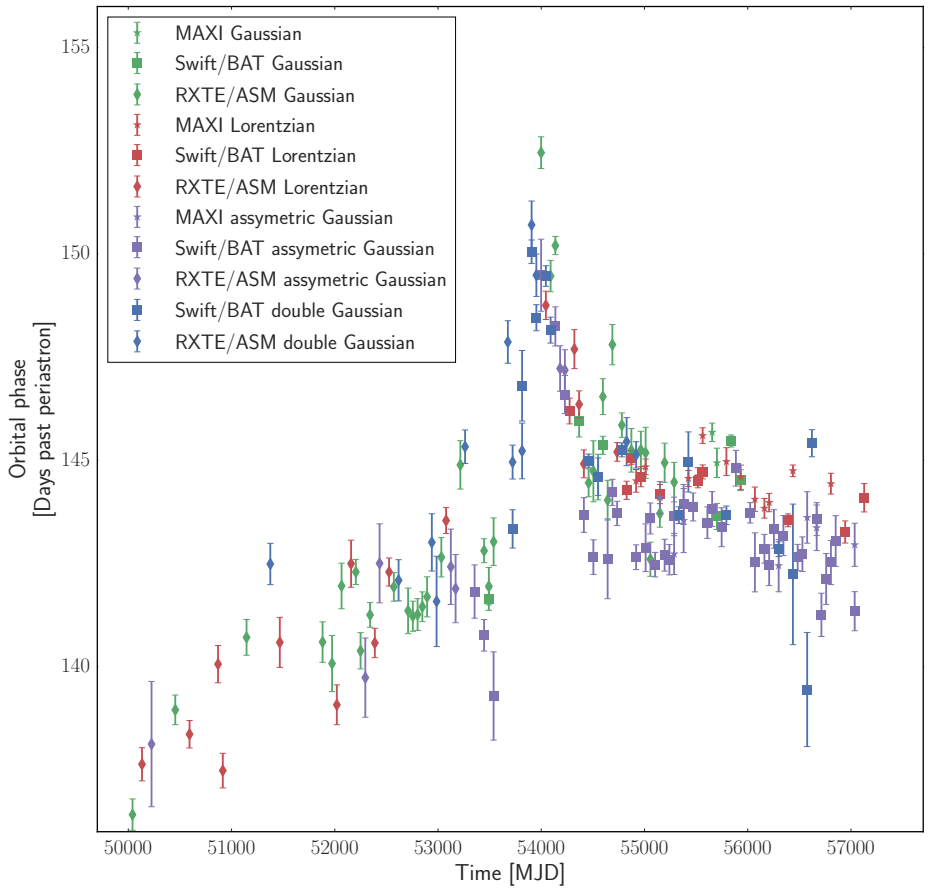

FIGURE 5.6: Orbital phase of the peak time of type I outbursts of EXO 2030+375 as a function of time. The various models used to obtain the peak time are indicated with different colors and the three instruments (RXTE/ASM, MAXI/GSC and Swift/BAT) are differentiated by the markers.

From this figure, it is apparent that the peak times are similar for both different models and different instruments. However, there seems to be a slight bias (1 day) by using the asymmetric Gaussian model, especially prominent in the Swift/BAT results. The existence of such a bias was probed by creating a histogram of the resulting orbital phases of the type I outbursts' peaks for this instrument, shown in Fig. 5.7.

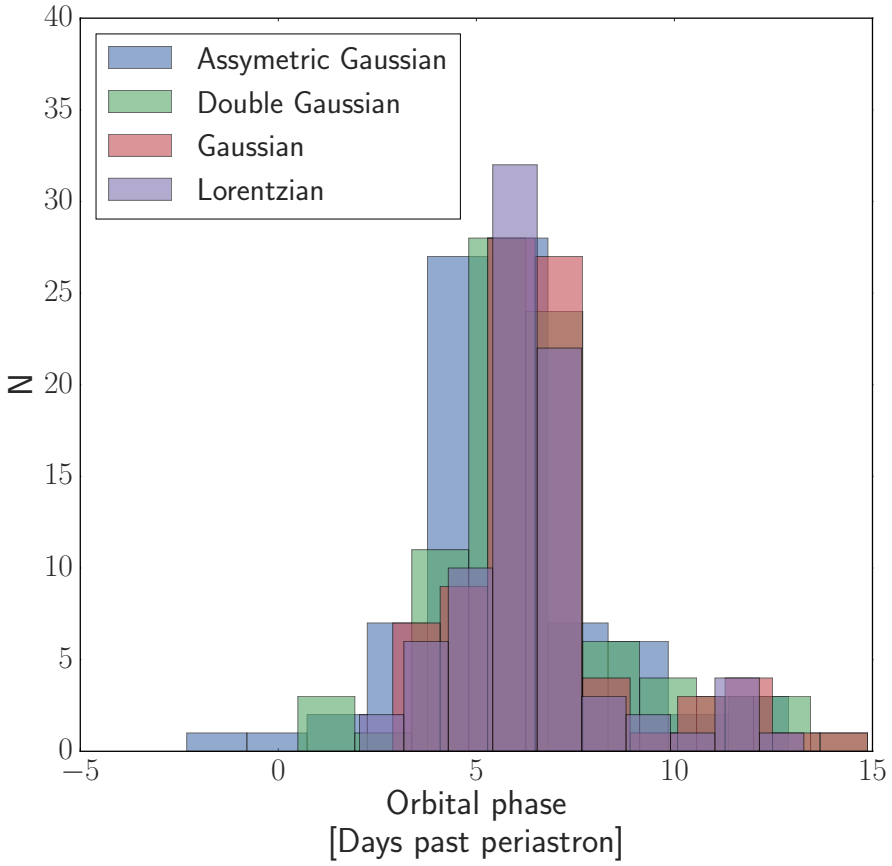

FIGURE 5.7: Histogram of the orbital phases of the peak times of type I outbursts obtained by fitting different models to Swift/BAT data.

While the results of asymmetric Gaussian fitting (by definition) indeed tends toward lower values, the results for all fitting functions are very similar on average and agree within ± 1 d.
The evolution of the orbital phases of the type I outbursts peaks is shown in Fig. 5.5, panel (d). The first measurements of the type I outbursts show a constant phase at about 5 days after periastron. The shift at around MJD 50000 reported by Wilson et al., 2002 is clearly seen with a sudden drop to 4 – 5 days *before* periastron, followed by a slow recovery to a stable phase of 3 – 4 days after periastron.
A shift of the same amplitude, but in the opposite direction was observed during the giant outburst Baykal et al., (2008) and Wilson, Finger, and Camero-Arranz, (2008). The peak phase changed from 3 – 4 days after periastron to 13 – 14 days *after* periastron (see also Fig. 3.3). After this event, the peak phased returned to a stable phase of about 5 days after periastron.

5.4 Type I outburst shape

As mentioned above, the shape of several outburst was found to be complex, and in several cases, a precursor could be observed in the light-curve data of the three monitoring instruments I analyzed. To understand the

origin and the properties of the precursors, I systematically searched for their presence in the 160 outbursts observed by RXTE/ASM, Swift/BAT and MAXI/GSC. Each outburst was fit separately for each instrument and the precursor time was converted to an orbital phase using the orbital solution of Wilson, Finger, and Camero-Arranz, (2008). Two main types of outburst shapes including a precursor were found: a sharp-peaked and short precursor with a duration of about 2 days and a broad-peaked, long-lasting precursor with a shape similar to that of the main outburst peak, which could perhaps be classified as "double-peaked". Examples of the outbursts and their precursor types are shown in Fig. 5.8.

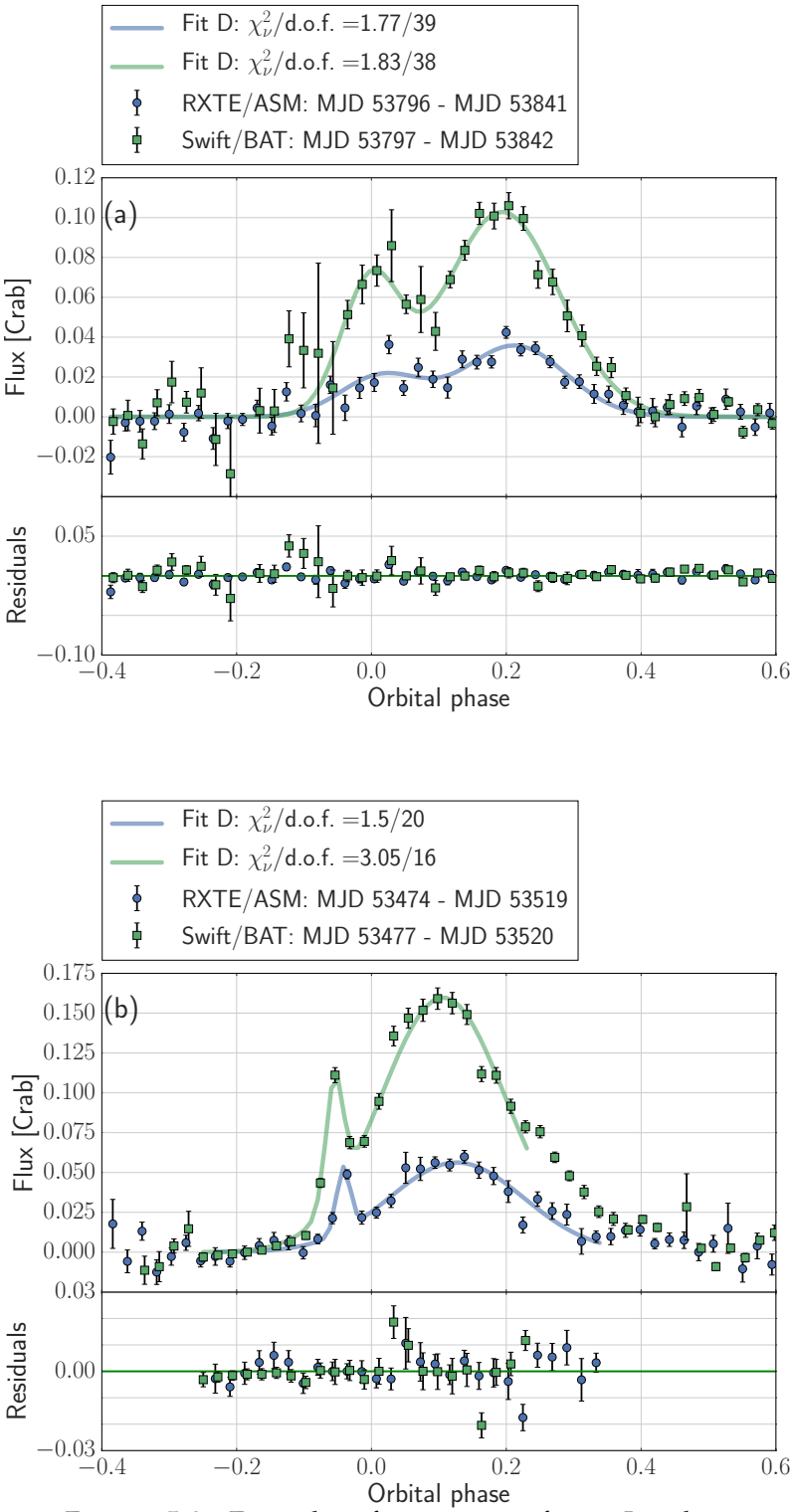

FIGURE 5.8: Examples of precursors of type I outbursts in EXO 2030+375 using RXTE/ASM and Swift/BAT data. Panel (a) shows an example of an outburst with two broad peaks, while a typical example for an outburst with a sharp-peaked precursor is shown in panel (b).

The evolution of the precursor phases can be observed in Fig. 5.9. The phases of the precursors remain roughly constant over time, at a phase of 0.9, about 4 – 5 days before periastron, contrary to the main peak of the

outburst. This phase is similar to the phase at which the main peak was observed during the OPS in 1995. This might imply that both this event and the precursors are caused by a similar mechanism.

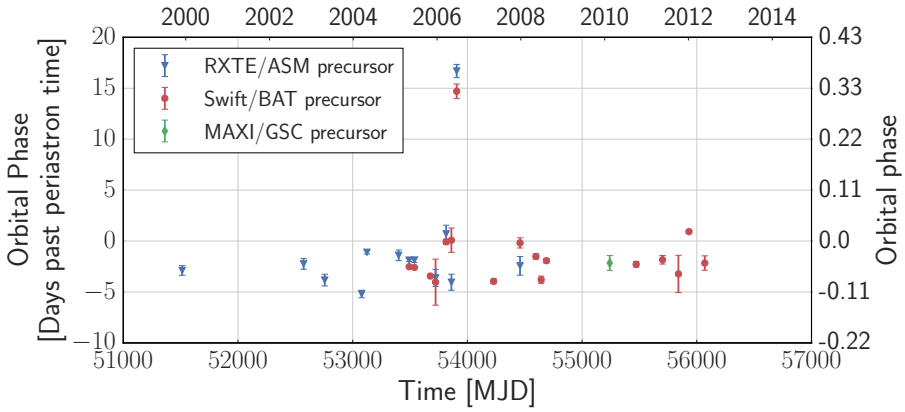

FIGURE 5.9: Evolution of the orbital phase of the precursors in EXO 2030+375.

The two precursors observed by RXTE/ASM and Swift/BAT with an orbital phase of 15 days are the fit to the possible precursor of the giant outburst in 2006 (see also (Baykal et al., 2008)). The fact that the phase at which it appeared is very different from the type I outburst indicate that it is generated by a different physical mechanism. In addition, I did not find the constant interval between the precursor peak and the outburst peak claimed by Camero Arranz et al., (2005), as can be verified in Fig. 5.8.

5.5 Indications for a long-term periodicity

As discussed in the previous section, the long-term behavior of EXO 2030+375 shows remarkable similarities between the recent trends and the ones observed 21 yr earlier (1995), with a drop in flux, missing outbursts, an increase Hα line equivalent width and a constant spin frequency. In addition, almost exactly in-between these events (2006 May – August), a giant outburst was observed, just as 21 yr earlier (1985). All these phenomenological similarities suggest the existence of an analogous underlying physical mechanism with a long-term recurrence period.
I estimated this recurrence period by folding the data. Since there is a large uncertainty associated to when the OPS in 1995 started (approximately three orbital periods, see Fig. 3.3), I matched the declining parts of both giant outbursts instead using data from EXOSAT/ME and RXTE/ASM, which have similar energy bands and are therefore comparable. I derived a period of 7746 d between two giant outbursts and therefore 3873 d between the orbital phase shifts and the giant outbursts. The possibly periodic events are summarized in Table 5.1 and the resulting folded data from Fig. 5.5 is shown in Fig. 5.10.

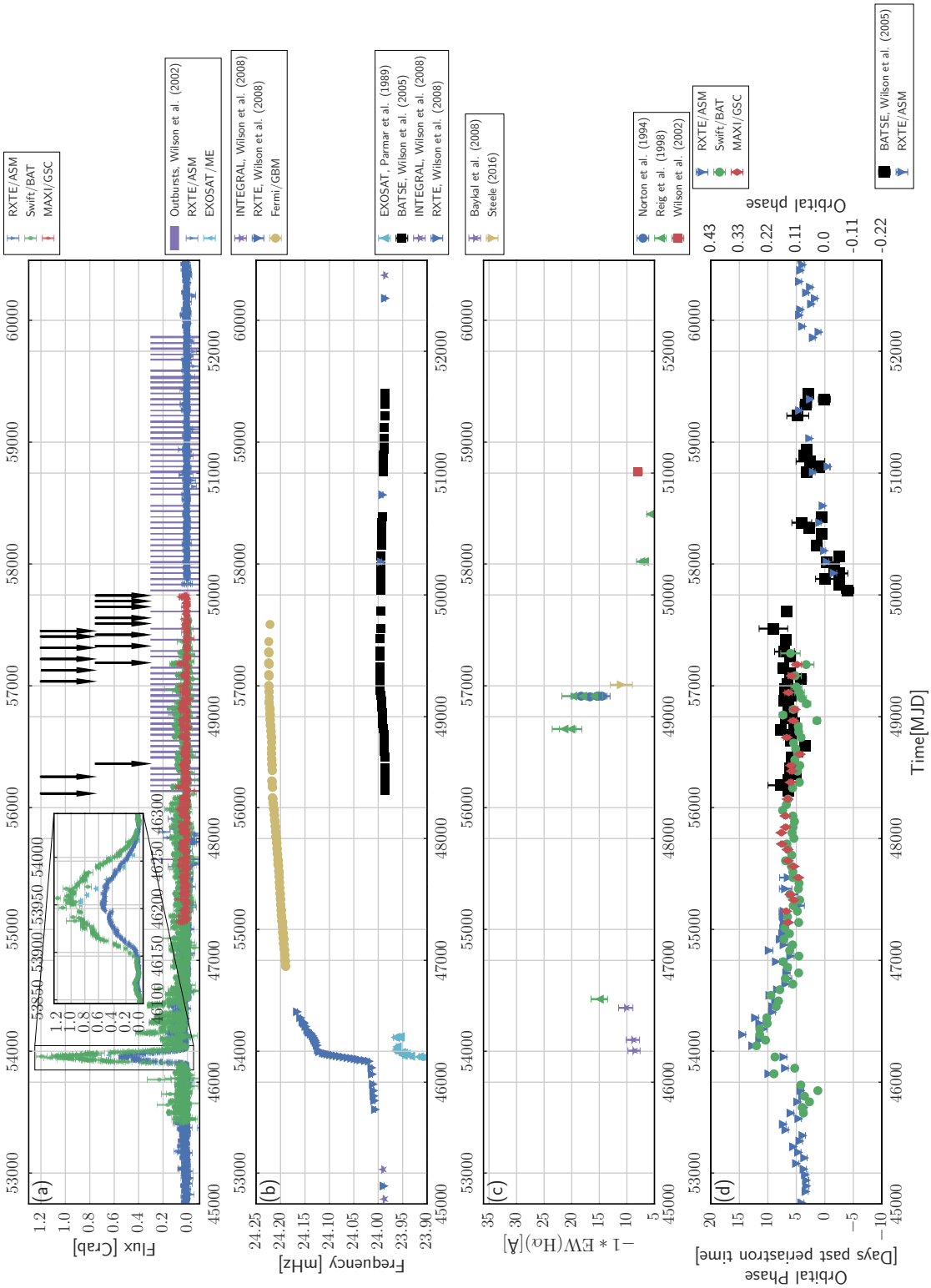

FIGURE 5.10: Data from Fig. 5.5 folded with a period of 7746 d. The MJD times before and after folding, and the corresponding legend are indicated above and below each plot, respectively. In panel (a), the inset shows a zoom of both giant outbursts for clarity. The arrows indicating the times of missing outburst have been shifted above and below, indicating their correspondence times before and after folding, respectively.

The giant outbursts also have a large associated uncertainty, since the discovery giant outburst in 1995 was observed close to its peak (see also Fig. 3.4) and it is unclear when it started. In addition, this outburst is believed to have been significantly brighter than the 2006 giant outburst (Klochkov et al., 2007). Kuehnel et al., (2015) have shown that there is a correlation between the duration and luminosity of an outburst, therefore, the giant outburst in 1985 very likely lasted longer than the 2006 outburst. Assuming half the period to be given by the duration between OPJ95 and OPJ06, the largest uncertainty is estimated to be on the order of the uncertainty on the time at which the OPJ95 occurred, that is, three orbital periods.

TABLE 5.1: Summary of the possibly periodic events and their occurrence time

Event	1985 giant outburst	1995 OPS	2006 giant outburst and 2016 OPS	Predicted OPS
Event start time [MJD]	<46204	49870	53880	57753
Event end time [MJD]	46290	50040	54034	-

From Fig. 5.10, I note that there is a good agreement between the folded data, regarding the light-curves, spin frequency, Hα line measurements and levels of the orbital phase of the outburst peaks. From these phenomenological similarities, I predicted the next orbital phase shift to occur at around MJD 57753d (December 2016).
In addition, the Fermi/GBM data indicated the beginning of a spin down of the source, which was confirmed by NuSTAR and Swift observations (Kretschmar et al., 2016).

5.5.1 Interpretations

These events are likely linked to the Be state, as interpretations for both giant outbursts and orbital phases shifts typically involve the interaction between the neutron star and a tilted/warped/eccentric disk (Wilson et al., 2002; Moritani et al., 2013; Nakajima et al., 2014). I therefore consider several possible interpretations involving various configurations of the Be disk and investigate the predictions associated to these interpretations.

5.5.2 Global one-armed oscillation scenario

In previous studies which attempt to interpret the global behavior of EXO 2030+375, and in particular the OPS in 1995, the preferred mechanism used to explain the observations is that of a global one-armed oscillation in the Be disk triggered by a major structural change inferred from optical and IR observations (see, e.g., Wilson et al., 2002; Baykal et al., 2008). Monitoring the peak change rate of the type I outbursts, the authors derived a propagation period of the density oscillations of 15 ± 3 yr (Wilson et al., 2002).
However, this is contradicted by the observation of a giant outburst in 2006,

during which the oscillation time must have been interrupted (Baykal et al., 2008). In addition, another migration of the outburst peak of the same amplitude, but in the opposite direction was observed after the giant outburst, further contradicting this hypothesis (Wilson, Finger, and Camero-Arranz, 2008).
As mentioned in section 2.4, the existence of these oscillations is mainly inferred from the observation of V/R variability (see, e.g., Reig, 2011). I note, however, that, to my knowledge, no V/R variability has been observed for EXO 2030+375. In addition, the typical orbital period of such an oscillation calculated from observations of V/R variability in BeXRBs is of 1 – 5 yr (Reig, 2011), significantly shorter than the inferred period. In isolated Be stars, this time-scale ranges from 6-11 yr with a mean period of 7 yr (Okazaki, 1997; Reig, 2011) and is thus significantly shorter than the derived period.
For the same reasons, considering a global one-armed oscillation as an explanation for the giant outbursts is contradicted by the time-scale, which would be of minimum 10.5 yr (between a giant outburst and an OPS), much larger than observed periods in BeXRBs. In addition, recent theoretical studies have found that the existence of such an oscillation alone is not a sufficient requirement for the formation of giant outbursts. In addition to begin warped, the disk must be significantly inclined with respect to the orbital plane (Okazaki, Hayasaki, and Moritani, 2013). Moreover, Martin et al., (2014a), have shown that this condition may still not be sufficient for the formation of a giant outburst, and that a high eccentricity of the Be disk is needed.

5.5.3 Precessing Be disk scenario

Another possible explanation for the observed phenomena is a Be disk precession scenario. This interpretation was first proposed by Negueruela and Okazaki, (2001) to explain the behavior of the BeXRB 4U 0115+63. In this model, a tilted Be disk starts to precess once it becomes warped, allowing the crossing of the neutron star orbit at times differing from periastron. The precessing Be disk model has since been applied to a larger sample of BeXRBs to explain optical observation of the Hα line during giant outburst by Bondi-Hoyle-Littleton accretion of matter by the neutron star from a misaligned and precessing disk Okazaki, Hayasaki, and Moritani, (2013) and Moritani et al., (2013).
Recently, this interpretation was discussed as an explanation for the observation of an orbital phase shift in the BeXRB A0535+262 along with a discovered 115d period between outburst precursors and giant outbursts in this system (significantly longer than the 111.1 d orbital period) (Nakajima et al., 2014). In particular, the authors argued that this model could account for the observation of opposed orbital phases of precursors and main peaks by the precession of the disk with a period of $\sim$8.5 yr. This particular case is thus reminiscent of the observations in EXO 2030+375.
In our case, a precession of the Be disk could explain the first orbital phase shift by a moving cross section between the precessing Be disk and the neutron star orbit. However, it remains unclear why the precession would stop after $\sim$200d (see Fig. 3.3) or how at the same time as the giant outburst, the disk would precesses in the opposite direction only to stop again suddenly

afterwards. In addition, the fact that the precursor phase has a stable value while the main peak shifts is also unexplained in this model.

5.5.4 Double Be disk scenario

In the previous sections, I have shown that a precessing disk is not sufficient to explain all the observations. I therefore consider the existence of a double disk.
Until now, no observational evidence for a double disk has been found in EXO 2030+375, although Wilson et al., (2002) reported double and even triple-peaked Hα line spectra of the source (see also Fig. 3.9).
Observational evidence for double Be disks have been reported for several single Be stars (μ Cen: Rivinius et al., (1998) and Rivinius et al., (2001b); 28 CMa and FV CMa: Rivinius et al., 2001a, and Pleione: Tanaka et al., (2007)), and for a single BeXRB system (X Per: Tarasov and Roche, (1995)).

The giant outburst would be explained classically as originating from the passage of the neutron star trough a large enough Be disk. In this case, the occurrence of giant outbursts would be quasi-periodic and have a time-scale similar to that of the disk-growth time-scale, which is about 6 yr for most BeXRBs (Reig, 2011). In fact, early studies showed that giant outbursts tended to occur quasi-periodically, such as in the case of 4U 0115+63 and Cep X-4, with a recurrence of 3 – 5 yr (Whitlock, Roussel-Dupre, and Priedhorsky, 1989; Okazaki and Negueruela, 2001; Boldin, Tsygankov, and Lutovinov, 2013) and 4 yr (McBride et al., 2007), respectively.
The double Be disk scenario can be pictured as follows. The Be star is surrounded by two circumstellar disks: a newer, inner disk which forms on the equatorial plane, and an older, outer disk, which is tilted and precessing due to gravitational interactions with the neutron star. The stable peak time of the type I outbursts until 1995 can be interpreted as originating from the outer disk. At the time of the missing outbursts, the disk expands and dissipates away, causing missing outbursts on time-scale of about 200 d. This time-scale is in agreement with optical observations of other Be systems, which showed changes in size and density on the order of 100 d (see Grundstrom et al., 2007; Arabacı et al., 2015). As the outer disk dissipates away, the inner disk, which has a different inclination, reaches far enough to interact with the neutron star, causing the OPS.
This model cannot explain the constant phase of the normal outbursts before the OPS, since the outer disk is expected to precess. In addition, I do not expect necessarily the same time-scale between the OPS and giant outbursts, since this time-scale is driven by the activity of the Be star and the expansion rate of the Be disks.

5.5.5 Kozai-Lidov oscillations scenario

Another possible interpretation of the global behavior of EXO 2030+375 is the existence of KL oscillations in the Be disk. As explained in section 2.3.6, when KL oscillations occur, the Be disk periodically oscillates between a state in which it is highly inclined and little eccentric and the opposite state, in which it is highly eccentric but little inclined.
I can estimate the KL time-scale for EXO 2030+375 using equation 5.5. With this interpretation, giant outbursts occur when the eccentricity of the Be

disk is high. Interestingly, applying this interpretation to EXO 2030+375, there can be two explanations for the orbital phase shifts, depending on the oscillation time-scale: enhanced inclination or enhanced eccentricity during a disk-loss phase.
I can estimate the time-scale of KL oscillations for EXO 2030+375 using equation 5.5. Given the uncertainty of this estimation (see section 2.4), I can approximate the orbital separation by the semi-major axis $a_{\rm sm}$ and the outer disk radius by the binary separation at periastron $D_{\rm peri}$. From ellipse geometry (see, e.g., *Encyclopaedia of Mathematics*), I can express both the binary separation and the periastron distance as a function of eccentricity e of the binary orbit

$$\frac{a}{R_{\rm out}} \approx \frac{a_{\rm sm}}{D_{\rm peri}} = \frac{1}{1-e}. \tag{5.4}$$

With this estimate, I can now express the KL time-scale solely as a function of parameters which can be constrained by observations

$$\frac{\tau_{\rm KL}}{P_{\rm orb}} \approx \frac{(4-p)}{\left(\frac{5}{2}-p\right)} \left(\frac{1}{1-e}\right)^{\frac{3}{2}} \sqrt{\frac{M_{\rm Be}}{M_{\rm NS}} \left(\frac{M_{\rm Be}}{M_{\rm NS}}+1\right)}, \tag{5.5}$$

with the power-law index of the surface density of the disk being the most difficult to estimate, with a typical value of 1.5 (Martin et al., 2014b; Fu, Lubow, and Martin, 2015a) and references therein.
Applying the equation 5.5 to EXO 2030+375, with $p = 1.5$ (Martin et al., 2014b), $M_{\rm Be} = 20 M_\odot$, and $M_{\rm NS} = 1.4 M_\odot$ (Okazaki and Negueruela, 2001) and $e = 0.4190$ Wilson, Finger, and Camero-Arranz, 2008, I obtain $\tau_{\rm KL} \approx 83\ P_{\rm orb} \approx 3820$ d. This estimation is close to the previously derived value of 3873 d (10.5 yr). This is an indication that KL oscillations provide a reasonable explanation for the behavior of the source. As shown in Fu, Lubow, and Martin, (2015a), this estimation is however only valid up to a factor of 2. As a result, two possible time-scales of the oscillations can be considered, in which the origin of the OPS differs:

1. A time-scale of 10.5 yr, in which both giant outbursts and OPS would be caused by an enhanced eccentricity of the disk, as my calculation suggests.

2. A time-scale of 21 yr, in which the giant outbursts would be caused by an increased eccentricity and the negative OPS by an increased inclination of the disk.

In the first interpretation, the giant outbursts are explained by an increased eccentricity of the disk, leading to the accumulation of a large amount of matter around the neutron star. In both cases, QPOs have been observed a few months after the giant outbursts occurred (see section 3.2.3 and Parmar et al., (1989) and Klochkov et al., (2011)), a strong indication for the existence of an accretion disk around the neutron star. From RXTE/ASM and Swift/BAT observations revealed that the 2006 giant outburst started at a similar phase (0.75) as the OPS in 1995. This can be interpreted as the cross section between the disk and the neutron star orbit. Precession effects or a disk loss scenario could explain the difference between the events. In a disk-loss scenario, around MJD 50000 the disk becomes less dense while becoming more eccentric because of KL oscillations. This is supported by

optical/IR observations around this time (see Fig. 5.5, 3.8, 3.9, and Wilson et al., (2002)). Therefore, the neutron star can capture some matter at a different phase from periastron, leading to an OPS. However, I note that from the previous infrared observations (Wilson et al., 2002) (see Fig. 3.8), the color did not seem to change, which is usually expected during disk-loss (Moritani et al., 2013).
In the second case, the origin of the giant outbursts is also the increased eccentricity of the Be disk. However, the orbital phase shift originates from another process, caused by an increased inclination of the disk. In the optical wavelength, the equivalent width of the Hα line decreases because the projected area of the Be disk becomes smaller. Similarly, the infrared flux drops, as is the case at the OPS in 1995 (Wilson et al., 2002). The accretion rate also drops because the eccentricity of the disk decreases. The higher inclination of the disk could then cause an orbital phase shift. However, I note that the time-scale of the changes of the outburst peaks observed around this time and of the changes of the Hα line (a few orbits) are significantly shorter than the KL oscillation time-scale (several years).

5.5.6 Predictions

With the different models detailed in the previous sections, I could make predictions for future observations of EXO 2030+375.

- For the first KL model, I predicted an increase of the disk eccentricity every 10.5 yr, forming a giant outburst accompanied by an OPS or only an OPS if the disk density is low. Consequently, I predicted the observation a giant outburst or an OPS in 2016 December. In addition, I expect to observe a giant outburst around August/September 2027. I expect the same observation from the double Be disk model.
- In the second KL oscillations model, I expect the eccentricity of the disk to reach a maximum every 21 yr. As a result, I expect to observe a giant outburst in 2027 August/September and I should have observed an OPS in 2016 December if the disk inclination is high enough.

5.6 2016 July OPS

In July 2016, a regular outburst of EXO 2030+375 was observed with regular MAXI and Swift monitoring (Laplace et al., 2016).

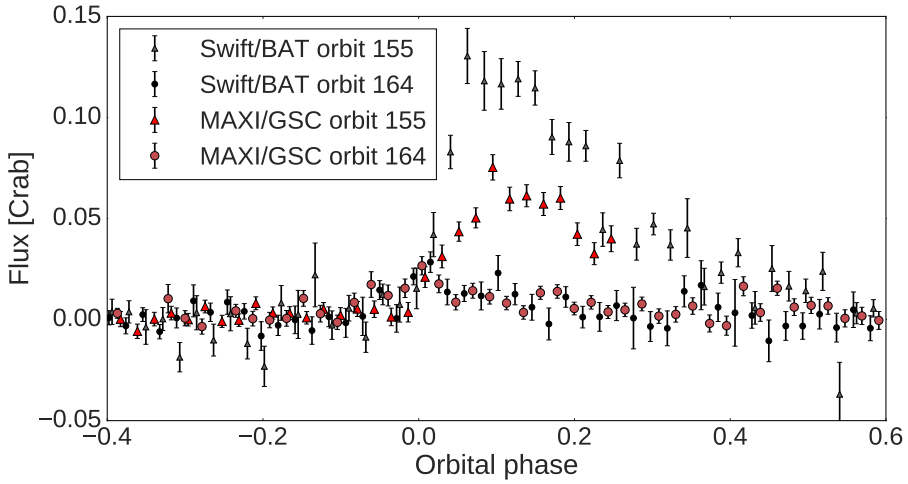

FIGURE 5.11: Folded light-curve of EXO 2030+375 with the orbital period of the last bright outburst in 2015 and of the observed outburst in 2016. The orbit number is calculated starting from the first periastron passage observed by RXTE/ASM, MJD 50086.967.

Contrary to the almost constant phase of the peak at about 0.13 in the 7 years before (see Fig. 5.5), the peak of this outburst was reached at an orbital phase of 0.015. This represents a shift of about 5 d, which is approximately half the shift of about 10 d observed during the OPS in 1995, but in the same direction. The folded light-curve of this outburst and the one before is shown in Fig. 5.11, where the shift of the outburst peak can clearly distinguished. In addition, the OPS can be seen in Fig. 5.5, panel (d).
This observation confirms the prediction of this event, even though it occurred earlier then expected.

5.6.1 Conclusion

I have studied the global behavior of EXO 2030+375 in the last 30 years since its discovery, studying the evolution of the light-curve, the spin frequency, the equivalent width of the Hα line, and computing the orbital phase of the type I outburst peaks. The recent changes in the source behavior are phenomenologically very similar to events which occurred about 21 years earlier, close to MJD 50000. From these similarities, and from noting that the two giant outbursts occur at peculiar times, about 10.5 years earlier than these changes, I derive a period of 10.5 or 21 years in the global source behavior and predict the occurrence of an orbital phase shift in December 2016.
In addition, I study the occurrence of outburst precursors in the source using data from MAXI/GSC, Swift/BAT and RXTE/ASM. I find that their orbital peak phase is constant over time and that the time interval between these precursors and the main peak is not constant, contradicting previous findings (Camero Arranz et al., 2005).
I discuss several models to explain the observation of a global cycle. Of these, the most promising is the KL oscillations model, which is based on the idea that KL oscillations occur in the Be disk, leading to periodic

changes of its eccentricity and inclination. The time-scale derived for EXO 2030+375 is surprisingly close to the derived observational period of 10.5 years. However, uncertainties in the calculation also allow the existence of a 21 years periodicity. Depending on the time-scale, I predict the observation of either an orbital phase shift or a giant outburst in December 2016 and a giant outburst in 2027.
Moreover, I report the observation of an orbital phase shift in 2016 July, which confirms my prediction and indicated that there is indeed a periodicity in the global source behavior. However, the model of KL oscillations needs to be verified by analyzing optical and infra-red observations of EXO 2030+375.

Chapter 6

Discussion and conclusion

6.1 Spectral properties

6.1.1 Summary

In this thesis, I have presented the first analysis of MAXI spectra of EXO 2030+375. I performed a systematic study of the outburst of EXO 2030+375 with MAXI and analyzed the spectral variability of the source during the average orbit and depending on the flux. In addition, I studied the spectral variability independently by folding MAXI light-curve and studying the hardness ratios. The results can be summarized as follows

- The phenomenological model of an absorbed power-law with high-energy cutoff used in this study is in good agreement with previous studies (Reig and Coe, 1999; Camero Arranz et al., 2005; Naik et al., 2013). However, at low energies, the spectrum is strongly background contaminated.
- I find indications for a weak luminosity-dependence of the photon index during the orbit of the source. At the onset and end of the outburst, the spectrum becomes softer then for the main outburst, during which the spectral parameters are remarkably constant. This supports findings from Reig and Coe, (1998).
- Folding the MAXI-light-curve reveals a small secondary peak at apastron. This confirms the findings of (Reig et al., 1998), who reported a similar peak at apastron from RXTE/ASM data at a comparable energy range (1 – 12 keV). I find a significant spectral variability during the peak in all energy bands by calculating the hardness ratios of MAXI.
- Flux resolved spectroscopy also shows indications for spectral variability between high fluxes and low fluxes.

6.1.2 Discussion

Owing to the low spectral resolution of MAXI and the low flux of MAXI, I do not find spectral variability during the last 7 years. However, I find indications for a softening of the spectrum at low fluxes and at the onset and end of the outbursts. A study of the spectral variations of the source during one outburst in 1996 July using RXTE was reported in Reig and Coe, (1999), who found a weak correlation between changes in the photon index with the luminosity. My study therefore independently supports this finding.

The small apastron peak found in the folded MAXI data is an interesting feature. The presence of such a small peak was reported before using RXTE/ASM data (Reig et al., 1998). Here, I report indications for strong spectral variability during this peak for the first time. The origin of this peak is intriguing and remains to be investigated.

6.2 Timing properties

To understand the origin of the recent changes observed in the timing behavior of EXO 2030+375, I have investigated the entire 30 yr history of the source, and investigated the evolution of the outburst peak phase and of the precursors of the type I outbursts. The results can be summarized as follows.

- Phenomenological similarities indicate the existence of a 10.5 or 21 yr long-term periodicity in the source. Both recently and 21 yr ago, the same behavior change can be observed in EXO 2030+375 (1) a drop in the X-ray flux with some outbursts becoming undetected; (2) a transition from slow spin-up to almost constant spin, then spin-down; (3) a strengthening of the Hα line equivalent width; (4) an orbital phase shift; (5) I note that before 10.5 yr earlier than these events, a giant outburst was observed.
- From all these similarities, a 3800-day or 7700-day periodicity of events can be derived, which can be related to the occurrence of type II outbursts and to orbital phase changes. Assuming the existence of such a periodicity, I could predict an orbital phase shift to occur around December 2016. At the same time, I predicted the possible appearance of a giant outburst.
- I have shown that a plausible explanation of the source behavior and the long-term cycle is the presence of KL oscillations of the Be disk.
- The observation of an orbital phase shift in 2016 July confirms the existence of a periodicity.

6.3 Outlook

- Optical and IR observations are necessary for determining disk state and the origin of the long-term periodicity.
- Additional studies of the narrow feature at apastron in the orbital profile are needed.
- The existence of a link between giant outbursts and KL oscillations of the disk in BeXRBs in general should be investigated.
- The predictability of EXO 2030+375 offers exciting possibilities for better understanding this object.
- The existence of a long-term periodicity will be further probed by my prediction of the observation of a giant outburst around August/September 2027.

Appendix A

Spectral studies of EXO 2030+375

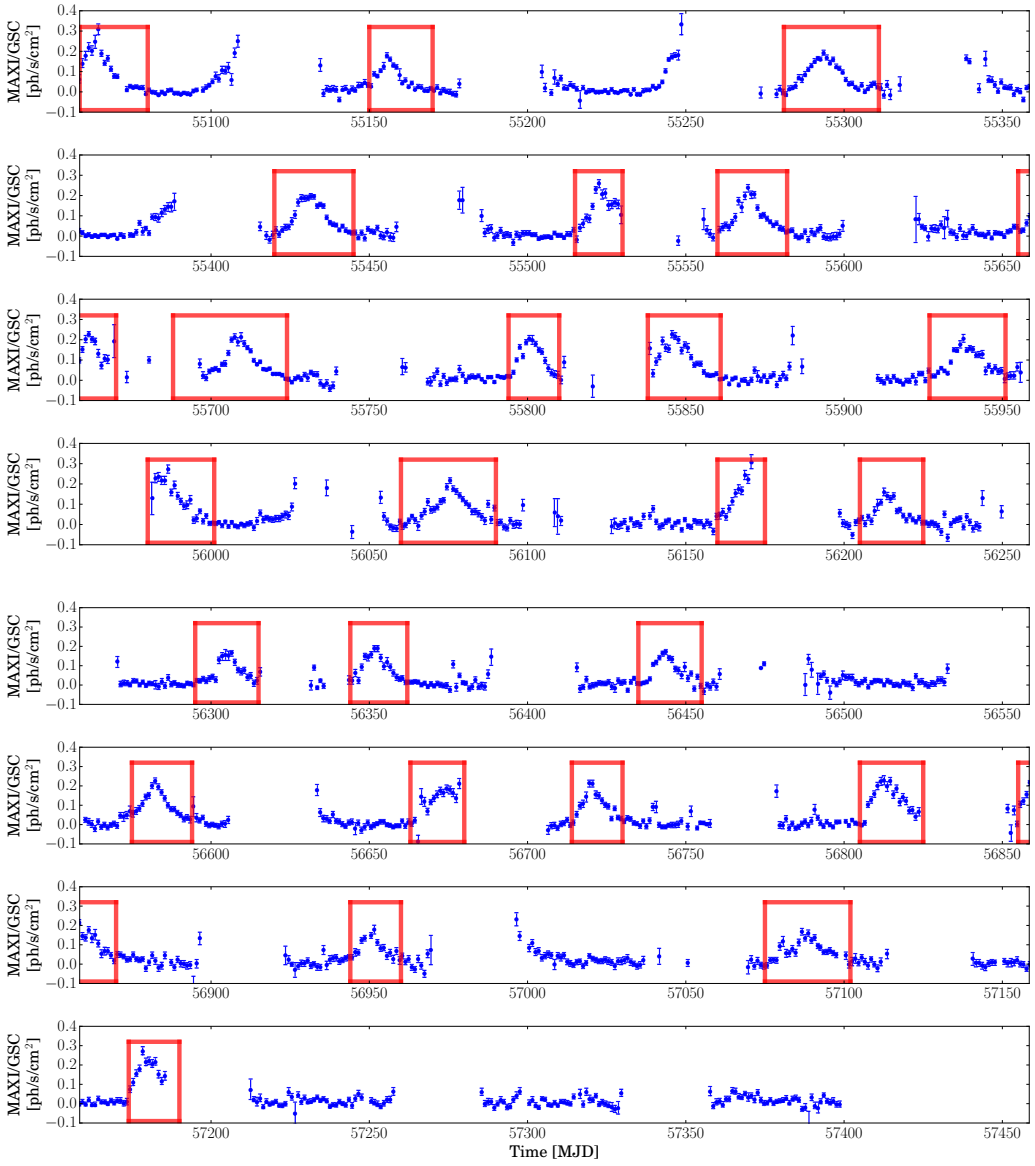

FIGURE A.1: Selected outbursts of the MAXI/GSC light-curve in the 2-20 keV energy band. The red boxes indicated the selection intervals.

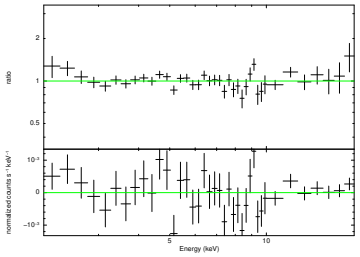

(a) Orbital phase 0.0 – 0.1

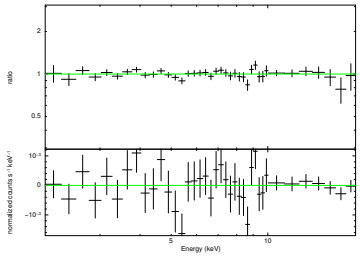

(b) Orbital phase 0.1 – 0.2

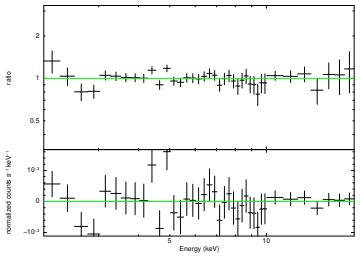

(c) Orbital phase 0.2 – 0.3

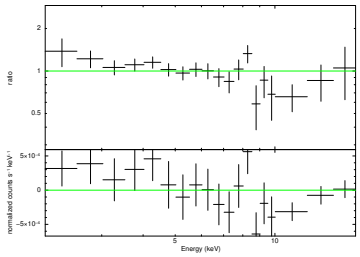

(d) Orbital phase 0.3 – 0.4

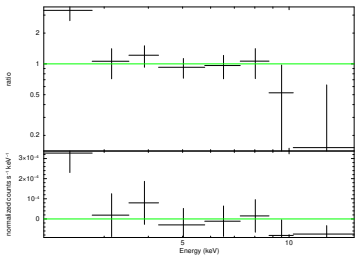

(e) Orbital phase 0.4 – 0.9

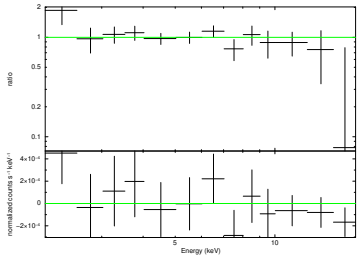

(f) Orbital phase 0.9 – 1

FIGURE A.2: Ratios of the best fit peak model and each of the orbital phase resolved spectra. Residuals are shown in the bottom panels.

Acknowledgements

Here, I wish to thank all the people who have helped, supported and advised me during my Master thesis.
Especially, I would like to thank **Prof. Andrea Santangelo**, together with **Mihara-san**, and **Makishima-sensei**, for giving me the remarkable opportunity to complete my master project in Japan in a collaboration between the IAAT and RIKEN. I wish to thank the RIKEN trainee and International Program Associate (IPA) programs and the IAAT for the support during my stay.
Prof. Andrea Santangelo, I would like to thank you for your help and advice throughout my master thesis, even from far away. Thank you for welcoming me in your group and for your generous guidance.
Mihara-san, thank you for your kind and generous supervision in Japan and for giving me the opportunity to discuss the work with other researchers. I am really glad to have had the chance to learn from you and I hope that we will continue to work together in the future.
Makishima-sensei, thank you so much for integrating me into the MAXI team and for the wonderful experience of working within your group. Your advice and comments greatly improved my work and I am very grateful for your explanations about Japan and the Japanese culture. I cannot thank you enough for giving me the opportunity through RIKEN to learn the basics of the Japanese language, to attend the RIKEN summer school, the meeting of the astronomical society of Japan, the 7 years of MAXI workshop and for allowing me to take some time to explore this beautiful country.
Nakajima-san and **Moritani-san**, thank you very much for our interesting and insightful discussions and for your kind and generous help for writing the paper! I am very glad to have met you and I hope to continue to work with you in the future!
Takagi-senpai, I wish to thank you for your incredibly generous and patient help during my stay in RIKEN. I will be forever thankful for your advice, your helpful comments and for inspiring me to be a good researcher. I hope to see you again soon!
I wish to thank the **MAXI team** in RIKEN in its entirety, with **Matsuoka-sensei**, **Takahashi-san**, **Sugizaki-san**, **Motoko-san**, **Iwakiri-san**, **Shidatsu-san**, **Juri-san**, **Aya-san**, **Takao-kun**, **Yatabe-kun**, **Sudo-kun** and all the other members for their exceptional generosity and for the wonderful time that I spent with them in RIKEN. I am very happy to have met you all and I sincerely hope that we will see each other again in the future. 本当にありがとうございます!
I also wish to thank all the people from the IAAT in Tübingen who helped me to complete my master thesis.
Lorenzo, thanks to you the quality of my master thesis greatly improved and I am very glad for your generous help and advices.
Daniel, vielen Dank für Deine freundliche und großzügige Hilfe und für die unterhaltsamen Kaffeepausen.
Christian thank you for your help during my master thesis and for your valuable advices about living in Japan!
Dima, thank you for the interesting discussions and for your helpful comments of my work.
Sara, with your kind and friendly way of being, you always make my days

in Tübingen happier.
Long, thank you for your helpful suggestions and for being a friendly office mate!
I wish to thank all the other members of the IAAT, including our lunch group with Conny, Samuel, Jörg, Alejandro G. and all the other members, especially the football team, and the Kaffeepause-Team with Heinz for creating a sympathetic and enjoyable atmosphere in the IAAT.
This work would never have been possible without the support of my friends and amazing visitors in Japan, thanks to whom I could bear the difficulties of living far away, and with whom my experience in this beautiful country became unforgettable.
I wish to thank my wonderful family for their love, kindness and support, and for making this experience possible in the first place.
Last, I would like to thank you, Alejandro, for everything.

Bibliography

Arabacı, M. Özbey et al. (2015). "Detection of a large Be circumstellar disk during X-ray quiescence of XTE J1946+274". In: *Astronomy & Astrophysics* 582, A53. ISSN: 0004-6361, 1432-0746. DOI: 10.1051/0004-6361/201425488. URL: http://www.aanda.org/10.1051/0004-6361/201425488 (visited on 06/13/2016).

Arnaud, K. A. (1996). "XSPEC: The First Ten Years". In: *Astronomical Data Analysis Software and Systems V* 101. URL: https://ui.adsabs.harvard.edu/#abs/1996ASPC..101...17A/abstract (visited on 03/25/2017).

Baade, W. and F. Zwicky (1934). "Remarks on Super-Novae and Cosmic Rays". In: *Physical Review* 46. DOI: 10.1103/PhysRev.46.76.2. URL: https://ui.adsabs.harvard.edu/#abs/1934PhRv...46...76B/abstract (visited on 04/12/2017).

Barthelmy, Scott D. et al. (2005). "The Burst Alert Telescope (BAT) on the SWIFT Midex Mission". In: *Space Science Reviews* 120.3, pp. 143–164. ISSN: 0038-6308, 1572-9672. DOI: 10.1007/s11214-005-5096-3. URL: http://link.springer.com/10.1007/s11214-005-5096-3 (visited on 05/10/2016).

Baykal, A. et al. (2008). "Recent RXTE/ASM and ROTSEIIId observations of EXO 2030+375 (V2246 Cygni)". In: *Astronomy and Astrophysics* 479, pp. 301–306. ISSN: 0004-6361. DOI: 10.1051/0004-6361:20078721. URL: http://cdsads.u-strasbg.fr/abs/2008A%26A...479..301B (visited on 02/25/2016).

Blackburn, J. K. (1995). "FTOOLS: A FITS Data Processing and Analysis Software Package". In: *Astronomical Data Analysis Software and Systems IV* 77. URL: https://ui.adsabs.harvard.edu/#abs/1995ASPC..77..367B/abstract (visited on 03/25/2017).

Boch, T. and P. Fernique (2014). "Aladin Lite: Embed your Sky in the Browser". In: *Astronomical Data Analysis Software and Systems XXIII* 485. URL: https://ui.adsabs.harvard.edu/#abs/2014ASPC..485..277B/abstract (visited on 03/10/2017).

Boldin, P. A., S. S. Tsygankov, and A. A. Lutovinov (2013). "On timing and spectral characteristics of the X-ray pulsar 4U 0115+63: Evolution of the pulsation period and the cyclotron line energy". In: *Astronomy Letters* 39.6, pp. 375–388. ISSN: 1063-7737, 1562-6873. DOI: 10.1134/S1063773713060029. URL: http://link.springer.com/article/10.1134/S1063773713060029 (visited on 05/20/2016).

Camero Arranz, A. et al. (2005). "INTEGRAL observations of the Be/X-ray binary EXO 2030+375 during outburst". In: *Astronomy and Astrophysics* 441, pp. 261–269. ISSN: 0004-6361. DOI: 10.1051/0004-6361:20053335. URL: http://cdsads.u-strasbg.fr/abs/2005A%26A...441..261C (visited on 01/12/2016).

Chadwick, J. (1932). "The Existence of a Neutron". In: *Proceedings of the Royal Society of London Series A* 136. DOI: 10.1098/rspa.1932.0112.

URL: https://ui.adsabs.harvard.edu/#abs/1932RSPSA.136..692C/abstract (visited on 04/12/2017).

Coe, M. J. et al. (1988). "The optical/IR counterpart to the newly-discovered X-ray source EXO 2030+375". In: *Monthly Notices of the Royal Astronomical Society* 232, pp. 865–871. ISSN: 0035-8711. DOI: 10.1093/mnras/232.4.865. URL: http://cdsads.u-strasbg.fr/abs/1988MNRAS.232..865C (visited on 03/07/2016).

Corbet, R. H. D. (1984). "Be/neutron star binaries : a relationship between orbital period and neutron star spin period." In: *Astronomy and Astrophysics* 141. URL: https://ui.adsabs.harvard.edu/#abs/1984A&A...141...91C/abstract (visited on 01/13/2017).

Corbet, R. H. D. and A. M. Levine (2006). "Outburst from EXO 2030+375". In: *The Astronomer's Telegram* 843. URL: http://cdsads.u-strasbg.fr/abs/2006ATel..843....1C (visited on 03/07/2016).

de Mink, S. E. et al. (2013). "The Rotation Rates of Massive Stars: The Role of Binary Interaction through Tides, Mass Transfer, and Mergers". In: *The Astrophysical Journal* 764. DOI: 10.1088/0004-637X/764/2/166. URL: https://ui.adsabs.harvard.edu/#abs/2013ApJ...764..166D/abstract (visited on 04/17/2017).

EXOSAT > EXOSAT Home Page. URL: https://www.cosmos.esa.int/web/exosat (visited on 04/03/2017).

Ferrigno, Carlo et al. (2016). "Glancing through the accretion column of EXO 2030+375". In: *Astronomy and Astrophysics* 593. DOI: 10.1051/0004-6361/201527837. URL: https://ui.adsabs.harvard.edu/#abs/2016A&A...593A.105F/abstract (visited on 03/21/2017).

Frank, Juhan, Andrew King, and Derek J. Raine (2002). "Accretion Power in Astrophysics: Third Edition". In: URL: https://ui.adsabs.harvard.edu/#abs/2002apa..book.....F/abstract (visited on 01/13/2017).

Fu, Wen, Stephen H. Lubow, and Rebecca G. Martin (2015a). "THE KOZAI–LIDOV MECHANISM IN HYDRODYNAMICAL DISKS. II. EFFECTS OF BINARY AND DISK PARAMETERS". In: *The Astrophysical Journal* 807.1, p. 75. ISSN: 1538-4357. DOI: 10.1088/0004-637X/807/1/75. URL: http://stacks.iop.org/0004-637X/807/i=1/a=75?key=crossref.91e6b7bbb6b786fada76ab86350532dc (visited on 05/17/2016).

— (2015b). "THE KOZAI–LIDOV MECHANISM IN HYDRODYNAMICAL DISKS. III. EFFECTS OF DISK MASS AND SELF-GRAVITY". In: *The Astrophysical Journal* 813.2, p. 105. ISSN: 1538-4357. DOI: 10.1088/0004-637X/813/2/105. URL: http://stacks.iop.org/0004-637X/813/i=2/a=105?key=crossref.2f3c9428e5f3c89d15cbe8f2faff1e3c (visited on 05/17/2016).

Fuerst, Felix et al. (2016). *ATel #8835: Fading outbursts of EXO 2030+375*. URL: http://www.astronomerstelegram.org/?read=8835 (visited on 04/26/2016).

Ghosh, P. and F. K. Lamb (1979). "Accretion by rotating magnetic neutron stars. III. Accretion torques and period changes in pulsating X-ray sources." In: *The Astrophysical Journal* 234. DOI: 10.1086/157498. URL: https://ui.adsabs.harvard.edu/#abs/1979ApJ...234..296G/abstract (visited on 03/03/2017).

Giacconi, R. et al. (1971). "Discovery of Periodic X-Ray Pulsations in Centaurus X-3 from UHURU". In: *The Astrophysical Journal* 167. DOI: 10.1086/180762. URL: https://ui.adsabs.harvard.edu/#abs/1971ApJ...167L..67G/abstract (visited on 01/13/2017).

Giacconi, Riccardo et al. (1962). "Evidence for x Rays From Sources Outside the Solar System". In: *Physical Review Letters* 9, pp. 439–443. ISSN: 0031-9007. DOI: 10.1103/PhysRevLett.9.439. URL: http://adsabs.harvard.edu/abs/1962PhRvL...9..439G (visited on 11/21/2016).

Granada, A. et al. (2013). "Populations of rotating stars. II. Rapid rotators and their link to Be-type stars". In: *Astronomy and Astrophysics* 553. DOI: 10.1051/0004-6361/201220559. URL: https://ui.adsabs.harvard.edu/#abs/2013A&A...553A..25G/abstract (visited on 04/17/2017).

Grundstrom, E. D. et al. (2007). "Joint H alpha and X-Ray Observations of Massive X-Ray Binaries. III. The Be X-Ray Binaries HDE 245770 = A0535+26 and X Persei". In: *The Astrophysical Journal* 660.2, p. 1398. ISSN: 0004-637X. DOI: 10.1086/514325. URL: http://stacks.iop.org/0004-637X/660/i=2/a=1398 (visited on 06/17/2016).

Hazewinkel, Michiel et al. *Encyclopaedia of Mathematics*. Ed. by Springer. URL: http://www.springer.com/la/book/9781556080104 (visited on 04/12/2017).

Hewish, A. et al. (1968). "Observation of a Rapidly Pulsating Radio Source". In: *Nature* 217. DOI: 10.1038/217709a0. URL: https://ui.adsabs.harvard.edu/#abs/1968Natur.217..709H/abstract (visited on 04/12/2017).

Hummel, W. and R. W. Hanuschik (1997). "Line formation in Be star envelopes. II. Disk oscillations." In: *Astronomy and Astrophysics* 320. URL: https://ui.adsabs.harvard.edu/#abs/1997A&A...320..852H/abstract (visited on 03/03/2017).

Kato, S. (1983). "Low-frequency, one-armed oscillations of Keplerian gaseous disks." In: *Publications of the Astronomical Society of Japan* 35. URL: https://ui.adsabs.harvard.edu/#abs/1983PASJ...35..249K/abstract (visited on 03/03/2017).

Klochkov, D. et al. (2007). "INTEGRAL and Swift observations of EXO 2030+375 during a giant outburst". In: *Astronomy and Astrophysics* 464, pp. L45–L48. ISSN: 0004-6361. DOI: 10.1051/0004-6361:20066801. URL: http://cdsads.u-strasbg.fr/abs/2007A%26A...464L..45K (visited on 01/12/2016).

Klochkov, D. et al. (2008). "Giant outburst of EXO 2030+375: pulse-phase resolved analysis of INTEGRAL data". In: *Astronomy and Astrophysics* 491, pp. 833–840. ISSN: 0004-6361. DOI: 10.1051/0004-6361:200810673. URL: http://cdsads.u-strasbg.fr/abs/2008A%26A...491..833K (visited on 01/12/2016).

Klochkov, D. et al. (2011). "Quasi-periodic flares in EXO 2030+375 observed with INTEGRAL". In: *Astronomy and Astrophysics* 536. DOI: 10.1051/0004-6361/201118185. URL: https://ui.adsabs.harvard.edu/#abs/2011A&A...536L...8K/abstract (visited on 03/01/2017).

Korte, De et al. (1981). "The X-Ray Imaging Telescopes on EXOSAT". In: *Space Science Reviews* 30. DOI: 10.1007/BF01246070. URL: https:

//ui.adsabs.harvard.edu/#abs/1981SSRv...30..495D/abstract (visited on 03/29/2017).

Kozai, Yoshihide (1962). "Secular perturbations of asteroids with high inclination and eccentricity". In: *The Astronomical Journal* 67, p. 591. ISSN: 00046256. DOI: 10.1086/108790. URL: http://adsabs.harvard.edu/cgi-bin/bib_query?1962AJ.....67..591K (visited on 05/17/2016).

Kretschmar, Peter et al. (2016). "EXO 2030+375 restarts in reverse". In: *The Astronomer's Telegram* 9485. URL: https://ui.adsabs.harvard.edu/#abs/2016ATel.9485....1K/abstract (visited on 03/09/2017).

Krimm, H. et al. (2006). "Swift/BAT detects an outburst from EXO 2030+375". In: *The Astronomer's Telegram* 861. URL: https://ui.adsabs.harvard.edu/#abs/2006ATel..861....1K/abstract (visited on 03/03/2017).

Krimm, H. A. et al. (2013). "The Swift/BAT Hard X-Ray Transient Monitor". In: *ApJS* 209.1, p. 14. ISSN: 0067-0049. DOI: 10.1088/0067-0049/209/1/14. URL: http://stacks.iop.org/0067-0049/209/i=1/a=14 (visited on 05/10/2016).

Kuehnel, M. et al. (2015). "The Be X-ray Binary Outburst Zoo II". In: p. 78. URL: http://cdsads.u-strasbg.fr/abs/2015int..workE..78K (visited on 03/07/2016).

Laplace, E. et al. (2016). "Orbital phase shift in a new type I outburst of the Be/X-ray binary EXO 2030+375". In: *The Astronomer's Telegram* 9263.

Laplace, Eva (2015). "Long-term variability of Be/X-ray binaries". Bachelor thesis. Universität Tübingen.

Laplace, Eva et al. (2017). "Possible regular phenomena in EXO 2030+375". In: *Astronomy and Astrophysics* 597. DOI: 10.1051/0004-6361/201629373. URL: https://ui.adsabs.harvard.edu/#abs/2017A&A...597A.124L/abstract (visited on 03/03/2017).

Lee, U., H. Saio, and Y. Osaki (1991). "Viscous excretion discs around Be stars". In: *Monthly Notices of the Royal Astronomical Society* 250. DOI: 10.1093/mnras/250.2.432. URL: https://ui.adsabs.harvard.edu/#abs/1991MNRAS.250..432L/abstract (visited on 03/03/2017).

Levine, Alan M. et al. (1996). "First Results from the All-Sky Monitor on the Rossi X-Ray Timing Explorer". In: *The Astrophysical Journal Letters* 469, p. L33. ISSN: 0004-637X. DOI: 10.1086/310260. URL: http://cdsads.u-strasbg.fr/abs/1996ApJ...469L..33L (visited on 05/10/2016).

Lidov, M.L. (1962). "The evolution of orbits of artificial satellites of planets under the action of gravitational perturbations of external bodies". In: *Planetary and Space Science* 9.10, pp. 719–759. ISSN: 00320633. DOI: 10.1016/0032-0633(62)90129-0. URL: http://linkinghub.elsevier.com/retrieve/pii/0032063362901290 (visited on 05/17/2016).

Longair, Malcolm S. (2011). "High Energy Astrophysics". In: URL: https://ui.adsabs.harvard.edu/#abs/2011hea..book.....L/abstract (visited on 01/13/2017).

Makishima, K. et al. (1990). "Discovery of a Prominent Cyclotron Absorption Feature from the Transient X-Ray Pulsar X0331+53". In: *The Astrophysical Journal* 365. DOI: 10.1086/185888. URL: https://ui.adsabs.harvard.edu/#abs/1990ApJ...365L..59M/abstract (visited on 01/13/2017).

Malacaria, C. et al. (2016). "Probing the stellar wind environment of Vela X-1 with MAXI". In: *Astronomy and Astrophysics* 588. DOI: 10.1051/0004-6361/201527009. URL: https://ui.adsabs.harvard.edu/#abs/2016A&A...588A.100M/abstract (visited on 04/10/2017).

Martin, Rebecca G. et al. (2014a). "Giant Outbursts in Be/X-Ray Binaries". In: *ApJ* 790.2, p. L34. ISSN: 2041-8205. DOI: 10.1088/2041-8205/790/2/L34. URL: http://stacks.iop.org/2041-8205/790/i=2/a=L34 (visited on 05/02/2016).

Martin, Rebecca G. et al. (2014b). "The Kozai-Lidov Mechanism in Hydrodynamical Disks". In: *The Astrophysical Journal Letters* 792, p. L33. ISSN: 0004-637X. DOI: 10.1088/2041-8205/792/2/L33. URL: http://cdsads.u-strasbg.fr/abs/2014ApJ...792L..33M (visited on 03/23/2016).

Matsuoka, Masaru et al. (2009). "The MAXI Mission on the ISS: Science and Instruments for Monitoring All Sky X-Ray Images". In: *Publications of the Astronomical Society of Japan* 61.5, pp. 999–1010. ISSN: 0004-6264, 2053-051X. DOI: 10.1093/pasj/61.5.999. arXiv: 0906.0631. URL: http://arxiv.org/abs/0906.0631 (visited on 05/10/2016).

McBride, V. A. et al. (2007). "On the cyclotron line in Cepheus X-4". In: *Astronomy and Astrophysics* 470.3, pp. 1065–1070. ISSN: 0004-6361, 1432-0746. DOI: 10.1051/0004-6361:20077238. URL: http://www.aanda.org/10.1051/0004-6361:20077238 (visited on 06/03/2016).

McCollough, M. L. et al. (2006). "INTEGRAL Observations of Activity in EXO 2030+375". In: *The Astronomer's Telegram* 868. URL: https://ui.adsabs.harvard.edu/#abs/2006ATel..868....1M/abstract (visited on 03/03/2017).

Meegan, Charles et al. (2009). "The Fermi Gamma-ray Burst Monitor". In: *The Astrophysical Journal* 702, pp. 791–804. ISSN: 0004-637X. DOI: 10.1088/0004-637X/702/1/791. URL: http://adsabs.harvard.edu/abs/2009ApJ...702..791M (visited on 05/10/2016).

Mihara, Tatehiro et al. (2011). "Gas Slit Camera (GSC) onboard MAXI on ISS". In: *Publications of the Astronomical Society of Japan* 63 (sp3), S623–S634. ISSN: 0004-6264, 2053-051X. DOI: 10.1093/pasj/63.sp3.S623. URL: http://pasj.oxfordjournals.org/lookup/doi/10.1093/pasj/63.sp3.S623 (visited on 05/10/2016).

Moritani, Yuki et al. (2013). "Precessing Warped Be Disk Triggering the Giant Outbursts in 2009 and 2011 in A0535+262/V725Tau". In: *Publications of the Astronomical Society of Japan* 65. ISSN: 0004-6264. DOI: 10.1093/pasj/65.4.83. URL: http://cdsads.u-strasbg.fr/abs/2013PASJ...65...83M (visited on 03/07/2016).

Munar-Adrover, P. et al. (2014). "Discovery of X-Ray Emission from the First Be/Black Hole System". In: *The Astrophysical Journal* 786. DOI: 10.1088/2041-8205/786/2/L11. URL: https://ui.adsabs.harvard.edu/#abs/2014ApJ...786L..11M/abstract (visited on 01/13/2017).

Naik, Sachindra and Gaurava K. Jaisawal (2015). "Suzaku observation of Be/X-ray binary pulsar EXO 2030+375". In: *Research in Astronomy and Astrophysics* 15. DOI: 10.1088/1674-4527/15/4/007. URL: https://ui.adsabs.harvard.edu/#abs/2015RAA....15..537N/abstract (visited on 03/03/2017).

Naik, Sachindra et al. (2013). "Timing and Spectral Properties of Be/X-Ray Pulsar EXO 2030+375 during a Type I Outburst". In: *The Astrophysical Journal* 764. DOI: 10.1088/0004-637X/764/2/158. URL: https://ui.adsabs.harvard.edu/#abs/2013ApJ...764..158N/abstract (visited on 03/01/2017).

Nakajima, Motoki et al. (2014). "Precursors and outbursts of A 0535+26 in 2009-2011 observed by the MAXI/GSC and the Swift/BAT". In: *Publications of the Astronomical Society of Japan* 66, p. 9. ISSN: 0004-6264. DOI: 10.1093/pasj/pst002. URL: http://cdsads.u-strasbg.fr/abs/2014PASJ...66....9N (visited on 02/19/2016).

Negueruela, I. and A. T. Okazaki (2001). "The Be/X-ray transient 4U 0115+63/V635 Cassiopeiae. I. A consistent model". In: *Astronomy and Astrophysics* 369. DOI: 10.1051/0004-6361:20010146. URL: https://ui.adsabs.harvard.edu/#abs/2001A&A...369..108N/abstract (visited on 03/03/2017).

Norton, A. J. et al. (1994). "Multiwavelength Observations of the Be-Star / X-Ray Binary EXO:3040+375 during Outburst". In: *Monthly Notices of the Royal Astronomical Society* 271, p. 981. ISSN: 0035-8711. DOI: 10.1093/mnras/271.4.981. URL: http://cdsads.u-strasbg.fr/abs/1994MNRAS.271..981N (visited on 03/09/2016).

Okazaki, A. T. (1997). "On the confinement of one-armed oscillations in discs of Be stars." In: *Astronomy and Astrophysics* 318. URL: https://ui.adsabs.harvard.edu/#abs/1997A&A...318..548O/abstract (visited on 03/03/2017).

Okazaki, A. T. and I. Negueruela (2001). "A natural explanation for periodic X-ray outbursts in Be/X-ray binaries". In: *Astronomy and Astrophysics* 377, pp. 161–174. ISSN: 0004-6361. DOI: 10.1051/0004-6361:20011083. URL: http://cdsads.u-strasbg.fr/abs/2001A%26A...377..161O (visited on 03/02/2016).

Okazaki, Atsuo T. (1996). "Emission-Line Profiles from Be-Star Envelopes with m=1 Perturbation Patterns". In: *Publications of the Astronomical Society of Japan* 48. DOI: 10.1093/pasj/48.2.305. URL: https://ui.adsabs.harvard.edu/#abs/1996PASJ...48..305O/abstract (visited on 03/03/2017).

Okazaki, Atsuo T., Kimitake Hayasaki, and Yuki Moritani (2013). "Origin of Two Types of X-Ray Outbursts in Be/X-Ray Binaries. I. Accretion Scenarios". In: *Publications of the Astronomical Society of Japan* 65. ISSN: 0004-6264. DOI: 10.1093/pasj/65.2.41. URL: http://cdsads.u-strasbg.fr/abs/2013PASJ...65...41O (visited on 02/23/2016).

Oppenheimer, J. R. and G. M. Volkoff (1939). "On Massive Neutron Cores". In: *Physical Review* 55. DOI: 10.1103/PhysRev.55.374. URL: https://ui.adsabs.harvard.edu/#abs/1939PhRv...55..374O/abstract (visited on 04/12/2017).

Pacini, F. (1967). "Energy Emission from a Neutron Star". In: *Nature* 216. DOI: 10.1038/216567a0. URL: https://ui.adsabs.harvard.edu/#abs/1967Natur.216..567P/abstract (visited on 04/12/2017).

Parmar, A. N., N. E. White, and L. Stella (1989). "The Transient 42 Second X-Ray Pulsar EXO 2030+375. II. The Luminosity Dependence of the Pulse Profile". In: *The Astrophysical Journal* 338. DOI: 10.1086/167205. URL: https://ui.adsabs.harvard.edu/#abs/1989ApJ...338..373P/abstract (visited on 03/03/2017).

Parmar, A. N. et al. (1985). "EXO 2030+375". In: *International Astronomical Union Circular* 4066. URL: https://ui.adsabs.harvard.edu/#abs/1985IAUC.4066....1P/abstract (visited on 03/03/2017).

Parmar, A. N. et al. (1989). "The transient 42 second X-ray pulsar EXO 2030+375. I - The discovery and the luminosity dependence of the pulse period variations". In: *The Astrophysical Journal* 338, pp. 359–372. ISSN: 0004-637X. DOI: 10.1086/167204. URL: http://cdsads.u-strasbg.fr/abs/1989ApJ...338..359P (visited on 02/03/2016).

Pilkington, J. D. H. et al. (1968). "Observations of some further Pulsed Radio Sources". In: *Nature* 218. DOI: 10.1038/218126a0. URL: https://ui.adsabs.harvard.edu/#abs/1968Natur.218..126P/abstract (visited on 04/12/2017).

Porter, John M. (1999). "On outflowing viscous disc models for Be stars". In: *Astronomy and Astrophysics* 348. URL: https://ui.adsabs.harvard.edu/#abs/1999A&A...348..512P/abstract (visited on 03/03/2017).

Rainey, Kristine (2014). *Weekly Recap From the Expedition Lead Scientist*. und. Text. URL: http://www.nasa.gov/mission_pages/station/research/news/wklysumm_week_of_29Jan14 (visited on 03/25/2017).

Reig, P. and M. J. Coe (1998). "Timing properties of the X-ray pulsar EXO 2030+375 during an X-ray outburst". In: *Monthly Notices of the Royal Astronomical Society* 294, p. 118. ISSN: 0035-8711. DOI: 10.1046/j.1365-8711.1998.01252.x. URL: http://cdsads.u-strasbg.fr/abs/1998MNRAS.294..118R (visited on 01/19/2016).

— (1999). "X-ray spectral properties of the pulsar EXO 2030+375 during an outburst". In: *Monthly Notices of the Royal Astronomical Society* 302. DOI: 10.1046/j.1365-8711.1999.02179.x. URL: https://ui.adsabs.harvard.edu/#abs/1999MNRAS.302..700R/abstract (visited on 03/03/2017).

Reig, P. et al. (1998). "Long-term variability of the Be/X-ray binary EXO 2030+375". In: *Monthly Notices of the Royal Astronomical Society* 301, pp. 42–48. ISSN: 0035-8711. DOI: 10.1046/j.1365-8711.1998.01989.x. URL: http://adsabs.harvard.edu/abs/1998MNRAS.301...42R (visited on 01/25/2016).

Reig, P. et al. (2014). "The high optical polarization in the Be/X-ray binary EXO 2030+375". In: *Monthly Notices of the Royal Astronomical Society* 445. DOI: 10.1093/mnras/stu2322. URL: https://ui.adsabs.harvard.edu/#abs/2014MNRAS.445.4235R/abstract (visited on 03/03/2017).

Reig, Pablo (2011). "Be/X-ray binaries". In: *Astrophysics and Space Science* 332, pp. 1–29. ISSN: 0004-640X. DOI: 10.1007/s10509-010-0575-8. URL: http://cdsads.u-strasbg.fr/abs/2011Ap%26SS.332...1R (visited on 05/02/2016).

Reynolds, A. P., A. N. Parmar, and N. E. White (1993). "The Luminosity Dependence of the X-Ray Spectrum of the Transient 42 Second Pulsar EXO 2030+375". In: *The Astrophysical Journal* 414. DOI: 10.1086/173076. URL: https://ui.adsabs.harvard.edu/#abs/1993ApJ...414..302R/abstract (visited on 03/03/2017).

Rivinius, Th et al. (1998). "Stellar and circumstellar activity of the Be star MU Centauri. I. Line emission outbursts". In: *Astronomy and Astrophysics* 333. URL: https://ui.adsabs.harvard.edu/#abs/1998A&A...333..125R/abstract (visited on 05/17/2016).

Rivinius, Th. et al. (2001a). "Evolution in circumstellar envelopes of Be stars: From disks to rings?" In: *Astronomy and Astrophysics* 379.1, pp. 257–269. ISSN: 0004-6361, 1432-0756. DOI: 10.1051/0004-6361:20011335. URL: http://www.edpsciences.org/10.1051/0004-6361:20011335 (visited on 05/17/2016).

Rivinius, Th et al. (2001b). "Stellar and circumstellar variability of the Be star mu Cen IV". In: *Journal of Astronomical Data* 7. URL: https://ui.adsabs.harvard.edu/#abs/2001JAD.....7....5R/abstract (visited on 05/17/2016).

Rodes-Roca, J. J. et al. (2015). "Orbital phase-resolved spectroscopy of 4U 1538-52 with MAXI". In: *Astronomy and Astrophysics* 580. DOI: 10.1051/0004-6361/201425323. URL: https://ui.adsabs.harvard.edu/#abs/2015A&A...580A.140R/abstract (visited on 03/25/2017).

Santangelo, Andrea and Rosalia Madonia (2014). "Fifty years of X-ray astronomy: A look back and into the (near) future". In: *Astroparticle Physics*. Centenary of cosmic ray discovery 53, pp. 130–151. ISSN: 0927-6505. DOI: 10.1016/j.astropartphys.2013.11.005. URL: http://www.sciencedirect.com/science/article/pii/S0927650513001631 (visited on 11/23/2016).

Sasaki, M. et al. (2010). "Analyzing X-ray pulsar profiles: geometry and beam pattern of EXO 2030+375". In: *Astronomy and Astrophysics* 517. DOI: 10.1051/0004-6361/200913863. URL: https://ui.adsabs.harvard.edu/#abs/2010A&A...517A...8S/abstract (visited on 03/03/2017).

Smith, M. A. (1994). "Photospheric Activity in Selected Be Stars: Lambda ERI and Gamma CAS". In: *Pulsation; Rotation; and Mass Loss in Early-Type Stars* 162. URL: https://ui.adsabs.harvard.edu/#abs/1994IAUS..162..241S/abstract (visited on 01/13/2017).

Steele, I. A. (2016a). "CORRECTION: Optical Spectroscopy of EXO2030+375 in ATel 9265 and 8927". In: *The Astronomer's Telegram* 9487. URL: https://ui.adsabs.harvard.edu/#abs/2016ATel.9487....1S/abstract (visited on 03/29/2017).

— (2016b). "Optical Spectroscopy of EXO 2030+375 during the current X-ray outburst". In: *The Astronomer's Telegram* 9265. URL: https://ui.adsabs.harvard.edu/#abs/2016ATel.9265....1S/abstract (visited on 03/29/2017).

— (2016c). "Optical Spectroscopy of EXO 2030+375 during the transition to low X-ray flux". In: *The Astronomer's Telegram* 8927. URL: https://ui.adsabs.harvard.edu/#abs/2016ATel.8927....1S/abstract (visited on 03/29/2017).

Stella, L., N. E. White, and R. Rosner (1986). "Intermittent stellar wind accretion and the long-term activity of Population I binary systems containing an X-ray pulsar". In: *The Astrophysical Journal* 308, p. 669. ISSN: 0004-637X, 1538-4357. DOI: 10.1086/164538. URL: http://adsabs.harvard.edu/doi/10.1086/164538 (visited on 05/02/2016).

Stollberg, Mark T. et al. (1999). "BATSE Observations and Orbit Determination of the BE/X-Ray Transient EXO 2030+375". In: *The Astrophysical Journal* 512. DOI: 10.1086/306733. URL: https://ui.adsabs.harvard.edu/#abs/1999ApJ...512..313S/abstract (visited on 03/03/2017).

Swift: About Swift - BAT Instrument Description. URL: https://swift.gsfc.nasa.gov/about_swift/bat_desc.html (visited on 04/03/2017).

Tanaka, Ken'ichi et al. (2007). "Dramatic Spectral and Photometric Changes of Pleione (28 Tau) between 2005 November and 2007 April". In: *Publications of the Astronomical Society of Japan* 59.4, pp. L35–L39. ISSN: 0004-6264, 2053-051X. DOI: 10.1093/pasj/59.4.L35. URL: http://pasj.oxfordjournals.org/lookup/doi/10.1093/pasj/59.4.L35 (visited on 05/17/2016).

Tarasov, A. E. and P. Roche (1995). "Double circumstellar disc structure in X Persei". In: *Monthly Notices of the Royal Astronomical Society* 276, pp. L19–L20. ISSN: 0035-8711. DOI: 10.1093/mnras/276.1.19L. URL: http://cdsads.u-strasbg.fr/abs/1995MNRAS.276L..19T (visited on 05/17/2016).

Tomida, Hiroshi et al. (2011). "Solid-State Slit Camera (SSC) Aboard MAXI". In: *Publications of the Astronomical Society of Japan* 63. DOI: 10.1093/pasj/63.2.397. URL: https://ui.adsabs.harvard.edu/#abs/2011PASJ...63..397T/abstract (visited on 03/25/2017).

Trümper, J. et al. (1978). "Evidence for strong cyclotron line emission in the hard X-ray spectrum of Hercules X-1." In: *The Astrophysical Journal* 219. DOI: 10.1086/182617. URL: https://ui.adsabs.harvard.edu/#abs/1978ApJ...219L.105T/abstract (visited on 04/12/2017).

Turner, M. J. L., A. Smith, and H. U. Zimmermann (1981). "The medium energy instrument on EXOSAT." In: *Space Science Reviews* 30. DOI: 10.1007/BF01246071. URL: https://ui.adsabs.harvard.edu/#abs/1981SSRv...30..513T/abstract (visited on 03/29/2017).

Whitlock, L., D. Roussel-Dupre, and W. Priedhorsky (1989). "Observations of the X-ray transient 4U 0115+63". In: *The Astrophysical Journal* 338, p. 381. ISSN: 0004-637X, 1538-4357. DOI: 10.1086/167206. URL: http://adsabs.harvard.edu/doi/10.1086/167206 (visited on 05/20/2016).

Wilson, Colleen A., Juan Fabregat, and Wayne Coburn (2005). "Discovery of a Transition to Global Spin-up in EXO 2030+375". In: *The Astrophysical Journal Letters* 620, pp. L99–L102. ISSN: 0004-637X. DOI: 10.1086/428838. URL: http://cdsads.u-strasbg.fr/abs/2005ApJ...620L..99W (visited on 01/12/2016).

Wilson, Colleen A., Mark H. Finger, and Ascensión Camero-Arranz (2008). "Outbursts Large and Small from EXO 2030+375". In: *The Astrophysical Journal* 678, pp. 1263–1272. ISSN: 0004-637X. DOI: 10.1086/587134. URL: http://cdsads.u-strasbg.fr/abs/2008ApJ...678.1263W (visited on 01/12/2016).

Wilson, Colleen A. et al. (2002). "A Decade in the Life of EXO 2030+375: A Multiwavelength Study of an Accreting X-Ray Pulsar". In: *The Astrophysical Journal* 570, pp. 287–302. ISSN: 0004-637X. DOI: 10.1086/339739. URL: http://cdsads.u-strasbg.fr/abs/2002ApJ...570..287W (visited on 01/12/2016).